EXPERIMENTAL INVESTIGATION ON NANOFLUIDS WITH AND WITHOUT THE EFFECTS OF EXTERNAL MAGNETIC FIELD

by

Alper Elkatmış

Submitted to the Institute of Graduate Studies in
Science and Engineering in partial fulfillment of
the requirements for the degree of
Doctor of Philosophy
In
Physics

Yeditepe University

2011

EXPERIMENTAL INVESTIGATION ON NANOFLUIDS
WITH AND WITHOUT THE EFFECTS OF EXTERNAL MAGNETIC FIELD

APPROVED BY:

Prof. Dr. Necdet Aslan
(Thesis Supervisor) .....

Assist. Prof. Dr. Ercüment Akat .....

Prof. Dr. Uğur Yahşi .....

Prof. Dr. Şahin Aktaş .....

Assoc. Prof. Dr. Sinan Keskin .....

DATE OF APPROVAL: …. /…. /…..

ACKNOWLEDGEMENTS

Firstly, I would like to express my gratitude and my deepest appreciation to my supervisor Professor Necdet Aslan for giving me the chance to study with him in the field of nanofluids that was not even related to his core research when I started. His advices, guidance and his trust on me gave me the courage and strength to overcome the challenges throughout this long journey.

I extend sincere thanks to Assoc. Prof. Dr. Seyda Malta from Chemical Engineering Department for allowing me to use her equipment in the laboratory and for her unlimited tolerance. Special thanks to Merve Yüksel for her study in preparation of ferrofluid samples. I also thank Assist. Prof. Dr. Ercüment Akat, Prof. Dr. Uğur Yahşi, Prof. Dr. Şahin Aktaş and Assoc. Prof. Dr. Sinan Keskin for serving on my thesis committee and for their suggestions to improve the manuscript quality.

I would like to thank TÜBİTAK UME for supporting my thesis research. This research project would not have been possible without the permission of the Institute to begin and complete this thesis.

Most importantly, I would like to thank my mother, Meral Özyiğit, and my sister, Banu Çelebi, for everything they have done for me.

This thesis is dedicated to my family.

ABSTRACT

EXPERIMENTAL INVESTIGATION ON NANOFLUIDS WITH AND WITHOUT THE EFFECTS OF EXTERNAL MAGNETIC FIELD

This thesis is mainly concerned with experimental studies on the magnetic and nonmagnetic nanofluids using Fe_3O_4 magnetite heptane/water/hexane and silicon dioxide (silica) dispersed in ethanol. TEM, SEM, DLS, X-Ray Diffraction and VSM analyses methods were used to investigate the characterization of nanoparticles and nanofluids. The thermophysical properties of the nanofluids at different temperatures and nanoparticle concentrations including density, viscosity and thermal conductivity directly affecting the heat transfer behaviors were investigated. Some theoretical models for density, viscosity and thermal conductivity taken from the literature were used to compare with the experimental results. In addition, a theoretical model was derived for the thermal conductivity of the magnetic nanofluids under the effect of external magnetic field. External magnetic field effects on thermal conductivity of magnetic nanofluids have been investigated for magnetite heptane/water, magnetite hexane and the results were compared with the theoretical derivation. In order to use the magnetic effect, a homemade electromagnet producing 0-1.7 Tesla was designed and manufactured. The results show that the density, viscosity and thermal conductivity of magnetic and nonmagnetic nanofluids increase with increasing particle weight concentration and decrease with increasing temperature. In addition, thermal conductivity enhancement for magnetic heptane/water under the full wave bridged DC voltage (full wave bridged by bridge diode of 160 A) external magnetic field and thermal conductivity reduction of the magnetite hexane under the full wave rectified DC voltage (full wave rectified by bridge diode of 160 A and capacitors of 4500 μF) external magnetic field were found and presented.

ÖZET

NANOAKIŞKANLARIN DIŞ MANYETİK ALAN ETKİSİNDE VE HARİCİNDE DENEYSEL OLARAK İNCELENMESİ

Bu tez, genel olarak manyetit Fe_3O_4 heptan/su/hegzan ve etanolda silisyum dioksit (silica) nanoakışkanlar üzerindeki deneysel çalışmalarla ilgilidir. Nanoparçaçık ve nanoakışkanların karakterizasyon ölçümleri TEM, SEM, DLS, X-Ray Diffraction ve VSM analiz yöntemleri kullanılarak gerçekleştirilmiştir. Farklı sıcaklık ve nano parçacık konsantrasyonlarındaki nanoakışkanların ısı transferi davranışını doğrudan etkileyen yoğunluk, viskozite ve ısıl iletkenlik büyüklüklerini içeren termofiziksel özellikleri araştırılmıştır. Yoğunluk, viskozite ve ısıl iletkenlik için literatürden seçilen bazı kuramsal modeller ile deneysel veriler karşılaştırılmıştır. Ayrıca, dış manyetik alan etkisi altındaki manyetik nanoakışkanlar için teorik model türetilmiştir. Ayrıca, dış manyetik alan etkisi altındaki manyetit heptan, manyetit su ve manyetit hegzan tip manyetik nanoakışkanların ısıl iletkenlikleri araştırılmış, kuramsal olarak türetilen sonuç ile karşılaştırılmıştır. Manyetik etki kullanımı için 0-1.7 Tesla üretebilen elektromıknatıs tasarlanmış ve üretilmiştir. Bu çalışma, manyetik ve manyetik olmayan nanoakışkanların yoğunluk, viskozite ve termal iletkenliklerinin parçacık konsantrasyon artışı ile arttığını ve sıcaklık ile azaldığını göstermektedir. Ayrıca, DC (160 A köprü diyot doğrultmalı) dış manyetik etki altındaki manyetit heptan/su nanoakışkanın ısıl iletkenliğinin zenginleştiği ve tam dalga DC (160 A köprü diyot ve 4500 μF kondansatör doğrultmalı) dış manyetik etki altındaki manyetit hegzan nanoakışkanın ısıl iletkenliğinin azaldığı bulunmuş ve sunulmuştur.

TABLE OF CONTENTS

ACKNOWLEDGEMENTS iii
ABSTRACT iv
ÖZET v
LIST OF FIGURES ix
LIST OF TABLES xiv
LIST OF SYMBOLS AND ABBREVIATIONS xvi
1. INTRODUCTION 1
1.1. SCOPE OF THE THESIS 1
1.2. A BRIEF HISTORY OF NANOFLUIDS 2
1.3. LITERATURE REVIEW 5
1.3.1. Magnetic Effect on Thermal Conductivity of Ferrofluids 6
1.3.2. Concentration Effect on Thermal Conductivty of Different Types of Nanofluids …..... 8
1.3.3. Different Effects on Viscosity of Different Types of Nanofluids 9
2. FERROFLUIDS AND FERROHYDRODYNAMICS 12
2.1. WHAT IS FERROFLUID? 12
2.2. FERROHYDRODYNAMICS. 15
2.3. STABILITY REQUIREMENTS OF FERROFLUIDS 17
2.3.1. Stability in a magnetic-field gradient 17
2.3.2. Stability against settling in a gravitational field 19
2.3.3. Stability against magnetic agglomeration 20
2.3.4. Necessity to guard against the Van der Waals attractive force 20
2.4. APPLICATION OF FERROFLUIDS 21
3. THEORETICAL BACKGROUND 23
3.1. THERMOPHYSICAL PROPERTIES OF FERROFLUIDS 23
3.1.1. Heat Transfer and Thermal Conductivity 23
3.1.2. Heat Transfer Mechanism in Nanofluids 24
3.1.2.1. Nanoparticle Motion 24
3.1.2.2. Liquid Layering at Liquid-Particle Interface 25

3.1.2.3. Nature of Heat Transport in Nanoparticles 26
3.1.2.4. Nanoparticle Clustering 26
3.2. MAGNETISM 28
3.2.1. Basic Definitions 28
3.2.1.1. Magnetic Induction, B 28
3.2.1.2. Magnetic Field Strength, H 29
3.2.1.3. Magnetic Moment, m 29
3.2.1.4. Magnetization, M 30
3.2.1.5. Magnetic Susceptibility, χ 31
3.2.2. Different Types of Magnetic Behaviour 31
3.2.3. Hysteresis Loop and Superparamagnetism 33
3.3. PREPARATION OF NANOFLUIDS 38
3.4. DERIVATION OF MAGNETIC EFFECT ON THERMAL CONDUCTIVITY OF MAGNETIC NANOFLUIDS 40
4. MEASUREMENTS TECHNIQUES 50
4.1. CHARACTERIZATION TECHNIQUES 50
4.1.1. Transmission Electron Microscopy (TEM) 50
4.1.2. Dynamic Light Scattering (DLS) 52
4.1.3. X-Ray Diffraction 55
4.1.4. Vibrating Sampling Magnetometer (VSM) 58
4.1.5. Scanning Electron Microscopy (SEM) 62
4.2. THERMOPHYSICAL MEASUREMENT TECHNIQUES 63
4.2.1. Density 63
4.2.2. Viscosity 64
4.2.3. Thermal Conductivity 66
5. RESULTS AND DICCUSSION 71
5.1. CHARACTERIZATION MEASUREMENTS OF THE SAMPLES 71
5.1.1. Transmission Electron Microscopy (TEM) Analyses of Ferrofluids 71
5.1.2. Dynamic Light Scattering (DLS) Analyses of Ferrofluids 72
5.1.3. X-Ray Diffractometer (XRD) Analyses of Ferrofluid 73
5.1.4. Vibrating Sample Magnetometer (VSM) Analyses of Ferrofluids 74
5.1.5. Scanning Electron Microscopy (SEM) and DLS Analyses of Silica 77
5.2. THERMOPHYSICAL MEASUREMENTS OF NANOFLUIDS 79

5.2.1. Density Measurements of Ferrofluid 79
5.2.2. Viscosity Measurements of Ferrofluid..... 82
5.2.3. Thermal Conductivity of Ferrofluids 85
5.2.4. Viscosity Measurements of Silica..... 89
5.3. MAGNETIC EFFECT MEASUREMENTS ON FERROFLUIDS 91
5.3.1. Magnetic Field Sources..... 91
5.3.1.1. Magnetic Coil 91
5.3.1.2. Homemade U-core DC Electromagnet..... 92
5.3.2. Thermal Conductivity of Magnetite Heptane and Water under magnetic effect..... 94
5.3.2.1. Using a Magnetic Coil..... 94
5.3.2.2. Using U-core Electromagnet 98
5.3.3. Thermal Conductivity of Magnetite Hexane under Magnetic Effect 100
6. CONCLUSION AND FUTURE WORK 104
APPENDIX A: UNCERTAINTY ESTIMATION AND ERROR ANALYSES OF THERMOPHYSICAL MEASUREMENTS 109
APPENDIX B: UNITS FOR MAGNETIC PROPERTIES..... 111
REFERENCES 113

LIST OF FIGURES

Figure 2.1. A schematic illustration of a common ferrofluid composition 12

Figure 2.2. Magnetization effect on the magnetic particles of a ferrofluid..... 14

Figure 2.3. Schematic representation of magnetic nanostructure morphologies 15

Figure 2.4. The concentration of magnetic particles in a magnetic nanofluid under the effect of a gradient magnetic field 19

Figure 3.1. Excess thermal-conductivity (*k*) enhancement owing to formation of highly conductive layered-liquid structure at liquid-particle interface.. 26

Figure 3.2. Excess thermal conductivity *k* enhancement owing to increased effective volume φ of highly conducting clusters…….. 28

Figure 3.3. Different types of magnetic behaviors..... 33

Figure 3.4. A typical magnetization hysteresis loop (M–H) of a ferromagnetic material…….. 34

Figure 3.5. The magnetic responses associated with different classes of magnetic material among others are illustrated by their corresponding M–H curves.……..... 35

Figure 3.6. The illustration of relationship between the coercivity in ultrafine particle systems and particle sizes……..... 36

Figure 3.7. Observation of superparamagnetism 38

Figure 3.8.	The experimental setup and solution domain	40
Figure 3.9.	Temperature gradient in a ferrofluid by applying a magnetic field…..	41
Figure 4.1.	Lens ray diagram of the imaging system of TEM…….	51
Figure 4.2.	Transmission Electron Microscope FEI - Tecnai G2 F30…….	52
Figure 4.3.	Particle size and particle motion dependency……	54
Figure 4.4.	Illustration of the scattered light sensing by detector……	54
Figure 4.5.	Bragg condition illustrating the diffraction of X-rays by a crystal……	56
Figure 4.6.	A basic schematic view of a X-ray diffractometer……	57
Figure 4.7.	The scheme of a vibrating sample magnetometer…….	59
Figure 4.8.	Scheme of a VSM with applied field transverse to the vibration axis...	60
Figure 4.9.	VSM equipment located at TÜBİTAK UME……	61
Figure 4.10.	Vertical rod holding the sample between coils……..	62
Figure 4.11.	Schematic diagramme of a SEM……...	63
Figure 4.12.	Density meter Anton Paar DMA 4100……...	64
Figure 4.13.	Brookfield DV-III Ultra Programmable Rheometer……..	65
Figure 4.14.	Comparison of the thermal conductivity measurement techniques for nanofluids……..	67

Figure 4.15. The thermal conductivity measuring device used in this study……. 70

Figure 5.1. TEM image of magnetite nanoparticles (Fe_3O_4) prepared by water synthesis……. 72

Figure 5.2. TEM image of magnetite nanoparticles (Fe_3O_4) prepared by oil synthesis……. 72

Figure 5.3. DLS Data for Fe_3O_4 particles……. 73

Figure 5.4. Magnetite–Oil X-Ray Diffractogram..... 74

Figure 5.5. Magnetization curves at different concentrations of Fe_3O_4 particles suspended in heptane at 296 K……... 75

Figure 5.6. Magnetization as a function of H in low fields for magnetite heptane nanofluids…….. 76

Figure 5.7. SEM image of Silica 2.86 N – 7T (SEM peak: 128.35 nm)…….. 77

Figure 5.8. DLS results for 2.86 N – 7T Intensity: 165.7 - 160.2……..... 78

Figure 5.9. DLS results for 2.86 N – 7T Volume : 155.2 -149.6……. 78

Figure 5.10. DLS results for 2.86 N – 7T Number : 108.4 -108.7……. 78

Figure 5.11. Density enhancement for magnetite nanoparticles dispersed in Heptane…….. 80

Figure 5.12. Comparison of density values for magnetite nanofluid at 25 °C……... 81

Figure 5.13. Viscosity enhancement for magnetite nanoparticles dispersed in heptane……... 82

Figure 5.14. Relative viscosities of magnetite nanofluids at 30 ^{o}C…… 83

Figure 5.15. Comparison of the viscosity data with theories for magnetite heptane nanofluid according to [114]…….. 84

Figure 5.16. Comparison of the viscosity data with theories for magnetite heptane nanofluid according to [115]…….. 85

Figure 5.17. Thermal conductivity enhancement of magnetite nanoparticles dispersed in heptane……... 86

Figure 5.18. Thermal conductivity enhancement of magnetic heptane at each weight concentration…….. 87

Figure 5.19. Relative enhancement of thermal conductivity upon addition of Fe_3O_4 in heptane as a function of concentration at 25^{o}C……..... 88

Figure 5.20. Comparison of Wasp model and experimental data obtained from this study for the thermal conductivity of Fe_3O_4 nanoparticles in Heptane at 25 °C…….. 89

Figure 5.21. Experimental values of viscosity for varying weight concentrations of silicon dioxide nanofluids (128.35 nm) with respect to temperature 90

Figure 5.22. Experimental values of viscosity for varying weight concentrations of silicon dioxide nanofluids (128.35 nm) with respect to temperature 90

Figure 5.23. Experimental setup for the thermal conductivity measurements at the external magnetic field……... 92

Figure 5.24. The U-core electromagnet and experimental setup for following experiments…… 93

Figure 5.25. The picture of the U-core electromagnet used in this study…….. 93

Figure 5.26. The full wave rectified DC circuit used for electromagnet……... 94

Figure 5.27. Relative enhancement of thermal conductivity in water-based magnetic fluid upon application of an external field……. 96

Figure 5.28. Relative enhancement of thermal conductivity in heptane-based magneticfluid upon application of an external field…….. 96

Figure 5.29. The thermal conductivity enhancement of heptane-based magnetic fluid which changes almost linearly by an external field…….. 97

Figure 5.30. A picture of the thermal conductivity measurement with the effect of external magnetic field……... 99

Figure 5.31. The ferrofluid located in the gap between magnetic poles…… 99

Figure 5.32. Relative enhancement of thermal conductivity in heptane-based magnetic fluid upon application of an external field……. 100

Figure 5.33. Relative reduction of thermal conductivity in hexane-based magnetic fluid upon application of an rectified DC external field…… 101

LIST OF TABLES

Table 1.1.	Thermal conductivity of additives and base fluids used in nanofluids..	5
Table 1.2.	Literature review on viscosity of different types of nanofluids…….	9
Table 3.1.	Typical magnitudes of magnetic induction……	29
Table 3.2.	Estimated critical single-domain sizes, D_c, for spherical particles with no shape anisotropy……...	36
Table 4.1.	Technical data for TEM - FEI Tecnai G2 F30……...	52
Table 4.2.	Zetasizer Nano Series specifications…….	55
Table 4.3.	Technical data for Anton Paar DMA 4100……	63
Table 4.4.	Viscosity units of measurement…….	65
Table 4.5.	Rheometer specifications……...	66
Table 4.6.	Thermal conductivity equipment specifications……	69
Table 5.1.	Viscosity theories and their formulae used in this study……...	84
Table A.1.	Comparison of experimental measurements of density of pure n-heptane with the literature values as a function of temperature at atmosferic pressure……	110
Table A.2.	Comparison of experimental measurements of viscosity of pure n-heptane with the literature values as a function of temperature at	

atmosferic pressure…… 110

Table B.1. Units for magnetic properties…… 111

LIST OF SYMBOLS AND ABBREVIATIONS

a	Thermal diffusivity
A	Current loop area
A_L	Heat transfer area of liquid
A_P	Heat transfer area of magnetic particles
$\boldsymbol{B}$	Magnetic flux density
$\boldsymbol{B_0}$	External magnetic induction
$\boldsymbol{B_{int}}$	Internal magnetic induction
c	Spring constant
c_p	Heat capacity
C	Integral constant
C_v, C_p	Specific heat values for the fluid
d	Diameter of nanoparticle
d'	Space between regular arrays in crystal
E	Electric field
E	Energy
f	Oscillating frequency
F	Force
g	Gravitational acceleration
$\boldsymbol{H}$	Magnetic field strength
H	Convection heat transfer coefficient
Ha	Hamaker Constant
H_c	Coercive field
I	Electric current
J	Current density
k	Thermal conductivity
k_B	Boltzmann's Constant
k_{eff}	Effective thermal conductivity
k_L	Thermal conductivity for polyatomic liquid
k_P	Thermal conductivity of magnetic particles
L	Elevation in the gravitational field

$\boldsymbol{m}$	Magnetic dipole moment
m	Mass
M	Magnetization
M_r	Remanence
M_s	Spontaneous magnetization
$\boldsymbol{n}$	Unit vector
N	Number of particles
P	Scalar pressure
P_m	Pressure of medium
q	Electric charge
$\dot{q}_L$	Heat source for liquid
$\dot{q}_p$	Heat source for magnetic particle
q_x	Heat transfer rate in the x-direction
r_L	Radius of magnetic liquid
r_p	Radius of magnetic particles
s	Surface-to-surface separation distance
T	Absolute temperature
v	Velocity
V	Volume
$\boldsymbol{V}$	Velocity of particle
$<V>$	Average molecular velocity
V_f	Magnetic fluid velocity
$\boldsymbol{V_r}$	Radial velocity
β	Expansion coefficient
γ	Euler's constant
ΔT	Temperature difference between surface and fluid
ε	Volume fraction of magnetic particles
η	Resistivity
λ	Wavelength
μ	Magnetic permeability
μ_0	Magnetic permeability of free space

μ_r	Relative permeability
ν	Viscosity
ρ	Density
ρ_{bf}	Density of base fluid
ρ_{ρ}	Density of metallic oxide particles
Φ_m	Mass concentration (%) of the dispersed fluid
Φ_v	Volume concentration (%) of the dispersed fluid
χ	Magnetic susceptibility
χ_0	Magnetic susceptibility at reference temperature
Ω	Total volume of medium

AFM	Atomic Force Microscope
DM	Diamagnetic
DLS	Dynamic Light Scattering
EA	European co-operaiton for Accreditation
ISO	International Organization for standardization
JCPDS	Joint Committee on Powder Diffraction Standards
MR	Magnetorheological fluid
NP	Nanoparticles
PM	Paramagnetic
SEM	Scanning Electron Microscope
SPM	Superparamagnetic
SQUID	Superconducting Quantum Interference Device
TEM	Transmission Electron Microscope
TÜBİTAK UME	National Metrology Institute of Scientific and Technological Research Council of Turkey
VSM	Vibrating Sample Magnetometer
XRD	X-Ray Diffractometer

1. INTRODUCTION

1.1. SCOPE OF THE THESIS

This thesis is mainly focused on the experimental studies of thermophyical properties such as density, viscosity and thermal conductivity of magnetic and nonmagnetic nanofluids, and the magnetic effect on the thermal conductivity of magnetic nanofluids. In order to get information about the characterization and experiments of nanoparticles, one must be aware of the definition of the nanofluid. A general introduction, brief history the detailed literature review given on nanofluids with regard to this study has been given in Chapter 1. Different magnetism terms of materials will be shortly summarized at the end of this chapter.

Some definitions and applications in addition to the stability requirements of ferrofluids are presented in Chapter 2.

Chapter 3 deals with the theoretical background on mainly heat transfer mechanism and general magnetism. The magnetic fluid preparation techniques are also presented in this chapter. The theoretical solution of conservation laws (Navier-Stokes Equations) along with Maxwell's equations for thermal conductivity as a function of external magnetic field has been derived in this chapter.

Chapter 4 deals with the experimental methodology and techniques on characterization and thermophysical measurements about nanofluids used in this study. The brief theoretical background and devices used were introduced in this chapter.

In Chapter 5, all the experimental results are given. These are mainly the characterization and thermophysical measurements and the magnetic effects on thermal conductivity of Fe_3O_4 magnetite nanoparticles both in water and in heptane and hexane by changing volume fraction and the strength of the external magnetic field. The design and construction studies of homemade magnetic field sources were summarized in this chapter, as well.

Finally, a conclusion and suggested future studies were proposed in Chapter 6.

The main specific questions being addressed in this dissertation are as follows:

i. How will nanoparticle loading or concentration affect the thermal conductivity, density and viscosity of nanofluids?
ii. How will the external magnetic field affect the thermal conductivity of different types of magnetic nanofluids?
iii. Are nanofluids better coolants than their base fluids?
iv. How is the comparison between the theoretical derivation and experimental results of thermal conductivity of magnetic nanofluids under the effect of external magnetic field.

1.2. A BRIEF HISTORY OF NANOFLUIDS

The heat transfer has been a time consuming challenge in science history. Additional researches have always been required in order to improve this process. Therefore, many researchers have conducted many experiments and tried different types of methods to remove heat from, for instance, computer chips, cooling systems, heat exchangers etc., since the beginning of 1950's. The understanding of the nature behind the nanoscale world has become an important issue after the physicist Nobel Prize winner Richard Feynman's famous talk at California Technology Institute (Caltech), "There is Plenty of Room at the bottom", introducing the micro and nanoscale concepts at the annual meeting of The American Physical Society on 29th of December 1959 [2]. He emphasized the manipulation and control of the tiny things in small scale in his speech. On the other hand, the term "Nanotechnology" has become pronounced after Norio Taniguchi, 1974 [3].

The main parameters affecting the thermal transport behaviours of fluids are thermal conductivity and viscosity within heat transfer applications. Thermal management and cooling are important technical difficulties facing numerous applications including microelectronics, communication, transportation, manufacturing, computing, optics and their devices and metrology [4].

The increasing power of these kinds of devices with decreasing size also calls for innovative cooling technology. However, it is important to note that miniaturized devices are not alone in looking for innovative cooling technology. Large devices (such as transportation trucks) and new energy technology (such as fuel cells) also require more efficient cooling systems with greater cooling capacities and decreased sizes. Thus, enhanced cooling technology is the real need of our time. It can be achieved by doing microchannels and miniature cryodevices as new designs for cooling devices. Another way is to enhance the heat transfer capability of the fluid itself. Since solid particles usually exhibit greater thermal conductivity than do liquids, one way to improve the thermal conductivity of liquids is to use suspensions that contain dispersed particles into base fluids. In fact, numerous theoretical and experimental studies of the effective thermal conductivity of dispersions that contain solid particles have been conducted since J.C. Maxwell's theoretical work was published more than 100 years ago [5]. Maxwell was the first scientist who thought that using suspension of solids would be a good alternative method to achieve this idea. He explained a theoretical basis for calculating the effective thermal conductivity of suspension. This work was extended further to examine polystyrene suspensions by Ahuja in 1975. He examined thermal conductivity of polystyrene-water based solutions with the size of about 40-100 μm in a tube and observed thermal conductivity enhancement by as mush as a factor 2 [6, 7]. However, all of the studies on thermal conductivity of suspensions have been confined to millimeter- or micrometer-sized particles. Maxwell's model shows that the effective thermal conductivity of suspensions that contain spherical particles increases with the volume fraction of the solid particles. It is also known that the thermal conductivity of suspensions increases with the ratio of the surface area to volume of the particle [8, 9]. Also, Liu *et al* (1988) worked on thermal enhancement of fluids containing micron particles and an industrial application test was carried out by them, in which the effect of particle volume loading, size and flowrate on the slurry pressure drop and heat transfer behaviour was investigated [10].

Traditional liquid coolants like water and lubricants have poor thermal conductivity. For example, water is roughly three orders of magnitude poorer in heat conduction than copper. Therefore, studies are focused on increasing the thermal conductivity of cooling fluids. Earlier studies focused on micro and macro sized particles, which have major

disadvantages like settling rapidly of particles, clogging the flow channels because of the large size of particles, increasing the pressure drop in the fluid [9].

These problems resulted in the birth of nanofluids which are a new class of solid-liquid composite materials consisting of solid nanoparticles, with sizes typically on the order of 1–100 nm, suspended in a heat transfer liquid [4]. Masuda *et al* presented their studies on thermal conductivity and viscosity of nanofluids containing nanoparticles such as Al_2O_3 and TiO_2 (27 nm) in 1993 [11]. The word "nanofluid" was conceived by Choi in 1995 from Argonne National Laboratory (ANL). The first impression of nanofluid is the observation of greater-than-expexted effective thermal conductivity with small nanoparticle volume fraction [12]. Large surface area and less particle momentum and high mobility features give chance to nanoparticles to be the best candidate for suspension in fluids. In other words, nanoparticles have extremely large surface areas and therefore have a great potential for application in heat transfer. With respect to conductivity enhancement, starting from copper, one can go up to multi-walled carbon nanotubes (MWCNTs), which at room temperature exhibit $2x10^4$ times greater conductivity than engine oil (Kim 2001). Higher heat conduction, stability, microchannel cooling without clogging, reducing the erosion of system components since nanoparticles have very small momentum and reduction of pumping power are the main benefits of nanofluids in this area [8, 9].

Theoretically, all solid nanoparticles with high thermal conductivity can be used as additives of nanofluids. These nanoparticles that have been often used to prepare nanofluids reported in literature are: (a) metallic particles (Cu, Al, Fe, Au and Ag); (b) nonmetal particles (Al_2O_3, CuO, Fe_3O_4, TiO_2, and SiC); (c) carbon nanotube; and (d) nanodroplet. The base fluids commonly used are water, oil, acetone, decene and ethylene glycol. Generally, the thermal conductivity of solids is typically higher than that of liquids, as seen from Table 1.1 [8, 13].

Table 1.1. Thermal conductivity of additives and base fluids used in nanofluids [8, 13]

Material		**Thermal conductivity (W/m.K) at Room-temperature**
Metallic solids	Si	429
	Ag	428
	Cu	401
	Au	318
	Al	237
	Fe	83.5
Nonmetalic solids	Diamond	3300
	Silicon	148
	Alumina (Al_2O_3)	40
	CuO	76.5
	Si	148
	SiC	270
	CNTs	≈3000 (MWCNTs)
		≈6000 (SWCNTs)
	BNNTs	260-600
Base fluids	Water	0.613
	Ethylene glycol (EG)	0.253
	Engine oil (EO)	0.145

1.3. LITERATURE REVIEW

A number of review articles have been published on nanofluids which are generally related to enhancement in the effective thermal conductivity and viscosity [14-27].

Thermal conductivity enhancement of a nanofluid can be affected by different parameters such as particle material, particle size, particle volume concentration, particle shape, base fluid material and temperature. According to the literature given briefly below,

we can say that nanofluids exhibit much higher thermal conductivities than their base fluids even when the concentrations of suspended nanoparticles are very low. It is clear that the thermal conductivity enhancement increases with increasing particle volume concentration. The general trend indicates that the thermal conductivity increases with increased temperature. The effective thermal conductivity of nanofluids increases with the decrease in the particle size (Murshed *et al.* 2008). Some of these parameters were summarized in the following sections.

1.3.1. Magnetic Effect on Thermal Conductivity of Ferrofluids

Li et al (2005) investigated the magnetic field effect on thermal conductivity enhancement with changing both orientation and field strength. According to their explanations, the orientation of an external magnetic field with respect to the temperature gradient affects the energy transport process of the fluid. They observed no substantial change in thermal conductivity for Fe-water magnetic fluid with the concentrations of between 1% and 5% under the effect of external magnetic field up to about 900 G which is perpendicular to the temperature gradient. On the other hand, when the magnetic field direction was kept parallel to the temperature gradient, they observed increased thermal conductivity for the same samples. For the Fe-water magnetic fluid of vol. 5%, thermal conductivity increased from 0.667 W/m K at 35 G to 0.833 W/m K at 240 G. Besides, they showed that the magnetic field effect was stronger at higher particle concentrations than that at lower particle concentrations. The orientation of an external magnetic field with respect to the temperature gradient was found to affect the energy transport process of the fluid where no change was observed when the magnetic field is perpendicular to the temperature gradient [28]. Heat transport ability of the magnetic fluid around a wire can be changed by changing either the orientation or the magnitude of an external magnetic field [29].

J. Philip et al., studied the thermal conductivity of magnetic fluid (Fe_3O_4 nanoparticles of average diameters 6.7 nm) during the formation of chains parallel and perpendicular to the thermal gradient. In the presence of applied external magnetic field, the thermal conductivity of magnetite nanofluids was found to increase with volume percentage of magnetic particles and increasing magnetic field strength. In the presence of

the external magnetic field parallel to the temperature gradient, the highest enhancement of thermal conductivity was 125% in nanofluid of 1.71 vol. % of particles and at field strength of 378 G. When the direction of magnetic field became perpendicular to the direction of heat flow, they observed no change in the thermal conductivity values, irrespective the magnetic field and the volumetric concentrations of the particles. They observed 300% thermal conductivity enhancement for 6.3 vol. % Fe_3O_4 at 82 G. This unusual increase is explained by the formation of chain-like linear aggregates which facilitate the heat transport [30].

Shima et al (2009) also observed effective thermal conductivity enhancement at different magnetic nanoparticles concentrations between 0.0011% and 0.0171% under the effect of magnetic field with the range of about 0-450 G which is parallel to the temperature gradient. Even though they observed no effective thermal conductivity enhancement at the lowest concentration, the enhancement increased with increasing magnetic field for the rest concentrations. The obtained enhancement of effective thermal conductivity is 50% at the 0.0057% concentration, while the viscosity data indicate no enhancement up to this concentration value. Additionally, they observed 300% effective thermal conductivity enhancement at 82 G for 0.078vol% of magnetic nanoparticles. In the second magnetic field region between 82-283 G, effective thermal conductivity (dimensionless) rapidly decreases to approximately 1.6. For upper magnetic field values up to about 700 G, viscosity increases dramatically and effective heat transfer coefficient has a constant value of 1.41 (dimensionless) [31].

Lajvardi et al (2010) studied on the laminar flow in order to see the convective heat transfer coefficient change in the effect of external magnetic field (up to 1200 G). They experimentally showed that an increase in heat transfer coefficient could be observed by increasing the magnitude of magnetic field and nanofluid (Fe_3O_4 nanoparticles of diameters 10 nm in water) concentration, which is attributed to the ferrofluid thermophysical properties, such as thermal conductivity or specific heat capacity under the influence of magnetic field [32]. This behaviour can explained by original theoretical derivations presented in Section 3.4 Equation (3.66).

1.3.2. Concentration Effect on Thermal Conductivity of Different Types of Nanofluids

About 10% enhancement upon addition of 0.5 vol. % copper (3 nm) and 2.3 vol. % copper oxide (15 nm) to ethylene glycol, 20% enhancement upon addition of 3 vol. % alumina (6.5 nm) nanoparticles [33], 7% with 2 vol. % copper oxide (20 nm) in water [34], 8 % with 4 vol. % alumina (30 nm) [33], 12.4 % and 8.5 % enhancements were obtained in ethylene glycol and synthetic oil respectively upon addition of 1 vol. % MWCNT [35], 29.7 % enhancement with 5 vol. % titanium oxide (15 nm) in water, 32.8 % if titanium oxide nano-rods [36]. For MWCNTs – water nanofluids 11 % enhancement in thermal conductivity with 1 vol. %, 5 % enhancement with 1 vol. % copper oxide and 9 % enhancement with 1 vol. % copper oxide nanoparticles in ethylene glycol was obtained. [37] For transformer oil–copper nanofluids, 44 % enhancement in thermal conductivity is obtained with 7.5 vol. % while for water – copper (100 nm) nanofluids the enhancement is 52 % with 5 vol. %. [38] A 30% increase in the thermal conductivity of water upon addition of 4.3 vol % alumina nanoparticles [39] and 21% increase with only 0.011 vol. % Au and Ag in water and in toluene was obtained [40]. Up to 60% improvement of thermal conductivity was achieved for only 5 vol. % of alumina, copper oxide and copper nanoparticles in water and oil base fluids [41]. Nanofluids with Fe particles have better thermal conductivity values than Cu nanofluids in ethylene glycol due to the agglomeration of Fe nanoparticles, which causes nonlinear interactions between solid metallic particles [42]. For very low particle loadings of gold and silver with thoriate and citrate as coatings in water and toluene base fluids 5% - 21% enhancement of the thermal conductivity for silver and water and silver themselves [43]. Thermal conductivity of carbon nanotubes are found to be anomalously greater than the theoretical predictions and were nonlinear with nanotube loadings [44].

According to *Buongiorno et al (2009)*, the results indicate the thermal conductivity enhancement with increasing particle concentration and decreasing base fluid thermal conductivity [45]. *Abareshi et al (2010)* investigated thermal conductivities of Fe_3O_4 nanofluids with different concentrations and temperatures ranging from 10°C to 40 °C. They obtained the highest enhancement of thermal conductivity as 11.4% for vol.3%

concentration sample and the thermal conductivity of the same sample with the 11.5% increment at 40 °C [46].

1.3.3. Different Effects on Viscosity of Different Types of Nanofluids

Namburu et al (2007) showed that the viscosity of SiO_2 nanofluids up to 10% nanoparticle volume concentration in ethylene glycol and water increases as the volumetric nanoparticle concentration increases. They examined 20 nm, 50 nm and 100 nm size particles for the temperature range -35°C and 50°C. For example, the viscosity of 10% SiO_2 particle volume concentration was found to be about 1.8 times the viscosity of the base fluid. As temperature increases, the viscosity of SiO_2 nanofluid decreases exponentially [57].

Nanoparticle type and size, solvent, concentration and temperature effect on viscosity of different kinds of nanofluids were investigated by many researchers. Literature review on this area is summarized as shown in Table 1.2 [47-71].

Table 1.2. Literature review on viscosity of different types of nanofluids

Sample	**Size (nm)**	**Solvent**	**Concent. (%)**	**Temp. (°C)**	**Viscosity or eff. viscosity enhancement**	**Ref.**
Cu	200	EG	<%2	-	-	47
Fe_2O_3	-	Water-%0,2 PVP Dio.water-%0,2 PEO	<%2 >%2	25 °C	-	48
TiO_2	-	-	%0,2-2	20-60 °C	Decreasing with temperature, increasing with particle concentration	49
Al_2O_3	43	Water	%1-5 <%2	Room Temp.	increasing with particle concentration	50
TiO_2	-	EG	%8	20-60 °C	-	51

Table 1.2. Literature review on viscosity of different types of nanofluids (*continue*)

Sample	Size (nm)	Solvent	Concent. (%)	Temp. (°C)	Viscosity or eff. viscosity enhancement	Ref.
γ-Al_2O_3 TiO_2 CuO	25 10 30-50	Water	%0.1-%4	5-45 °C	-	52
Ag	40	Dietilen Glikol	%0.1-4,4	25 °C	-	53
TiO_2	-	Water	0.05-0.12	-	-	54
TiO_2	21	Water	<%3	13-55 °C	-	55
CuO	10-30	EG	-	25°C	-	56
SiO_2 CuO	20,50, 100	EG Water	<%10 %0-6.12	<-10°C >-10°C-50°C	Increasing with decreasing particle dimater	57
Al_2O_3 CuO	36 47 29	Water	<%4;>%4 <%4;>%4	20-75 °C	μ; μ_1 μ; >μ_1 μ_{maks}	58
Al_2O_3	28-13	Water	-	-	-	59
ZnO	10-20	EG	<0.02 >0.03	20-60 °C	Decreasing with increasing temp.	60
TiO_2 Al_2O_3 Al Al	-	Water EG EG M. Oil	%4 %5	20-60 °C	%80	61
UDD Ag SiO_2	-	EG Water Water	%1 %2 %3	-	%50 %30 %20	62
Al_2O_3 TiO_2	- 27	- Water	- %4.3	- -	- %60	63

Table 1.2. Literature review on viscosity of different types of nanofluids (*continue*)

Sample	**Size (nm)**	**Solvent**	**Concent. (%)**	**Temp. (°C)**	**Viscosity or eff. viscosity enhancement**	**Ref.**
Al_2O_3	28	Water EG	%5 %3,5	-	%86 %40	64
γ-Al_2O_3 TiO_2	13 27	Water	%10	Room Temp.	200 (rel.vis.) 3 (rel.vis.)	65
Al_2O_3 CuO	-	Water	%1-%4	21°C-51°C	-	28-66
Al_2O_3	-	PG	%3	Independent	%30	67
Al_2O_3	11-20-40	Water EG	-	23°C	-	68
TiO_2	95 145 210	Water	%0.24-%0.6- %1.18	22°C	-	69
Al_2O_3	-	Water	%0.01-0.3	20-40 °C	Decreasing with temperature, nonlinear increasing with particle concentration	70
Cu	-	Water	-	-	Concentration Independent	71

2. FERROFLUIDS AND FERROHYDRODYNAMICS

2.1. WHAT IS FERROFLUID?

Ferrofluid, also called magnetic fluid, is a magnetic colloidal suspension consisting of a carrier liquid and supermagnetic nanoparticles with a size of about 10 nm in diameter coated with a surfactant layer. A colloid is a suspension of finely divided particles in a continuous medium, including suspensions that settle out slowly. Each nanoparticle inside the liquid has a single magnetic dipole moment responding strongly to external magnetic fields. The magnetic material most often used is magnetite (Fe_3O_4), and carrier liquids like water, kerosene or various oils are available [72].

The colloidal ferrofluid must be manufactured since ferrofluids normally do not occur in nature. Also, it is quite different than the “magnetic fluids” for clutches and brakes introduced in the late 1940’s. The clutch fluids containing micron-and larger-size iron particles can solidify under the influence of an applied magnetic field. In comparison, colloidal ferrofluids as a smart fluid retain liquid flowability like the Newtonian carrier fluids in the most intense applied magnetic fields and the magnetic features of ferrofluid similar to those of the bulk magnetic materials. It can be seen from the schematics of a common ferrofluid composition as given in Figure 2.1. A ferrofluid has three main parts, first of which is magnetic particle in nanosize, second is a carrier liquid and the last one is a surfactant material that coats the particle (coating thickness=δ). A typical ferrofluid contains 10^{23} particles per cubic meter and is opaque to visible light [72,73].

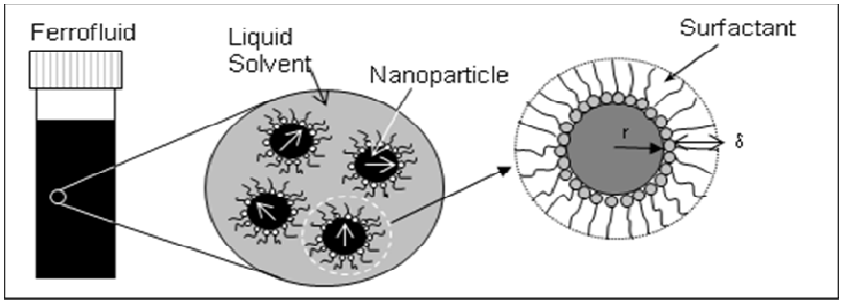

Figure 2.1. A schematic illustration of a common ferrofluid composition

The surfactant has to overcome the Van der Waals and magnetic forces in order to prevent agglomeration and precipitation of the magnetic nanoparticles. Van der Waals forces are forces of attraction and repulsion between atoms, molecules and particles that arise from statistical correlations in the fluctuating polarizations of nearby particles [72].

The orientation of nanoparticles is dictated by thermal fluctuations in the absence of a magnetic field. When no magnetic field is applied, magnetic moments of particles inside the suspension are randomly oriented. In order to use ferrofluids in the technological area, their stability against sedimentation in gravitational and magnetic field and against aggregation of the particles is needed. To achieve this, the thermal energy of a particle must be greater than the gravitational and magnetic energy of the particle. The maximum diameter of the particles, on the order of 10 nanometers can satisfy these stability requirements. In other words, the nanoparticles must have a specific size in order to remain dispersed in the liquid carrier, around 3 to 15nm. In this range, thermal molecular motion keeps the particles from settling out [72].

The prevention of agglomeration of the particles is due to balancing mainly three attractive forces: i. Magnetic, ii. Gravitational, and iii. Van der Waals forces. Aggregation of particles can occur because of Van der Waals forces. Due to steric hindrance, the surfactant layer attached to the particles prevents agglomeration by maintaining a sufficient distance between the particles to have Van der Waals interaction. Brownian motion keeps the particles from settling in an external magnetic field [72].

In Figure 2.2, one can see the external magnetic field effect on the magnetic moment of a nanoparticle. Stability requirements will be explained in the Section 2.3. in detail.

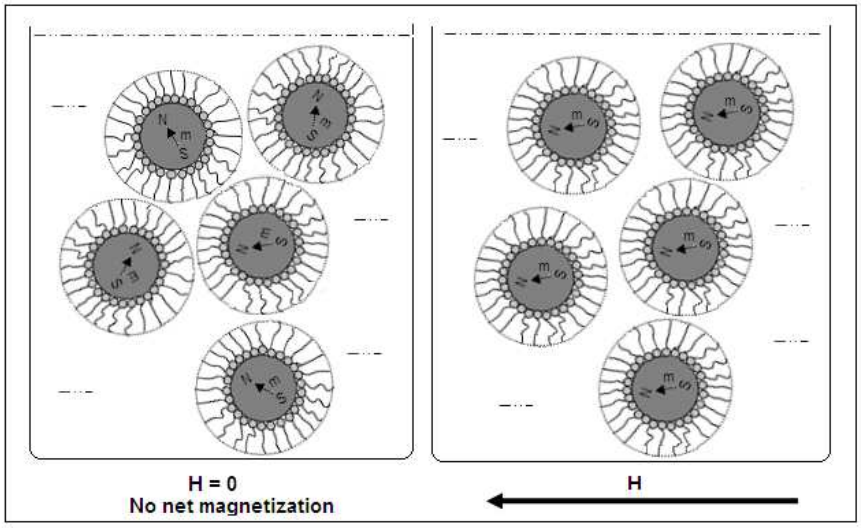

Figure 2.2. Left: The net magnetization of the ferrofluid is zero since there is no external field. Right: Magnetic moment of each particle is aligned in the direction of a magnetic field with strength of H

The term “nanostructured” describes materials with structure on length scales from 1 to 100 nm. The nanostructure morphology of magnetic nanomaterials can be classified according to the relationship between nanostructure and magnetic properties, which emphasizes the physical mechanisms responsible for the behaviour of magnetic nanomaterials In this study, we are interested in first group (type A) as ferrofluids among four general groups describing of magnetic nanostructured materials. Non-interacting particles with nano-scale diameters are grouped as type A, the magnetic properties of which strickly from the reduced size of the components, with no interparticle interactions. In a type A material, the inter-particle spacing is large enough to approximate the particles as non-interacting. Magnetic nanofluids, ferrofluids, in which magnetic particles are surrounded by long surfactant molecules preventing interactions, are a subgroup of type A materials as shown in Figure 2.3. In a bulk material, a significant fraction of the sample volume (up to 50 %) is composed of grain boundaries and interfaces which denotes type D. The magnetic properties of a bulk material are dominated by the interactions between the nanoparticles unlike type A. The other intermediate groups are type B and type C, first of which include ultrafine particles with core-shell morphology. The presence of a shell can help prevent particle-particle interactions, but the interactions between the core and the shell may affect the magnetic properties of the sample. The shells themselves may be

magnetic or are formed via oxidation. In type C nanocomposites consisting of magnetic particles distributed in throughout a matrix, the magnetic interactions between the magnetic particles are mainly determined by the volume fraction of the magnetic particles and the character of the matrix [74].

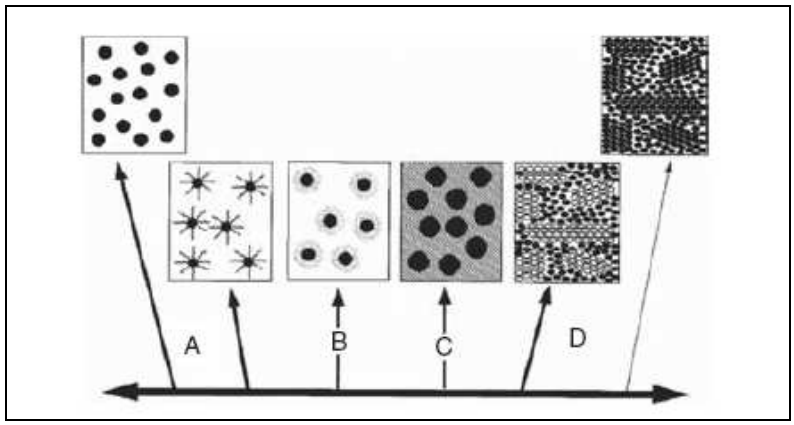

Figure 2.3 Schematic representation of magnetic nanostructure morphologies. In a type A, the inter-particle spacing is large enough to approximate the particles as non-interacting. Ferrofluids, in which magnetic particles are surrounded by a surfactant preventing interactions, are a subgroup of Type A materials. Type B materials are ultra-fine particles with a core–shell morphology. Type C nanocomposites are composed of small magnetic particles embedded in a chemically dissimilar matrix. The matrix may or may not be magnetoactive. Type D materials consist of small crystallites dispersed in a non-crystalline matrix. In this type, the nanoparticles may be in a distinct phase from the matrix, or both the nanoparticles and the matrix are made of the same material as the ideal case [74]

2.2. FERROHYDRODYNAMICS

The term ferrohydrodynamics was introduced in 1964 by Neuringer and Rosensweig in their paper that is the first publication in this area [75]. This attractive area comes from the interest which describes ferrofluids in the presence of magnetic fields in order to convert magnetic energy into motion without the use of moving macroscopic mechanical parts.

The interaction of electromagnetic fields and fluids has been attracting increasing attention in the area of applications such as nuclear fusion, chemical reactor engineering, medicine and high-speed silent printing. The study of various field and fluid interactions may be divided into three main categories [72]:

i. EHD (Electrohydrodynamics): the branch of fluid mechanics concerned with electric force effects;
ii. MHD (Magnetohydrodynamics): the study of the interaction between magnetic fields and fluid conductors of electricity;
iii. FHD (Ferrohydrodynamics): the subject of this thesis dealing with the mechanics of fluid motion influenced by strong forces of magnetic polarization. In other words, the field of ferrohydrodynamics deals with the mechanics of fluid motion under the influence of magnetic polarization body forces [72].

The difference between ferrohydrodynamics and the relatively better-known discipline of magnetohydrodynamics must be explained at this point. In MHD the body force acting on the fluid is the Lorentz force that arises when electric current flows at an angle to the direction on an impressed magnetic field. However, in FHD there need be no electric current flowing in the fluid. The body force in FHD is due to polarization force, which in turn requires material magnetization in the presence of magnetic field gradient or discontinuities [72].

On the other hand, magnetorheological fluids should not be confused with ferrofluids since they have micron sized magnetic particles and they can be solidify under the effect of strong magnetic fields, whereas, ferrofluids retain its fluidity even in the presence of a magnetic field as mentioned before. Ferrofluids indicate a significant magnetic response in relatively weak field since the magnetic susceptibility of ferrofluids is large. This is because of the magnetization of the nanoparticles is much larger than that of the individual atoms. This can be explained by their superparamagnetic feature [72].

2.3. STABILITY REQUIREMENTS OF FERROFLUIDS

On the microscopic scale, there are a number of different forces supplying physics of certain mechanisms that are responsible for the existence of the ferrofluid. Gravity, magnetic field gradients, dipole-dipole interaction forces (sometimes repulsive but more often attractive), van deer Waals attractive forces all act to bring the particles together. Only thermal effects (Brownian motion) steric repulsion force them apart. Dimensional reasoning may be used to arrive at criteria for physicochemical stability. It is helpful to write expressions for various energy terms. These energies per particle are

$$\text{thermal energy} = k_B T\,, \tag{2.1}$$

$$\text{magnetic energy} = \mu_0 MHV\,, \tag{2.2}$$

$$\text{gravitational energy} = \Delta\rho VgL\,, \tag{2.3}$$

$$\text{dipole-dipole interaction energy} = \mu_0 M^2 V/12\ . \tag{2.4}$$

Equation 2.4 is valid when the particles are in contact. Here, k_B = 1.38 x 10^{-23} $J.K^{-1}$ is Boltzmann's constant, T is the absolute temperature in degrees Kelvin, $\mu_0 = 4\pi$ x 10^{-7} $Henry.m^{-1}$ is the magnetic permeability of free space, M is the magnetization of the volume in Ampere/meter, H is the strength of the magnetic field in Ampere/meter, V is the volume $\pi d^3/6$ for a spherical particle, d is the particle diameter in meters, ρ is the density of the fluid, g = 9.8 $m.s^{-2}$ is the acceleration due to gravity, L is the elevation in the gravitational field in meter [72].

2.3.1. Stability in a magnetic-field gradient

In order for the ferrofluid particle to have stability against settling in a magnetic field gradient, one must have the ratio of thermal to magnetic energies be greater than "1" as follows:

$$\frac{thermal\ energy}{magnetic\ energy} = \frac{k_B T}{\mu_0 MHV} \geq 1 \tag{2.5}$$

Rearranging the equation using particle volume gives an expression for the maximum particle size:

$$d \leq \left(\frac{6 k_B T}{\pi \mu_0 MH} \right)^{1/3}. \tag{2.6}$$

Consider the conditions existing in a beaker of magnetic fluid containing magnetite (Fe_3O_4) particles subject to the magnetic gradient field of a typical hand-held permanent magnet. The values are as follows: H = 8 x 10^4 A.m^{-1} (equivalently μ_0 H ≅ 0.1 Tesla), M = 4.46 x 10^5 A.m^{-1} (equivalently μ_0 M = 0.56 Tesla), T = 298 K.

Here, H corresponds to an induction of ~ 1000 Gauss in CGS units, the strength of a typical hand-held magnet, the magnetization of magnetite M given corresponds to 5600 Gauss. The particle size, computed from (2.6), is $d \leq 8.1$ nm. Actual particle sizes of stable colloids range up to about 10 nm [72].

Another physical feature limits the concentration of particles in regions of more intense magnetic field. As seen from Figure 2.4, steric resistance puts an upper limit on the particle number concentration. Although concentration gradients can be established in situations like this, when the field is removed particles of a well-stabilized ferrofluid spontaneously redistribute throughout the fluid volume over a period of time [72].

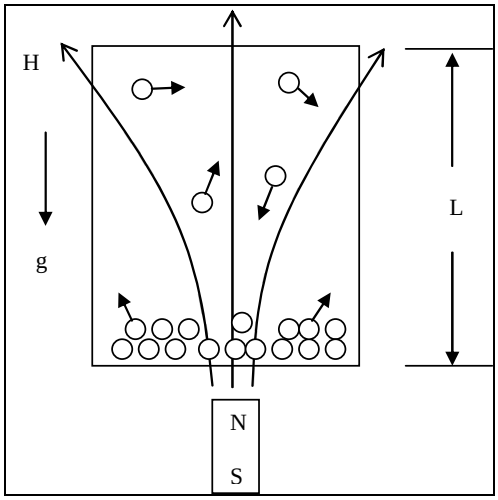

Figure 2.4 The concentration of magnetic particles in a magnetic nanofluid under the effect of a gradient magnetic field is limited by diffusion due to particle thermal motion and steric resistance due to finite particle size [72]

2.3.2. Stability against settling in a gravitational field

A similar analysis can be done for settling due to gravity. Gravity constantly pulls an individual particle downward in the beaker while thermal agitation tends to keep the particle dispersed throughout the fluid medium. The relative influence of gravity to magnetism is described by the ratio

$$\frac{gravitational\ \ energy}{magnetic energy} = \frac{\Delta\rho g L}{\mu_0 M H} \tag{2.7}$$

By choosing L = 0.05 m and $\Delta\rho = \rho_{solid} - \rho_{fluid} \cong 4300$ kg.m^{-3} with g = 9.8 g.s^{-2} the ratio from (2.7) is 0.047. Thus gravity is less of threat to the segregation of these magnetic fluids than is a magnetic field [72].

Another approach is to use thermal energy against gravitational energy for finding out the limitation on the diameter of the particle for stability.

$$d \leq \left(\frac{6k_B T}{\Delta\rho\pi g L} \right)^{1/3} \tag{2.8}$$

Equation 2.8 gives $d \leq 16$ nm. This value is larger than the minimum diameter needed for stability in a magnetic field. As is seen, the maximum stable diameter d is inversely proportional to L [72].

2.3.3. Stability against magnetic agglomeration

Thermal agitation is available to disrupt the agglomerates, with the effectiveness of the disruption governed by the ratio

$$\frac{thermal\ \ energy}{dipole - dipole\ \text{interaction}\ \ energy} = \frac{12k_B T}{\mu_0 M^2 V} \tag{2.9}$$

Accordingly, for particles to escape agglomeration, this ratio must be greater than unity, so the particle size is given by

$$d \leq \left(72k_B T / \pi\mu_0 M^2\right)^{1/3}. \tag{2.10}$$

For the magnetite particles at room temperature, Equation (2.10) requires $d \leq 7.8$ nm. This estimate shows that normal magnetic fluids having particle size in the range up to 10 nm are on the threshold of agglomerating but manage to escape this fate [72].

2.3.4. Necessity to guard against the Van der Waals attractive force

However, there is still one more force to be accounted which is Van der Waals attraction force. This attractive force arises spontaneously between neutral particles. This force represents the quantum mechanical interaction due to fluctuating orbital electrons in one particle inducing oscillating dipoles in the other. The London model predicts an inverse sixth power law between point particles. Hamaker extended the theory to apply to equal spheres and obtained the following expression for the dipole fluctuation energy.

$$Hamaker\ Energy = -\frac{H_a}{6}\left[\frac{2}{\ell^2+4\ell}+\frac{2}{(\ell+2)^2}+ln\frac{\ell^2+4\ell}{(\ell+2)^2}\right] \quad (2.11)$$

where, H_a is the Hamaker constant for Fe, Fe_2O_3 or Fe_3O_4 in hydrocarbon, and equals 10^{-19} N.m. In addition, $\ell = 2s/d$, with s the surface-to-surface separation distance. The Hamaker energy is not significant for distant spheres but for close spheres it changes with ℓ^{-1}, meaning that the energy required to separate touching spheres is infinite. If the colloid is to remain stable, particles must be prevented from coming into contact with one another [72].

2.4. APPLICATION OF FERROFLUIDS

The research field of magnetic fluids is a multi-disciplinary area including Chemistry, Physics, Engineering and Biology. Chemists study their synthesis and preparation of ferrofluids, Physicists study their physical properties and the theory behind them, engineers study the technology and applications of ferrofluids and biologists study their biomedical possibility in medicine and medical area like drug targeting for cancer research [76].

Heat conversion to work without mechanical parts and manipulation of the liquids in the space with no gravitation gave some opportunities for development in this field in the 1960's. In these times, researchers from the NASA Research Centre investigated methods for controlling liquids in space. Magnetic nanofluids (ferrofluids) were found to act a stable colloidal suspensions of single-domain magnetic nanoparticles, such as Fe_3O_4, having number density of the order 10^{23} per m^3 dispersed in appropriate carrier liquid. The nanoparticles typically have sizes of about between 3-15 nm [72]. Ferrofluids show normal liquid behaviour coupled with superparamagnetic properties meaning that one can control the flow of ferrofluids by means of magnetic fields in the order of about 50 mT. Due to its unique characteristics, ferrofluids behave as a smart fluid and has found many applications in a variety of fields such as aerospace, mechanical engineering, bioengineering including magnetic hyperthermia in cancer treatment, loudspeakers,

bearings, drug targeting, high-speed computer disk drives etc. Remote positioning and control of magnetic fluid using external magnetic fields are the other applications [77].

3. THEORETICAL BAKGROUND

3.1. THERMOPHYSICAL PROPERTIES OF FERROFLUIDS

3.1.1. Heat Transfer and Thermal Conductivity

There are three types of energy transfer: i- Conduction, ii-convection, and iii-radiation. All heat transfer processes use one or more of these transfer types. In the molecular interaction mechanism, one can say that conduction is the transfer by molecular motion of heat between one part of a body another part of the same body, or between different bodies contacting each other. A molecule at a higher temperature transfers energy to adjacent molecules at lower energy levels. This type of transfer, of course, occurs in the situation of temperature gradient and in fluids heat is conducted by almost elastic collisions of the molecules. The second mechanism is due to free electrons. The pure metals are the best conductors since they have high concentration of free electrons [78, 79].

The basic equation explaining the heat conduction mechanism in fluids and solids was first stated in 1822 by Fourier as follows:

$$\frac{\vec{q}}{A} = -k\vec{\nabla}T \quad \text{or} \quad \frac{q_x}{A} = -k\frac{dT}{dx} \quad \text{in 1 dimension} \tag{3.1}$$

where q_x is the heat transfer rate in the x-direction, in Watts (W), A is the area normal to the direction of heat flow in m^2, T is the temperature in Kelvin (K), dT/dx is the temperature gradient in the x direction in K/m. Here first ratio is heat flux and proportional to the temperature gradient. "k" expresses the proportionality between heat flux and the temperature gradient and is called the "thermal conductivity of the material" in Watts per meter per Kelvin (W/m.K). Since the heat flow is in the opposite direction to the temperature gradient, there exists a negative sign in this equation [78, 79].

Convection involves a mass movement of fluids between a surface and an adjacent fluid. The density difference resulting from the temperature difference leads to circulation

and energy transfer by mass movement which is called free or natural convection. If a pump or a fan is used for mass motion, the process is called “forced convection”. The equation for convective heat transfer was first expressed by Newton in 1701 which is called “Newton’s law of cooling” as follows [78, 79]:

$$\frac{q}{A} = h\Delta T \tag{3.2}$$

where q is the rate of convective heat transfer in Watts (W), A is the area normal to the direction of heat flow in m^2, T is the temperature in Kelvin (K), ΔT is the temperature difference between surface and fluid. In addition, h is the “convection heat transfer coefficient”, $W/m^2.K$ [78, 79].

3.1.2. Heat Transfer Mechanism in Nanofluids

Particle size, particle shape and volume fraction, and assuming diffusive heat transfer both in fluid and solid phases can give a good prediction for micrometer or larger-size solid and fluid systems for macroscopic solution. But these are not sufficient to explain the unusual heat transfer characteristics of nanofluids. In order to explain the reasons for the unusual or anomalous increase of thermal conductivity in nanofluids, more explanations are needed. Therefore, Keblinski *et al.* and Eastman *et al.* proposed four possible mechanisms in this area: Browninan motion of the nanoparticles, Liquid Layering at Liquid-Particle Interface, anomalous nature of heat transport among the nanoparticles and nanoparticle clustering. However, they only focused on stationary nanofluid [80, 81].

3.1.2.1. Nanoparticle Motion

As the particles move and collide with each other within the nanofluid, there will be an energy exchange between nanoparticles arising from the contact between them. This effect could result in an enhancement of the thermal conductivity. Even though there has not been a collision, the Brownian motion of the particles might enhance thermal conductivity.

The Brownian motion in the nanofluid is an effective heat transfer mechanism than thermal diffusion in the fluid. However, Keblinski *et al.* have shown that a nanoparticle

with a diameter of 10 nm takes 2×10^{-7} s to move a distance equal to its size. By contrast, the time required to move heat the same distance through the liquid is only 4×10^{-10} s which means thermal diffusion is much faster than Brownian diffusion. Therefore, Brownian motion cannot directly cause an enhancement of the thermal conductivity but it could have an important indirect role in producing particle clustering which is described later on. Therefore, the effect of Brownian motion can be ignored since contribution of thermal diffusion is much greater than Brownian diffusion [80, 81].

Wang et al. measured the effective thermal conductivities of fluids with Al_2O_3 and CuO nanoparticles dispersed in water, vacuum pump fluid, engine oil and ethylene glycol and they argued that the thermal conductivity of nanoparticle fluid mixtures is dependent on the microscopic motion (Brownian motion) and particle structure [82].

Xuan and Li also discussed several possible reasons including the interaction and collision among particles [83]. *Chon and Kihm* stated that Brownian motion is key mechanisms of enhanced thermal conductivity since there become millions of interactions between nanoparticles and base fluid molecules. According to them, the smaller nanoparticles increase their surfaces and the number of interactions which leads to the more enhanced thermal conductivity of a nanofluid [84].

3.1.2.2. Liquid Layering at Liquid-Particle Interface

Liquids tend to show a significant amount of structural ordering at solid-liquid interfaces. If this were to enhance the thermal transport in the layer liquid region, then it could result in an increase in the thermal conductivity. To estimate an upper limit for this effect, let us assume that the thermal conductivity of this interfacial liquid is the same as that of the solid. The resultant larger effective volume of the particle-layered-liquid structure would enhance the thermal conductivity, shown in Figure 3.1 [80, 81].

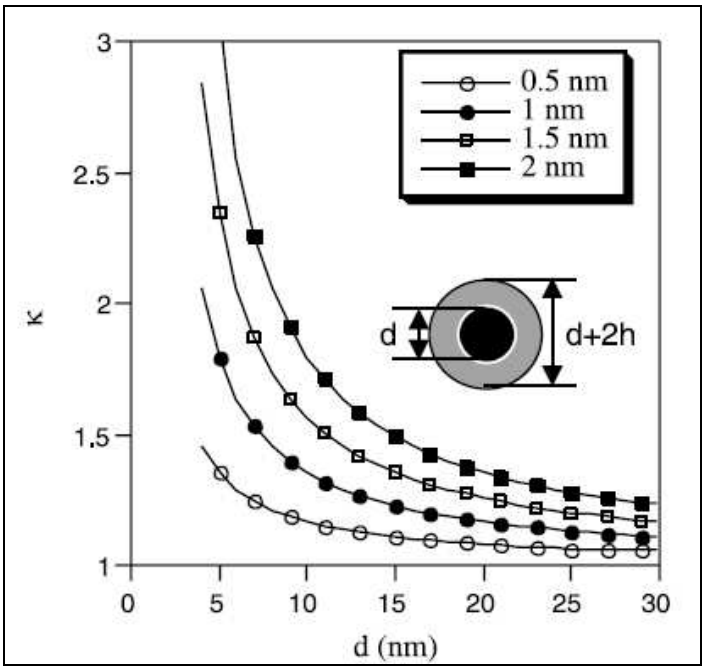

Figure 3.1. Excess thermal-conductivity (*k*) enhancement owing to formation of highly conductive layered-liquid structure at liquid-particle interface for several values of layer thickness *h* as a function of particle diameter, *d*. [80, 81]

3.1.2.3. Nature of Heat Transport in Nanoparticles

Heat carried by phonons in crystalline solids is transported by diffusion according to macroscopic theories. Such phonons propagating in random directions are scattered by each other and by defects and therefore justify the use of the macroscopic description of heat transfer. In the situation of the size of the nanoparticles in a nanofluid smaller than the phonon mean-free path, phonons cannot diffuse across the nanoparticle and their motion will be ballistically without any scattering. It is difficult to envision how ballistic phonon transport could be more effective than a very-fast diffusion phonon transport, particularly to the extent of explaining the order-of magnitude- larger increase of thermal conductivity in Cu nanofluids. In particular, for both ballistic and fast-diffusive phonon transport, the temperature within the solid particle will be essentially constant, providing the same boundary condition for heat flow in a low-thermal-conductivity liquid [80, 81].

3.1.2.4. Nanoparticle Clustering

If particles could cluster into percolating networks, they would create paths of lower thermal resistance and thereby have a major effect on the effective thermal conductivity

(k_{eff}). The effect of clustering is illustrated in Figure 3.2, which shows the excess thermal conductivity enhancement resulting from the increased effective volume of highly conducting clusters as a function of the packing fraction of the cluster φ (ratio of the volume of the solid particles in the cluster to the total effective volume of the cluster). With decreasing packing fraction, the effective volume of the cluster increases, thus enhancing thermal conductivity [80, 81].

Even for a cluster of closely packed spherical particles, ~25% of the volume of the cluster consists of liquid filling the space between particles, which increases the effective volume of a highly conductive region by ~30% with respect to a dispersed nanoparticle system. For more loosely packed clusters the effective volume increase will be even larger [80, 81].

A further dramatic increase of κ can take place if the particles do not need to be in physical contact, but just within a specific distance, allowing rapid heat flow between them. Such “liquid mediated” clusters exhibit a very low packing fraction and thus a very large effective volume and, in principle, are capable of explaining the unusually large experimentally observed enhancements of high thermal resistance reducing the thermal conductivity [80, 81].

Clustering may result in a negative effect on heat transfer enhancement since small particles settle out of the liquid and create large “particle free regions” liquid with high thermal resistance reducing the thermal conductivity [80, 81].

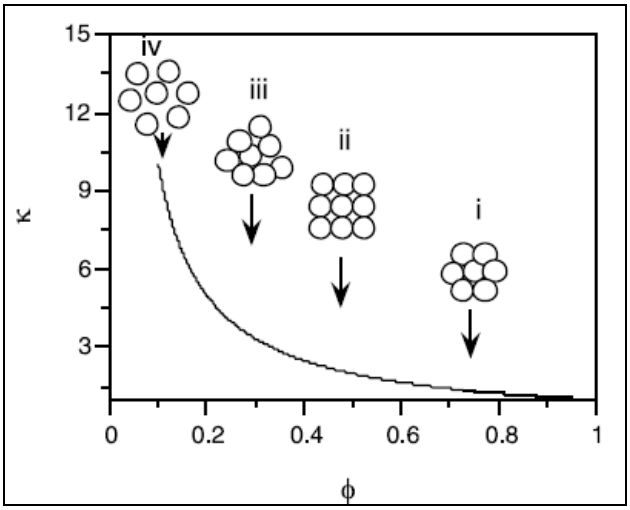

Figure 3.2. Excess thermal conductivity *k* enhancement owing to increased effective volume φ of highly conducting clusters. Schematic diagrams indicate (right to left) (i) closely packed fcc arrangement of particles, (ii) simple cubic arrangement, (iii) loosely packed irregular structure of particles in physical contact, and (iv) clusters of particles separated by liquid layers thin enough to allow for rapid heat flow among particles [80, 81]

3.2. MAGNETISM

To understand the behaviour of magnetite nanofluids, we need to be aware of some of the fundamental concepts of magnetism, which will be recalled briefly here.

3.2.1. Basic Definitions

3.2.1.1. Magnetic Induction, B

The magnetic induction, B, of a magnet may be described by its magnetic field lines. The magnetic field lines are always in closed loops. According to Lorentz's law, an electric charge, *q*, moving at velocity, *v*, is subjected to a force, *F*, given below

$$\vec{\mathrm{F}} = q\left(\vec{\mathrm{E}} + \vec{\mathrm{v}} \times \vec{\mathrm{B}}\right). \tag{3.3}$$

where $\vec{E}$ is the electric field and $\vec{B}$ is the magnetic field.

This equation describes the coupling of electrical and magnetic fields with electric charges. The unit of B is called Tesla, 1 Tesla is the magnetic induction at a point in space which exerts a force of 1 Newton on an electric charge of 1 coulomb moving with a velocity of 1 m/s normal to magnetic induction. Table 3.1 gives typical magnitudes for the magnetic induction. Magnetic induction is sometimes named the magnetic flux density. The name, magnetic flux intensity, is perfectly correct because the magnetic flux penetrating a surface is the product of the magnetic induction, B, and the area of the surface, when **B** is normal to the surface. The unit for the magnetic flux is the "weber", which is a Tesla.m^{-2} [85].

Table 3.1. Typical magnitudes of magnetic induction [85]

Source	**B** (Tesla)
Magnetic induction at the surface of the Earth	5×10^{-5}
Permanent magnets	10^{-2} to 1
Iron-core electromagnets	up to 3
Superconducting magnets	up to 20

3.2.1.2. Magnetic Field Strength, H

In vacuum, the magnetic induction, **B**, is related to the magnetic field strength, **H**, by

$$\mathrm{B} = \mu_0 \mathrm{H} = 4\pi \times 10^{-7}\,\mathrm{H}, \tag{3.4}$$

therefore, the unit of the magnetic strength, H, is Ampere/m [85].

3.2.1.3. Magnetic Moment, m

A planar loop of electric current, *I*, with area *A*, has a magnetic dipole moment, **m**, given by expression

$$\mathrm{m} = IA\,\mathrm{n}, \tag{3.5}$$

where **n** is the unit vector normal to the plane of the loop. The unit of the magnetic dipole moment is then Ampere.m^2 [85].

3.2.1.4. Magnetization, M

The magnetization, **M**, is the magnetic moment per unit volume of a material,

$$\vec{M} = n\vec{m}, \tag{3.6}$$

where *n* is the number of magnetic dipole moments, **m**, per cubic meter. The unit of magnetization is thus A/m, the same as the magnetic field strength, **H** [85].

When a material is placed in an external magnetic induction, $\mathbf{B_0}$, three general types of magnetic behaviour , *diamagnetism*, *paramagnetism* and *feromagnetism*, are possible as will be defined in the next section. Within the diamagnetic material, the internal magnetic induction, $\mathbf{B_{int}}$, is slightly smaller than the external magnetic induction, $\mathbf{B_0}$. Within a paramagnetic material, the internal magnetic induction, $\mathbf{B_{int}}$, is slightly larger than the external magnetic induction, $\mathbf{B_0}$. Within a ferromagnetic material, the internal magnetic induction, $\mathbf{B_{int}}$, is substantially larger than the external magnetic induction, $\mathbf{B_0}$. In other words, the magnetic induction lines are diluted by a diamagnetic material, concentrated by a paramagnetic material and strongly concentrated by a ferromagnetic material [85].

Measurements on diamagnetic and paramagnetic materials, in small applied field, show that the magnetic induction, $\mathbf{B_{int}}$, is directly proportional to the magnetic moment as

$$B_{int} = \mu_r \mu_0 M \quad . \tag{3.7}$$

If a material is placed in an external magnetic induction, $\mathbf{B_0}$, or an external magnetic field of strength, **H**, the internal magnetic induction, $\mathbf{B_{int}}$, in the material is given by

$$\mathbf{B_{int}} = \mathbf{B_0} + \mu_0 \mathbf{M} = \mu_0 (\mathbf{H} + \mathbf{M}) \tag{3.8}$$

where μ_r, is the *relative permeability* of the magnetic material and is a unitless constant at a given pressure and temperature [85]. Equation 3.8 shows that the internal magnetic field increases with external field.

3.2.1.5. Magnetic Susceptibility, χ

The magnetic susceptibility is defined by:

$$\vec{M} = \chi \vec{H} . \tag{3.9}$$

It is unitless and is also known as the volume susceptibility. It measures the ease with which a given material may be magnetized. For a diamagnetic material, χ is negative and of the order of 10^{-6}, indicating that the magnetization in the sample is antiparallel to the magnetic field strength. In this situation, the internal magnetic induction is smaller than the applied external magnetic induction. For a paramagnetic material, χ is positive and of the order of 10^{-4}, indicating that it is easy to magnetize such a material and that the internal magnetic induction is larger than the applied external magnetic induction [85].

3.2.2. Different Types of Magnetic Behaviour

Materials are placed in a class based on their response to an externally applied magnetic field. The orientations of magnetic moments help to identify different forms of magnetism observed in nature. There are five types of magnetism that can be described: Diamagnetism, paramagnetism, ferromagnetism, antiferromagnetism and ferrimagnetism [72].

In diamagnetism the orbital motion of the electrons responds to oppose the applied field. Diamagnetism represents the weakest type of magnetic behaviour and is prominent only in materials with closed electron shells. Inert gases, many metals, most nonmetals and many organic compounds are diamagnetic.

Paramagnetism occurs when each atom carries a magnetic moment which partially aligns in an applied magnetic field and enhances the magnetic flux density. There is no long range order and there is only a small positive magnetic susceptibility. As a result, paramagnetism is the behaviour resulting from the tendency of molecular moments to align with the applied magnetic field but in the absence of long-range order.

Ferromagnetic materials have aligned atomic magnetic moments of equal magnitude. Alignment of the moments in ferromagnetic materials can cause a spontaneous magnetization in the absence of an applied field. Materials that retain this permanent magnetization in the absence of an applied field are known as hard magnets. Ferromagnetism is exhibited by iron, nickel, cobalt and many of their alloys.

Antiferromagnetic materials have atomic magnetic moments of equal magnitude arranged in an antiparallel fashion. The result of the magnetic moments cancelling each other is a net magnetization of zero. In other words, antiferromagnetic materials exhibit no net moment and temperature.

Ferrimagnetism is similar to antiferromagnetism in that there are magnetic moments arranged in an antiparallel fashion. However the moments are not equal in magnitude and thus a net magnetization occurs. Therefore, in ferrimagnetism the net moment is smaller than that in typical ferromagnetic materials. Ferrites of the general formula $MO.Fe_2O_3$ exhibit ferrimagnetism where M stands for Fe, Ni, Mn, Cu, Mg. Magnetite, having composition Fe_3O_4 and possessing cubic crystalline structure, is the best known ferrite [72,73].

A colloidal magnetic fluid consists of a collection of ferro-or ferromagnetic single-domain particles with no-long range order between particles. The resultant behaviour , termed superparamagnetism, is similar to paramagnetism except that the magnetization in low to moderate fields is much larger [72, 73].

The magnetite particles used in this study are superparamagnetic. Magnetic anisotropy, which keeps particles spin magnetized in a certain direction, is proportional to the volume of the particle. As the particle size decreases, anisotropy energy decreases until the thermal energy is sufficient to overcome any preferential orientation of a particle’s magnetic moment, maintaining the magnetite particles as single domain species. A single domain particle that reaches magnetization equilibrium in a short amount of time relative to measurement time is referred to as superparamagnetic [72,73].

Figure 3.3 illustrates in a schematic manner the difference between different types of magnetic behaviour . Ferromagnetism, antiferromagnetism and ferrimagnetsim give spontaneous domain formation, whereas paramagnetism and diamagnetism give no domain. Both types of magnetism have no-long-range order. Alignment is in the direction of the applied field in paramagnetism, while in the opposite direction in diamagnetism.

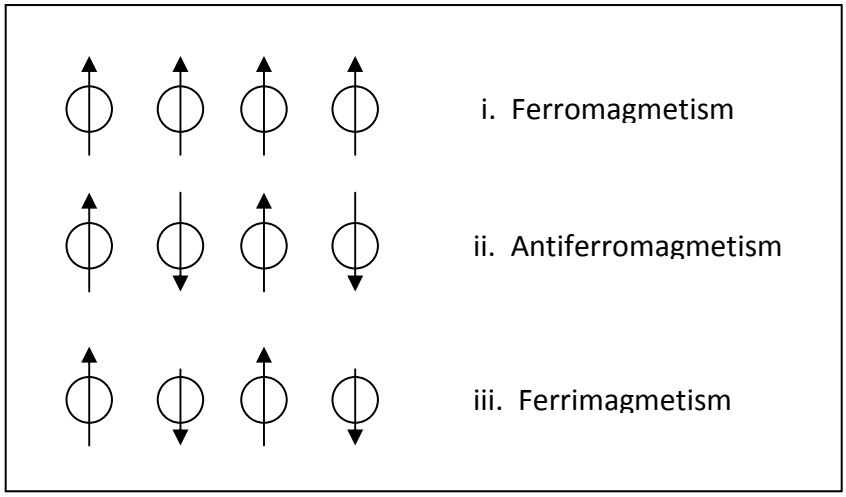

Figure 3.3. Different types of magnetic behaviors. Colloidal ferrofluids exhibit superparamagnetism. i. Ferromagnetic ordering with all spins parallel. ii. Antiferromagnetic ordering with spin moments equal but in opposite direction. iii. Ferrimagnetic ordering with spin moments antiparallel but unequal in magnitute giving a net magnetization in one direction. [72, 86]

3.2.3. Hysteresis Loop and Superparamagnetism

When the external magnetic field is sufficiently large, all the spins within a magnetic material align with the applied magnetic field. In this situation, the magnetization of the material reaches its maximum value which is called the saturation magnetization, M_s. As the magnitude of the field decreases, the spins in the material cease to be aligned with the magnetic field, so the total magnetization of the material decreases. When the external magnetic field decreases to zero for a ferromagnetic material, the material still has a residual magnetic moment, and the value of the magnetization at zero field is called the remanent magnetization, M_r. Remanence represents the magnetization obtained after applying a large field to the specimen and then removing it. The remanence ratio is defined

as the ratio of the remanent magnetization to the saturation magnetization, M_r/M_s, which varies from 0 to 1. In order to bring the material back to zero magnetization, an external magnetic field in the negative direction has to be applied, and the magnitude of the field is called the coercive field, H_c. In other words coercive field is needed to bring the magnetization from remanent value to zero. The coercive field measures the order of magnitude of the fields that must be applied to a material in order to reverse its magnetization. Figure 3.4 schematically illustrates a hysteresis curve of a ferrfomagnetic material [74].

In most cases, the hysteresis loop of a magnetic material can be experimentally measured using a vibrating sample magnetometer (VSM) or superconducting quantum interference device SQUID magnetometer [74].

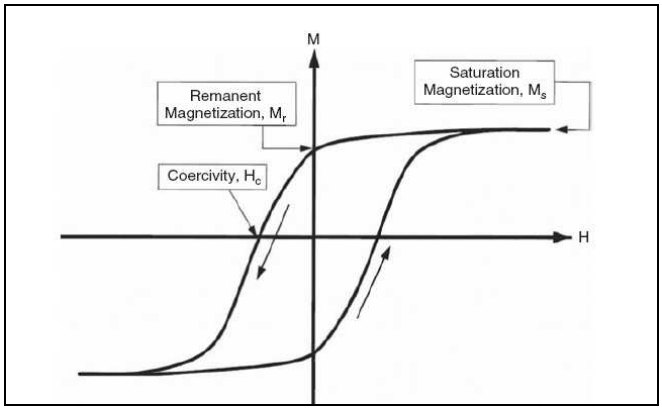

Figure 3.4. A typical magnetization hysteresis loop (M–H) of a ferromagnetic material. Saturation magnetization, M_s, remanent magnetization, M_r, and coercivity, H_c , are shown here as important parameters [74]

The susceptibility in ordered materials depends on applied magnetic field H and temperature. This magnetic field gives rise to the characteristic sigmoidal shape of the M–H curve, with M approaching a saturation value at high magnetic field. In ferromagnetic and ferrimagnetic materials, hysteresis loops can be observed, as shown in Figure 3.5. The shape of a hysteresis curve is partly determined by the particle size. In large particles in the order of micron size or more has a multi-domain structure. Since it is easy to move the domain walls, the hysteresis loop of such particles is narrow. In a smaller particle, there is

a single-domain structure leading to a broad hysteresis loop. When particle size becomes even smaller, in the order of tens of nanometers or less, one can see superparamagnetism. The magnetic moment of a superparamagnetic particle as a whole is free to fluctuate in response to thermal energy, while the individual atomic moments maintain their ordered state relative to each other. As shown in Figure 3.5, the M–H curve of a superparamagnetic particle is anhysteretic, but still sigmoidal [87].

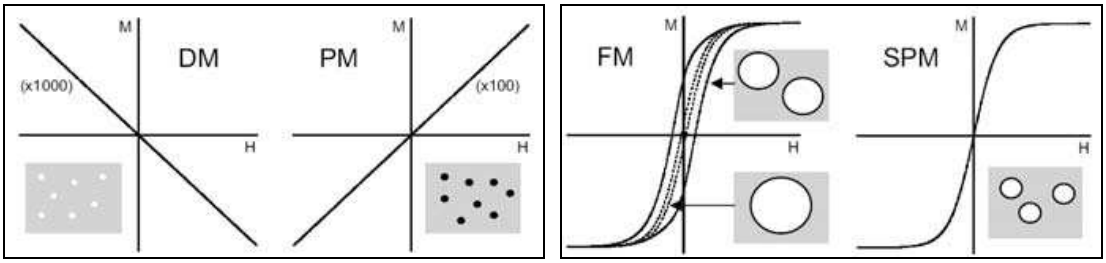

Figure 3.5. The magnetic responses associated with different classes of magnetic material among others are illustrated by their corresponding M–H curves. The particles can be diamagnetic (DM), paramagnetic (PM), ferromagnetic (FM) or superparamagnetic (SPM), depending on their size of the particle. Ferromagnetic materials can be multi-domain (- - - - in FM diagram) or single-domain (in FM diagram) [87]

A domain is a group of spins whose magnetic moments are in the same direction, and in the magnetization procedure, they act cooperatively. In a bulk material, domains are separated by domain walls, which have a characteristic width and energy associated with their formation and existence. The motion of domain walls is a primary means of reversing magnetization and a main source of energy dissipation. Figure 3.6 schematically illustrates the relationship between the coercivity and particle sizes. In large particles, energetic considerations favor the formation of domain walls, forming a multi-domain structure. The magnetization of such a particle is realized through the nucleation and movement of these walls. As the particle size decreases toward a critical particle diameter, D_c, the formation of domain walls becomes energetically unfavorable. Therefore, there is no domain wall in such a particle which is called a single-domain particle. For a single-domain particle, changes in the magnetization can no longer occur through domain wall movement and the magnetization procedure is realized through the coherent rotation of spins, causing larger coercivities. As the particle size is much smaller than Dc, the spins are affected by thermal

fluctuations, and such a single-domain particle becomes superparamagnetic particle. Frenkel and Dorfman (1930) theoretically predicted the existence of single-domain particles. The D_c values for some common magnetic materials of spherical shape are given in Table 3.2 [74].

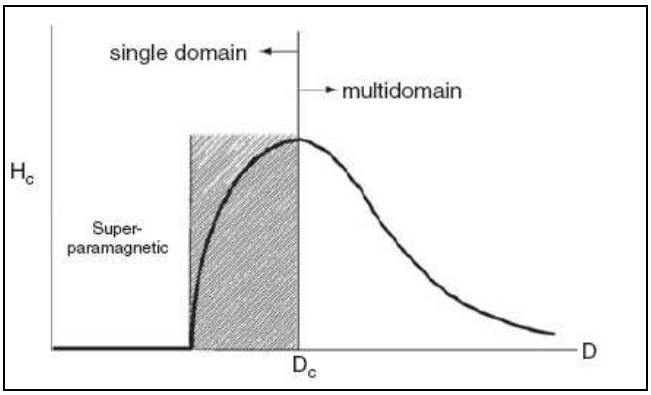

Figure 3.6. The illustration of relationship between the coercivity in ultrafine particle systems and particle sizes [74]

Table 3.2. Estimated critical single-domain sizes, D_c, for spherical particles with no shape anisotropy [74]

Material	**D_c (nm)**
Co	70
Fe	14
Ni	55
Fe_3O_4	128
γ-Fe_3O_4	166

Neel (1949) theoretically demonstrated that H_c approaches zero when particles become very small since the thermal fluctuations of very small particles prevent the existence of a stable magnetization. This is a typical phenomenon of superparamagnetism. [74].

The physics behind the superparamagnetism is based on the relaxation time τ of the net magnetization of a magnetic particle (Brown 1963):

$$\tau = \tau_0 \exp\left(\frac{\Delta E}{k_b T}\right) \tag{3.10}$$

where ΔE is the energy barrier to moment reversal, and $k_B T$ is the thermal energy. For non-interacting particles the pre-exponential factor τ_0 is in the order of 10^{-10}–10^{-12} s and only weakly dependent on temperature. The energy barrier has several origins, including both intrinsic and extrinsic effects such as the magnetocrystalline and shape anisotropies. In the simplest cases, it is given by $\Delta E = KV$, where K is the anisotropy energy density and V is the particle volume. The direct proportionality between ΔE and V is important for superparamagnetism-the thermally activated flipping of the net moment direction- for small particles since ΔE is comparable to $k_B T$ at room temperature in this situation [87].

The observation of superparamagnetism is dependent not only on temperature, but also on the measurement time τ_m of the experimental technique used [88]. As shown in Figure 2.8, if τ much shorter than τ_m, the flipping is fast relative to the experimental time window and the particles appear to be paramagnetic (PM); while if τ much longer than τ_m, the flipping is slow, and such a state is called a blocked state. In a block state, the quasi-static properties of the material can be observed. The blocking temperature T_B is obtained by assuming $\tau = \tau_m$. In typical experiments, the measurement time τ_m can range from the slow timescale of 10^2 s for DC magnetization, and medium timescale of 10^{-1}–10^{-5} s for AC susceptibility, through to the fast timescale of 10^{-7}–10^{-9} s for ^{57}Fe Mössbauer spectroscopy [87].

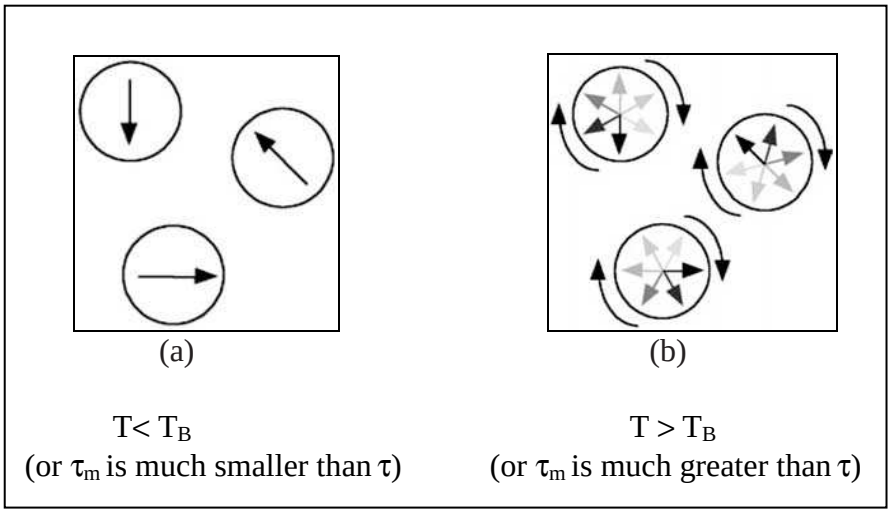

Figure 3.7. Observation of superparamagnetism. The circles depict three magnetic nanoparticles, and the arrows represent the net magnetization direction in those particles. In case (a), at temperatures well below the measurement-technique-dependent blocking temperature T_B of the particles, or for relaxation times τ (the time between moment reversals) much longer than the characteristic measurement time τ_m, the net moments are quasi-static. In case (b), at temperatures well above T_B, or for τ much shorter than τ_m, the moment reversals are so rapid that in zero external field the time-averaged net moment on the particles is zero [87]

3.3. PREPARATION OF NANOFLUIDS

The ferrofluids used in this study were synthesized at the Department of Chemical Engineering of Yeditepe University based on the procedure reported by Wooding et al. [1], in which co-precipitation of Fe(II) and Fe(III) salts by NH_4OH at 60 ^oC were carried out in the presence of a fatty acid surfactant.

Preparation of ferrofluids will be given in summary in this section since the details are out of the scope of this thesis.

Two methods have been conducted to produce nanofluids. First is a single-step method and the other is a two-step method. The single-step method is a combining method using nanoparticles directly prepared by physical vapour deposition (PVD) technique or

liquid chemical method and synthesized nanofluids together. The agglomeration of nanoparticles is minimized in this method, so ferrofluid stability is higher [88].

The second method involves the dispersing nanoparticles into base fluids. First of all, nanoparticles are produced as a dry powder by some different methods given below, then these particles are dispersed into a fluid as second step. The probability of occurrence agglomeration is higher than that of first method, single-step method, which causes clogging of microchannels and decreasing the thermal conductivity of the fluid. Adding the surfactants to the fluids has been used in order to escape agglomeration and enrich the dispersion behaviour of the fluid. The main problem that has to be overcome is to get stabilized suspensions in this method [88].

Preparation of ferrofluids can be divided into two steps at two-step method: (1) The preparation of nano-sized magnetic particles and (2) the dispersion of the particles in various liquids. Most commonly used ferrites are magnetite (Fe_3O_4) and maghemite (γ-Fe_2O_3). There have been different types of ways to produce nano-sized ferrite particles as follows [73]:

Wet-grinding: The method takes a very long time (1000 hours) involved wet-grinding ferrites in a ball-mill in the presence of a suitable surfactant until the ferrite is in a colloidal state. This is the main disadvantage of the method; therefore, a simple and fast method involving the co-precipitation of metal salts in aqueous solution took place in the survey.

Co-precipitation methods: This conventional method usually conducted between 0 °C and 100 °C uses aqueous Fe^{2+} and Fe^{3+} salt solutions which are in use to obtain iron oxides (either Fe_3O_4 or γ-Fe_2O_3).

Microemulsion techniques: This method involves the preparation of two microemulsions, one containing an aqueous solution of a metal salt or a mixture of metal salts and the other an aqueous solution of an alkali and mixture of metal salts in the appropriate ratio.

3.4. DERIVATION OF MAGNETIC EFFECT ON THERMAL CONDUCTIVITY OF MAGNETIC NANOFLUIDS

The Navier-Stokes (NS) and Maxwell's equations (along with Bousinessq approximation) are used in order to describe the fluid flow exposed to external magnetic and gravitational fields. The solution domain used for derivation is shown in Figure 3.8.

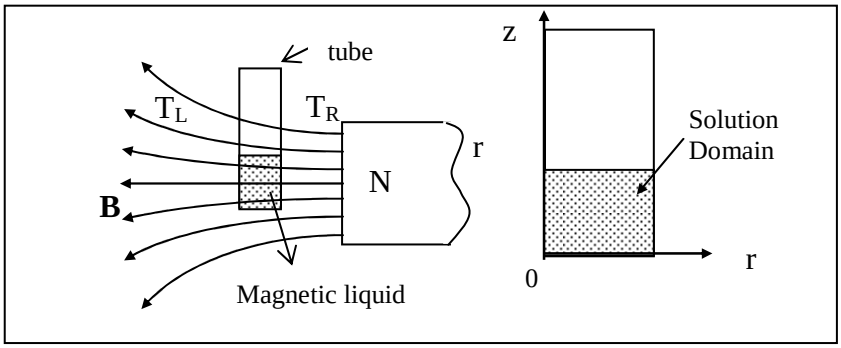

Figure 3.8. The experimental setup and solution domain

The following assumptions on static pressure and velocity are considered:

$$\frac{\partial P}{\partial r} = 0 \quad ; \frac{\partial P}{\partial z} \neq 0 \tag{3.11}$$

Since pressure gradients are in the vertical direction on liquids in cylindrical containers. It was also assumed that the variables show azimuthal symmetry, i.e. $\frac{\partial}{\partial \theta}(\ ) = 0$ so that one has

$$V_\theta = 0\,,\ V_r, V_z = f(r,z)\,. \tag{3.12}$$

The Navier-Stokes (NS) equations describing mass, momentum and energy for an incompressible fluid are given by:

$$\nabla \cdot V = 0 \tag{3.13}$$

$$\frac{\partial \mathbf{V}}{\partial t} + \mathbf{V}\cdot\nabla\mathbf{V} = -\frac{1}{\rho_0}\nabla P + \nu\nabla^2\mathbf{V} + \beta\mathbf{g}(T - T_0) + \frac{1}{\rho_0}(\mathbf{J}\times\mathbf{B} + \mathbf{M}\cdot\nabla\mathbf{B}) \qquad (3.14)$$

$$\rho_0 C_v\left(\frac{\partial T}{\partial t} + V\cdot\nabla T\right) = \dot{q}_p + \dot{q}_l + \eta\,\mathbf{J}\cdot\mathbf{J} + k\nabla^2 T \qquad (3.15)$$

where **V** is velocity, ρ_0 is the density, P is the scalar pressure, ν is viscosity, β is expansion coefficient (due to Boussinesq approximation), **g** is gravitational acceleration, T is temperature, **J**, **B**, and **M** are current density, magnetic flux density, and magnetization respectively. In addition, $C_v \cong C_p$ are specific heat values for the fluid, $\dot{q}_p$ and $\dot{q}_L$ are heat sources for magnetic particle and liquid respectively, η is resistivity, and k is the thermal conductivity. Note that as the magnetic field is applied, the magnetic particles align along the radial direction so that the temperature gradients in the fluid and solid particles are in local equilibrium and thus the same (Figure 3.9). Note also that the right face of the tube is heated by the heat produced by the electromagnet.

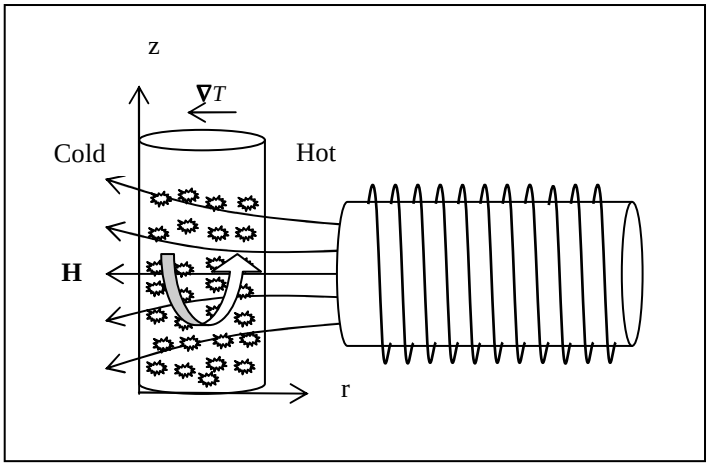

Figure 3.9. Temperature gradient in a ferrofluid by applying a magnetic field

Assume that heat transfer areas and the radii of magnetic particles and liquid are constant and given by: A_f, A_L and r_p, r_L respectively. If the volume fraction (concentration) of magnetic particles is ε, then that of liquid is $1-\varepsilon$. Using these one can show that the combined effect of magnetic particles and liquid to the heat transfer turns into:

$$q = q_p + q_L = -(k_p A_p + k_L A_L)\frac{dT}{dr} = -k_{eff} A_L \frac{dT}{dr} \tag{3.16}$$

$$k_{eff} = k_L\left(1 + \frac{k_p \varepsilon r_L^2}{k_L(1-\varepsilon) r_p^2}\right) \tag{3.17}$$

k_{eff} is the effective thermal conductivity.

This expression shows that the thermal conductivity gets higher by increasing the volume fraction of magnetic particles which is exactly what has been observed in previous experiments in the absence of a magnetic field. The effective thermal conductivity can be complete when magnetic field and temperature gradient effects are included into above expression. This can only be done by combining the above equation set by Maxwell`s equations.

Maxwell`s equations are given by:

$$\mathbf{J} = \nabla \times \mathbf{H} \;;\; \nabla \cdot \mathbf{B} = 0 \tag{3.18}$$

$$\frac{\partial \mathbf{B}}{\partial t} - \nabla \times (\mathbf{V} \times \mathbf{B}) = \frac{\eta}{\mu_0} \nabla^2 \mathbf{B} \tag{3.19}$$

where **H** is magnetic field intensity. **B**, **H**, and **M** are related through the following equations:

$$\mu = \mu_0(1+\chi),\ \mathbf{B} = \mu\mathbf{H} = \mu_0(\mathbf{H}+\mathbf{M}),\ \mathbf{M} = \chi\mathbf{H} \tag{3.20}$$

where χ is magnetic susceptibility, μ and μ_0 are magnetic permeability of the fluid and free space respectively.

In order to perform simple calculations, some assumptions were made. Firstly, as the tube filled with magnetic fluid is cylindrical, the cylindrical geometry was used. Because the magnetic field produced by magnet is nearly constant in *r* direction, only radial velocity, V_r was considered as relevant component of velocity, other components of velocity were taken as negligible. The temperature closer to magnet, T_R is slightly greater than T_L, so the temperature gradient was observed to be in radial direction experimentally and assumed to be linear for these calculations (Figure 3.9).

Assuming that T changes only in *r* direction, the energy equation can be written as

$$\rho_0 C_v \left(\frac{\partial T}{\partial t} + V_r \frac{\partial T}{\partial r} + Vz \frac{\partial T}{\partial z}\right) = \dot{q}_f + \dot{q}_l + \eta J \cdot J + k\nabla^2 T, \tag{3.21}$$

Note that Joule heating term is zero since H=constant, i.e.,

$$\mathbf{J} = \nabla \times \mathbf{H} = 0 \text{ , Therefore } \eta \vec{J} \cdot \vec{J} = 0. \tag{3.22}$$

$$\frac{\partial T}{\partial t} \to 0 \ ; \ \frac{\partial T}{\partial z} \to 0 \text{ ,} \tag{3.23}$$

$$\left(\rho_0 C_v V_r \frac{1}{k}\right) \frac{\partial T}{\partial r} = \frac{\dot{q}_{env.}}{k} + \left(\frac{\partial^2 T}{\partial r^2} + \frac{1}{r}\frac{\partial T}{\partial r}\right) \tag{3.24}$$

$$\left(\rho_0 C_v V_r \frac{1}{k} - \frac{1}{r}\right) \frac{\partial T}{\partial r} = \frac{\dot{q}_{env.}}{k} \tag{3.25}$$

where $\partial^2 T / \partial r^2$ is negligible since $\partial T / \partial r$ is linear and small and subscript env. denotes environmental.

The terms with 1/*r* were neglected since Corriolis force is neglected. With all the assumptions described so far, the steady state energy equation then becomes

$$\rho_0 C_p V_r \frac{dT}{dr} = \dot{q} \tag{3.26}$$

where V_r is the average fluid velocity in the radial direction. The magnetic and gravitational forces in the radial direction are negligible in the momentum equation since external **B** is much greater than the induced field and is constant. In that case, momentum equation in radial direction turns into hydrodynamic force balance in radial direction given by equation

$$\beta g(T - T_0) = 0 \quad \text{(in z-direction)} \tag{3.27}$$

$$\frac{1}{\rho_0}(J \times B) = 0 \quad (\perp \text{ to r-z plane } \theta \text{ direction}) \tag{3.28}$$

$$M = \chi H \;; \quad B = \mu H = \mu_0 (H + M) \tag{3.29}$$

$$\begin{gathered} \nabla B = (\nabla \mu) H \quad ; \quad H = cons.; \\ B = \mu_0 (1 + \chi(T)) H \end{gathered} \tag{3.30}$$

$g = 0$ in radial direction and in cylindrical coordinates (with $\partial / \partial \theta \to 0$):

$$\frac{D}{Dt} \equiv \frac{\partial}{\partial t} + V_r \frac{\partial}{\partial r} + V_z \frac{\partial}{\partial z} \tag{3.31}$$

$$\nabla^2 \equiv \frac{\partial}{\partial r^2} + \frac{1}{r}\frac{\partial}{\partial r} + \frac{\partial^2}{\partial z^2} \tag{3.32}$$

$$\frac{\partial V}{\partial t} + V_r \frac{\partial V_r}{\partial r} + V_z \frac{\partial V_r}{\partial z} = -\frac{1}{\rho_0}\frac{\partial P_m}{\partial r} + \nu\left(\frac{\partial^2 V_r}{\partial r^2} + \frac{1}{r}\frac{\partial V_r}{\partial r} + \frac{\partial^2 V_r}{\partial z^2}\right) \tag{3.33}$$

$$V_r \frac{\partial V_r}{\partial r} + V_z \frac{\partial V_r}{\partial z} = -\frac{1}{\rho_0}\frac{\partial P_m}{\partial r} + \nu \frac{1}{r}\frac{\partial}{\partial r}\left(r \frac{\partial V_r}{\partial r}\right) + \frac{\partial^2 V_r}{\partial z^2} \tag{3.34}$$

$$\frac{\partial V}{\partial t} \to 0 \text{ and } \frac{\partial V_r}{\partial z} \to 0 \quad \frac{\partial^2 V_r}{\partial z^2} \to 0 \tag{3.35}$$

$$\frac{1}{2}\frac{\partial V^{2}{}_{r}}{\partial r}-\frac{\nu}{r}\frac{\partial}{\partial r}\left(r\frac{\partial V_{r}}{\partial r}\right)=-\frac{1}{\rho_{0}}\frac{\partial P_{m}}{\partial r} \tag{3.36}$$

and Equation 3.14 get its final form

$$\left(V_{r}-\frac{\nu}{r}\right)\frac{\partial V_{r}}{\partial r}-\nu\frac{\partial^{2}V_{r}}{\partial r^{2}}=-\frac{1}{\rho_{0}}\frac{\partial P_{m}}{\partial r}=-\frac{F_{m}}{\rho} \tag{3.37}$$

$$\frac{\partial \mathrm{P_m}}{\partial \mathrm{r}}=\nu\frac{1}{\mathrm{r}}\frac{\partial}{\partial \mathrm{r}}(\mathrm{r}\frac{\partial \mathrm{V_r}}{\partial \mathrm{r}}) \tag{3.38}$$

$$V_{r}=f(r)\frac{dP}{dr} \tag{3.39}$$

$$\frac{\nu}{r}\frac{\partial}{\partial r}\left(r\frac{\partial V_{r}}{\partial r}\right)=\frac{1}{\rho_{0}}\frac{\partial P_{m}}{\partial r} \tag{3.40}$$

$$\frac{\rho_{0}\nu}{\partial P_{m}/\partial r}\frac{\partial}{\partial r}\left(r\frac{\partial V_{r}}{\partial r}\right)=r \quad ; \quad \rho_{0}\nu\frac{\partial}{\partial r}\left(r\frac{\partial V_{r}}{\partial r}\right)=r\frac{\partial P_{m}}{\partial r}\,. \tag{3.41}$$

If

$$C=\frac{\rho_{0}\nu}{\partial P_{m}/\partial r} \tag{3.42}$$

then

$$r\frac{\partial V_{r}}{\partial r}=f(r); \qquad C\frac{\partial f}{\partial r}=r \tag{3.43}$$

$$f=\frac{1}{C}\frac{r^{2}}{2}+c' \quad ; \quad \frac{dV_{r}}{dr}=\frac{1}{C}\frac{r}{2} \tag{3.44}$$

This results in

$$V_r = \frac{1}{C}\frac{R^2 - r^2}{4} \tag{3.45}$$

$$C = \frac{R^2 - r^2}{4V_r} \tag{3.46}$$

$$\frac{1}{\rho_0 \nu}\frac{\partial P_m}{\partial r} = \frac{4V_r}{R^2 - r^2} \tag{3.47}$$

$$\frac{\partial P_m}{\partial r} = \frac{4V_r}{R^2 - r^2}\rho_0 \nu \quad . \tag{3.48}$$

By assuming constant pressure gradient and assuming also V_r vanishes at the tube boundaries (at $r = R$), the solution to Equation (3.38) becomes:

$$\mathrm{V_r} = \frac{\partial \mathrm{P}/\partial \mathrm{r}}{4\nu}(\mathrm{r}^2 - \mathrm{R}^2) \tag{3.49}$$

The magnetic susceptibility has temperature [89] dependence given by:

$$\chi = \frac{\chi_0}{1 + \alpha(\mathrm{T} - \mathrm{T_0})} \tag{3.50}$$

where χ_0 is the magnetic susceptibility at the reference temperature, $\mathrm{T_0}$. This shows that although the magnetic field intensity obtained by the magnet is constant in time and space, magnetic flux density is space dependent through the following equation:

$$\mathrm{B} = \mu\mathrm{H} = \mu_0[1 + \chi(\mathrm{T})]\mathrm{H} \tag{3.51}$$

According to the energy principle, the total energy in the medium is given by [91]

$$E = \int_{\Omega} (\frac{1}{2}\mathbf{H}\cdot\mathbf{B} - \mathbf{F}\cdot\mathbf{r})d\Omega \tag{3.52}$$

where Ω is the total volume of medium and $\mathbf{F} = dP/d\,\mathbf{r}$ is the constant force due to pressure gradient given by Equation 3.38. For stability, the differential change in this total energy should be minimized, i.e.:

$$\delta E = \int_{\Omega} (\frac{1}{2}\mathbf{H}\cdot\delta\mathbf{B} - \mathbf{F}\cdot\delta\mathbf{r})d\Omega = 0 \tag{3.53}$$

By taking

$$\mathbf{H}\cdot\delta\mathbf{B} = \mathbf{H}\cdot\mathbf{H}\delta\mu = \mathbf{H}\cdot\mathbf{H}\nabla\mu\cdot\delta\mathbf{r} \tag{3.54}$$

$$\delta\mu = -\delta\mathbf{r}\cdot\nabla\mu \tag{3.55}$$

[90] and realizing that

$$\mathbf{H}\nabla\mu = \mu_0\mathbf{H}\frac{d\chi}{dT}\nabla T = \mu_0\frac{d\mathbf{M}}{dT}\nabla T\,. \tag{3.56}$$

One can obtain the differential change in the energy

$$\delta E = \int_{\Omega} (-\frac{\mu_0}{2}\mathbf{H}\cdot\frac{d\mathbf{M}}{dT}\frac{dT}{d\mathbf{r}} - \mathbf{F})\cdot\delta\mathbf{r}d\Omega = 0 \tag{3.57}$$

which is true only if the integrand vanishes, i.e.,

$$F = \frac{dP}{dr} = -\frac{\mu_0}{2}H\frac{dM}{dT}\frac{dT}{dr} = -\frac{1}{2}H^2\frac{d\mu}{dT}\frac{dT}{dr}\,. \tag{3.58}$$

Thus V_r given by Equation 3.49 can be written as

$$V_r = \frac{1}{8\nu}(r^2 - R^2)H^2 \frac{d\mu}{dT}\left(\frac{dT}{dr}\right). \tag{3.59}$$

Using Equation 3.26 this can be written as:

$$V_r = \frac{\mu_0}{8\nu}(r^2 - R^2)H^2 \frac{d\mu}{dT}\left(\frac{\dot{q}}{\rho_0 C_p V_r}\right) \tag{3.60}$$

Using Equation 3.51 this equation then leads to

$$V_r^2 \approx V_f^2 = \frac{\mu_0 \alpha \chi_0 \dot{q}(R^2 - r^2)}{8\nu\rho_0 C_p (1 + \alpha(T - T_0))^2} H^2 \tag{3.61}$$

where V_f is the magnetic fluid velocity given as

$$V_f = \frac{(V_p n_p + V_L n_L)}{n_p + n_L} \tag{3.62}$$

where n_L and n_p are the number of liquids and particles, respectively. If $n_L >> n_p$ then

$$V_f = \frac{V_p n_p + V_L n_L}{n_L} \approx V_L + V_p \frac{n_p}{n_L} \approx V_L \tag{3.63}$$

According to [91], the thermal conductivity for polyatomic liquids is given by:

$$k_L = (N/V)^{2/3} m C_p < V_L > \tag{3.64}$$

where N is the number of particles in volume V, m is the mass, and <V> is the average molecular velocity which is nothing but the fluid velocity in this analysis: $V_f \approx V_L$ then,

$$k_L \approx (N/V)^{2/3} mC_p < V_f > . \tag{3.65}$$

The previously defined conductivity defined by Equation 3.17 can be written as

$$k_{eff} = k_L + k_p \left(\frac{\varepsilon r_L^2}{(1-\varepsilon) r_p^2}\right) \tag{3.66}$$

Inserting $k_L \approx (N/V)^{2/3} mC_p < V_f >$ in the equation above, one obtains

$$k_{eff} = (N/V)^{2/3} mC_p < V_f > + k_p \left(\frac{\varepsilon r_L^2}{(1-\varepsilon) r_p^2}\right) . \tag{3.67}$$

When the velocity given by Equation 3.60 is used, one finds that the thermal conductivity of magnetic fluid is given by

$$k_{eff} = (N/V)^{2/3} mC_p \left(\frac{\mu_0 \alpha \chi_0 \dot{q}(R^2 - r^2)}{8\nu\rho_0 C_p (1+\alpha(T - T_0))^2}\right)^{1/2} H + k_p \left(\frac{\varepsilon r_L^2}{(1-\varepsilon) r_p^2}\right) \tag{3.68}$$

This expression shows that thermal conductivity is linearly dependent on the volume fraction of magnetic particles, externally applied magnetic field intensity and radial temperature gradient. All these were shown here experimentally.

4. MEASUREMENTS TECHNIQUES

4.1. CHARACTERIZATION TECHNIQUES

Transmission Electron Microscopy (TEM), Scanning Electron Microscopy (SEM), Dynamic Light Scattering (DLS) and X-Ray diffraction (XRD) techniques are used to characterize the magnetic nanoparticles in order to obtain their size and its distributions and crystalline structure. In addition, the samples are subjected to measurements by a vibrating sample magnetometer (VSM) in order to obtain their magnetic behaviour s about the structure of the magnetite particles contained in the magnetic nanofluid. In this chapter, the devices used in this study are introduced and the brief theories behind of them are given.

4.1.1. Transmission Electron Microscopy (TEM)

Evaluation of particle size before dispersion in liquids is carried out using electron microscopy techniques. One of them is transmission electron microscope which uses an electron beam with high energy to determine the structure of the samples [92].

Transmission electron microscope (TEM) operates on the same fundamental principle as a light microscope but uses electrons instead of light. The active components that compose the TEM are arranged in a column, within a vacuum chamber. An electron gun at the top of the microscope emits electrons that travel down through the vacuum towards the specimen stage. Electromagnetic electron lenses focus the electrons into a narrow beam and direct it onto the test specimen. The majority of the electrons in the beam travel through the specimen. Some of the electrons in the beam are scattered depending on the density of the material and removed from the beam. At the base of the microscope the unscattered electrons hit a fluorescent viewing screen and produce a shadow image of the test specimen with its different parts displayed in varied darkness according to their density. This image can be viewed directly by the operator or photographed with a camera. The limiting resolution of the modern TEM producing two-dimensional images is of the order of 0.05 nm with aberration-corrected instruments [92].

In a TEM, the electrons are accelerated at high voltages (100-1000 kV) to a velocity approaching the speed of light (0.6-0.9 *c*). The associated wavelength is five orders of magnitude smaller than the light wavelength (0.04-0.008 Å). Nevertheless, the magnetic lens aberrations limit the convergence angle of the electron beam to 0.5° (instead of 70° for the glass lens used in optics) and reduce the TEM resolution to the order of Å. The ultimate limit of resolution of an electron microscope is determined by the wavelength of the electron [93]. The basic structure of the device is schematically given in Figure 4.1.

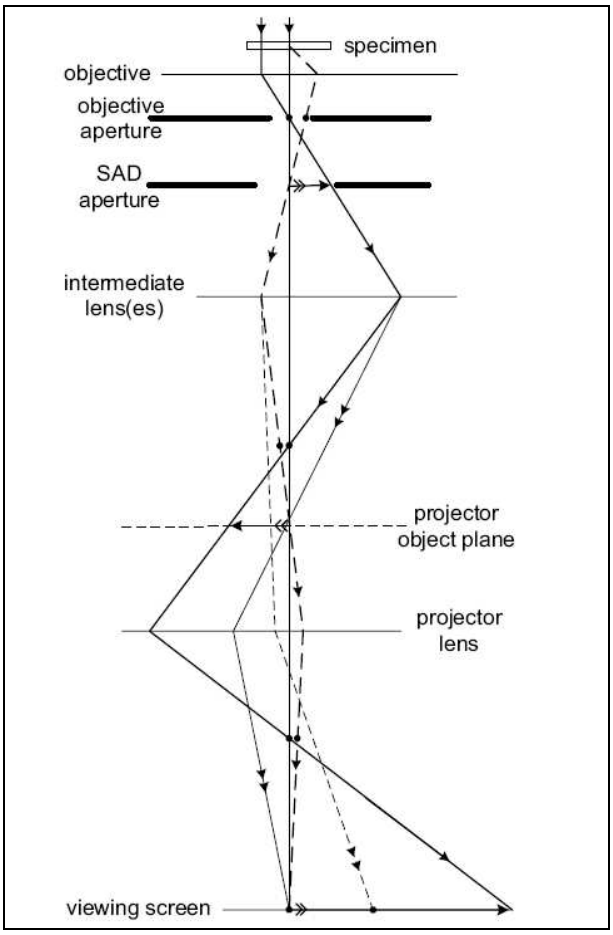

Figure 4.1. Lens ray diagram of the imaging system of a TEM. Image planes are represented by horizantal arrows and diffraction planes by horizantal dots. Rays leading to a TEM –screen diffraction pattern are identified by the double arrow heads [94]

In order to characterize the magnetite in this study, Model FEI, Company: Tecnai^{TM} G2 F30 series which is a service of National Nanotechnology Research Centre UNAM,

Bilkent University, Turkiye, was used. The corresponding technical data and the photograph of the device are given in the Table 4.2 and in Figure 4.2, respectively.

Table 4.1. Technical data for TEM - FEI Tecnai G2 F30 [95]

TEM Magnification Range	60 x – 1000 kx
TEM Point Resolution	0.20 nm
TEM Line Resolution	0.102 nm
Minimum Focus Step	1.8 nm
Maximum Diffraction Angle	$\pm 12^{o}$
Information Limit	0.14 nm

Figure 4.2. Transmission Electron Microscope FEI - Tecnai G2 F30 [95]

4.1.2. Dynamic Light Scattering (DLS)

Dynamic Light Scattering (DLS) also known as Photon Correlation Spectroscopy (PCS) is one of the most popular methods used to determine the size and size distribution of particles and molecules dispersed in a liquid such as proteins, polymers, colloidal sand suspensions. Illuminating the spherical particles in the solution in Brownian motion with a laser beam results in a change in the wavelength of the incoming light since the beam hits

the particle. The Doppler Shift gives the sphere size distribution and a description of the particle's motion in the fluid and the intensity fluctuations in the scattered light [96,97].

In this study, magnetite nanoparticles in hydrophobic and hydrophilic conditions were examined through dynamic light scattering for their size and size distributions. The theory is based on two assumptions, one of which is the "particles are in Brownian motion". Brownian motion is the random movement of particles in a liquid due to the bombardment by the molecules that surround them and this speed of movement is used to determine the size of the particles. The second assumption is that "the beads used in the experiment, are spherical particles with a diameter small compared to the molecular dimensions". As mentioned earlier, the particles suspended in a liquid are constantly moving due to Brownian motion, not stationary. An important feature of Brownian motion for DLS is that small particles move quickly and large particles move more slowly as shown in Figure 4.3. The relationship between the size of a particle and its speed due to Brownian motion is defined in the Stokes-Einstein equation.

$$D = k_B T / 6\pi\eta a \tag{4.1}$$

where a is the radius of the beads, k_b is the Boltzmann constant, T is the temperature in K (in this experiment it will be considered as if it is taking place at room temperature) and η is the viscosity of the solvent. Since from the light scattering it is possible to obtain information about the position of the particles, the formula given above is easy to get the radius of the beads [96,97].

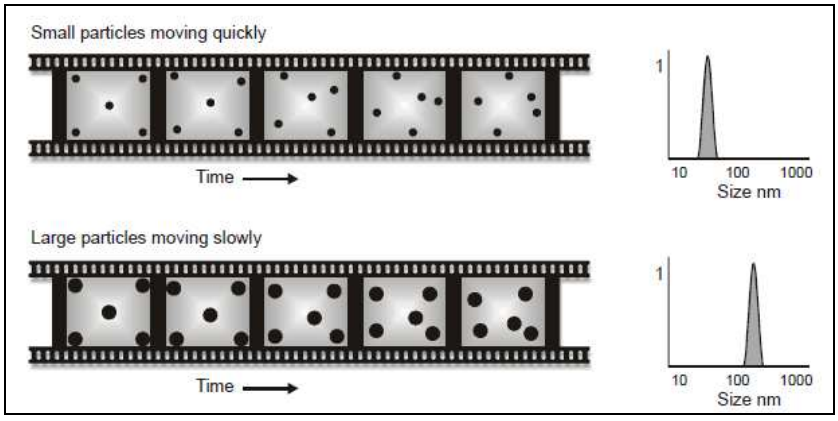

Figure 4.3. Particle size and particle motion dependency [97]

Figure 4.4 illustrates the scattered light and intensity dependency in the manner of dark and bright areas. The intensity at any particular point appears to fluctuate for this reason. The Zetasizer Nano system measures the rate of the intensity fluctuations which yields the velocity of the Brownian motion and fluctuation and then uses this to calculate the size of the particles using the Stokes-Einstein relationship.

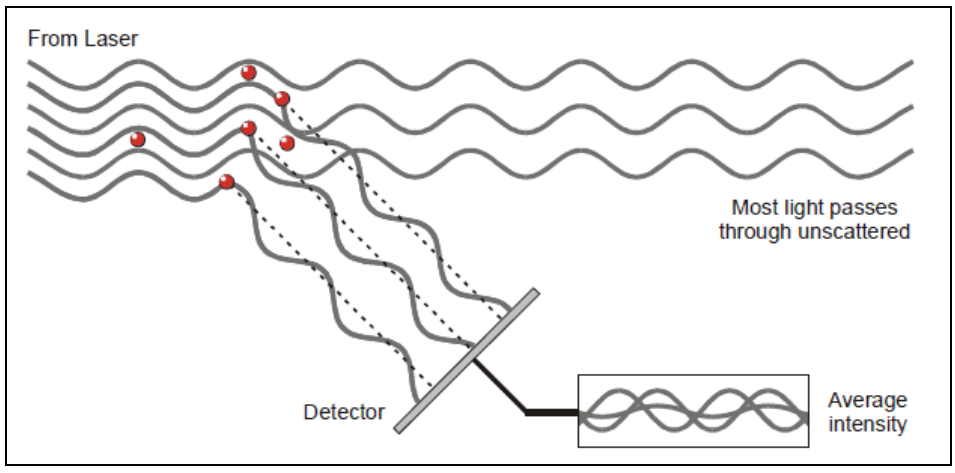

Figure 4.4. Illustration of the scattered light sensing by detector. The intensity of the scattered light fluctuates at a rate that is dependent upon the size of the particles [97]

Table 4.2. Zetasizer Nano Series specifications [97]

Zetasizer	**Size range (diameter)**	**Size range for zeta potential (diameter)**	**Molecular weight range**
Nano S	0.6 nm to 6μm	-	1000 to $2x10^7$ Daltons
Nano Z	-	5 nm to 10μm	-
Nano ZS	0.6 nm to 6μm	5 nm to 10μm	1000 to $2x10^7$ Daltons
Nano S90	1 nm to 3μm	-	10,000 to $2x10^7$ Daltons
Nano ZS90	1 nm to 3μm	5 nm to 10μm	10,000 to $2x10^7$ Daltons

4.1.3. X-Ray Diffraction

Most of solid materials can be described as crystalline in which the atoms are arranged in a regular pattern and there is a smallest volume element that by repetition in three dimensions describes the crystal. When X-rays interact with a crystalline substance, a diffraction pattern like a fingerprint of the substance is obtained. In 1919 A.W.Hull gave a paper titled, “A New Method of Chemical Analysis”, and he pointed out that “Every crystalline substance gives a pattern; the same substance always gives the same pattern; and in a mixture of substances each produces its pattern independently of the others. “ The powder diffraction method is therefore ideally used for characterization and identification of polycrystalline phases [98].

X-ray diffraction crystallography for powder samples is well-established and widely used in the field of materials characterization to obtain information on the atomic scale structure of various substances in a variety of states. There have been many advances in this field, since the discovery of X-ray diffraction from crystals in 1912 by Max von Laue and in 1913 by W.L. Bragg and W.H. Bragg [99].

X-rays with energies ranging from about 100 eV to 10 MeV are classified as electromagnetic waves. X-rays show wave nature with wavelength ranging from about 10 to 10^{-3} nm. When a high voltage with several tens of kV is applied between two electrodes, the high-speed electrons with sufficient kinetic energy, drawn out from the cathode, collide with the anode (metallic target). The electrons rapidly slow down and lose kinetic energy. Since the slowing down patterns (method of losing kinetic energy) vary with electrons, continuous X-rays with various wavelengths are generated. X-rays entering a sample are scattered by electrons around the nuclei of atoms in the sample. The scattering usually occurs in various different directions other than the direction of the incident X-rays, even if photoelectric absorption does not occur. As a result, the reduction in intensity of X-rays which penetrate the substance is necessarily detected [99].

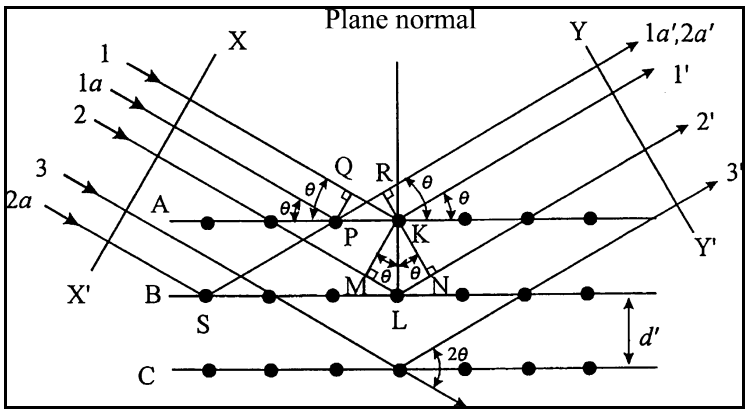

Figure 4.5. Bragg condition illustrating the diffraction of X-rays by a crystal [99]

Two geometrical facts are worth remembering [101]:

i. The incident beam, the normal to the reflecting plane and the diffracted beam are always coplanar and ii. The angle between the diffracted X-ray beam and the transmitted beam is always 2θ. This is known as the “diffraction angle”.

Diffraction in general occurs only when the wavelength of the wave motion is of the same order of magnitude as the repeating distance between scattering centre. This requirement follows from the Bragg law [100].

As an incident beam, with the wavelength of λ, collides a crystal, diffraction beam of sufficient intensity is detected only when Bragg condition given below is satisfied:

$$2d \sin\theta = n\lambda \tag{4.2}$$

where n is the number of wavelengths in the path difference between diffracted X-rays from adjacent crystal planes shown in Figure 4.5. d is the spacing between regular arrays in crystal [100].

There are various methods for measuring the intensity of a scattered X-ray beam from crystalline materials. The most common method is to measure the X-ray diffraction intensity from a powder sample as a function of scattering angle (it is also called diffraction angle) by using a diffractometer [99].

The device in question, measures the intensity data of a diffracted X-ray beam, as a function of angle, in order to satisfy Bragg's law under the condition of X-rays of known wavelength. The basic design of the device is illustrated in Figure 4.6. Three components, X-ray source (F), sample holder (S), and detector (G), lie on the circumference of a circle, as known as the focusing circle [99].

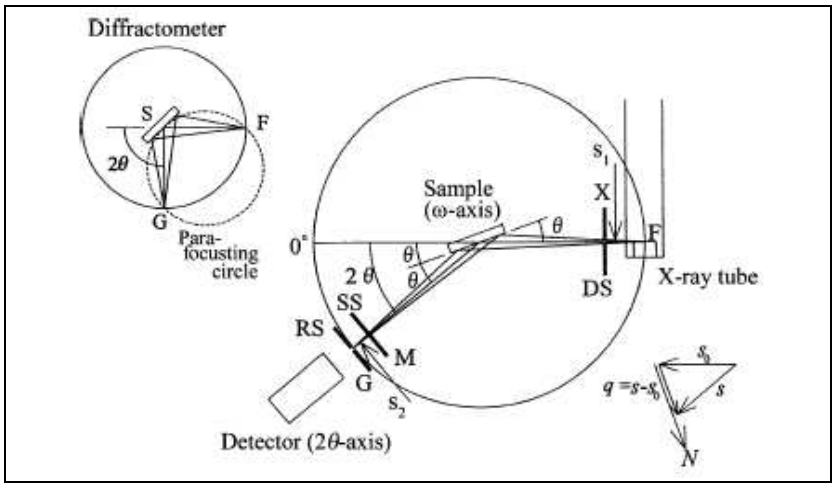

Figure 4.6. A basic schematic view of a X-ray diffractometer [99]

4.1.4. Vibrating Sampling Magnetometer (VSM)

The flux linked with a sensing coil located at a certain distance from an open sample subjected to an intense magnetizing field can be seen as the sum of a main contribution due to such field plus a perturbation originating from the sample. The main issue is to measure such a perturbation. A kind of AC magnetometric method is used in order to separate this perturbation from the background. In this method, the linkage of the sensing coil with the signal generated by the sample is made to vary rapidly with time, all the rest remaining unaltered. This can be done by driving the sample mechanically and giving to that a vibration in order to produce an AC signal while making a DC characterization. In this way, any background constant flux is automatically filtered out and signal optimization can be pursued if some degree of flexibility exists in the amplitude and frequency (ω) of the oscillation and the arrangement of the sensing coils. As a result, the sample moves periodically in a region of homogeneous applied field. The vibrating sample magnetometer (VSM) is based on this principle (S.Foner, 1959). The field may be transversal to the axis of vibration. The pick-up coil is constructed in two separate sections wound in series opposition, also transverse to the vibration axis and oppositely wound. The sample moves around the centre of symmetry of both coils in Figure 4.9. A moving dipole will therefore induce in these coils the instantaneous voltage which is proportional to the magnetic moment of the sample

$$u(t) = KMdz\omega \sin \omega t \tag{4.3}$$

where K is a geometrical factor that is determined by calibration with a sample of known M, and dz is the amplitude of the periodic displacement of the sample, ω is the angular frequency of voltage variation [100, 101]. The voltage induced in the detection coils is a function of many variables including the finite dimensions of the coils and the sample, as well as the geometrical arrangement of the coil assembly. This method permits obtaining the magnetic hysteresis.

According to Figure 4.7, the feedback driven by continuous reading by an interfaced Hall unit controls the field strength. The current is generated by means of a bipolar power supply driven by an interfaced DC source. The voltage induced in the pickup coils is

amplified by means of a lock-in amplifier, whose internal reference signal, driven via a computer-controlled procedure relying on the signal generated by the vibrating reference magnet, is used to feed the power amplifier supplying the vibrator. Figure 4.8 illustrates the scheme of a VSM with applied field transverse to the vibration axis [101].

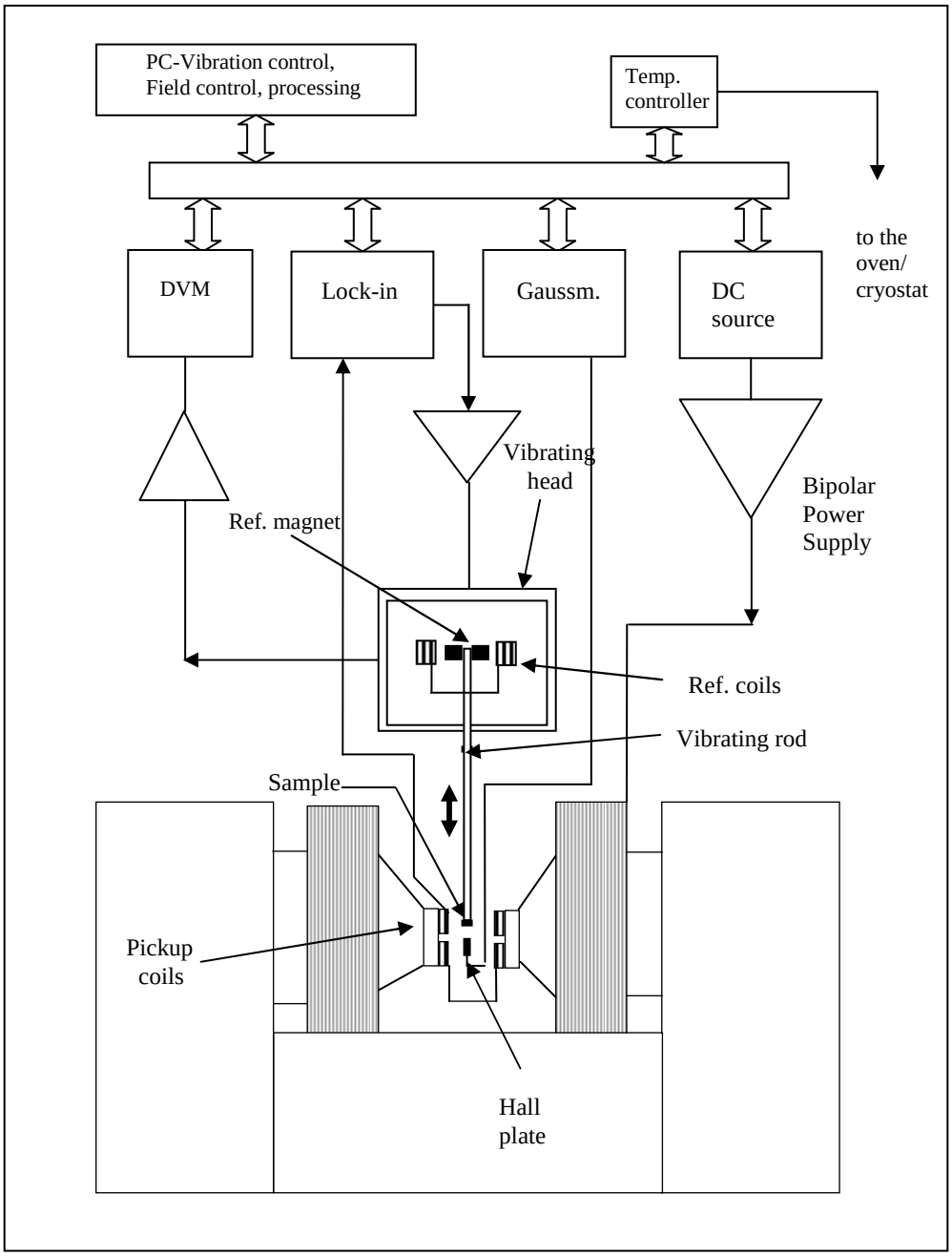

Figure 4.7. The scheme of a vibrating sample magnetometer [101]

The measurement of the magnetic moment of the test sample as a function of the field strength can be performed by continuous variation of the field with time. The voltage simultaneously induced in the pickup coils is again simultaneously detected and processed to determine the magnetic moment. The lower limit for measurable magnetic moment is typically around 10^{-9} Am^{-2} in commercial setups. On the other hand, the upper limit can be of the order of 0.1 Am^{-2} and higher (for example, the magnetic moment of a 7 mm diameter iron sphere is around 0.3 Am^{-2}) [101, 102].

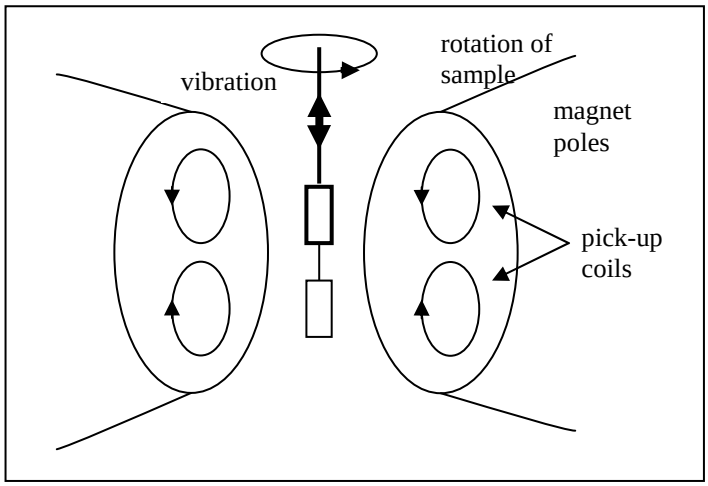

Figure 4.8. Scheme of a VSM with applied field transverse to the vibration axis. The rod supporting the sample may be rotated [101]

It is better to mention about some aspects such as hysteresis, remanence and coercive fields at this point.

Hysteresis is at the heart of the behaviour of magnetic materials. All applications, from electric motors to transformers and permanent magnets, from various types of electronic devices to magnetic recording, rely heavily on particular aspects of hysteresis. Hysteresis loops may take many different shapes and it is important to list a few parameters that give some prime characterization of loop properties. Three quantities of particular importance in this respect are the saturation magnetization M_s, remanent magnetization or *remanence*, M_r, and the *coercive field*, H_c, described in detail in 3.2.1 [103].

The device used for magnetization measurement is 9600 model Vibrating Sample Device (VSM, LDJ Electronics, Inc, 9300 Power supply electromagnet drive 2400 Watt, 30 Amper, 80 V AC) with the magnetic field strength about 1 Tesla located at TÜBİTAK UME Magnetic Measurements Laboratory, Kocaeli Turkiye.

Magnetization was recorded over the whole magnetic field range from negative to positive saturation. The mass values were determined experimentally by filling the container with the sample and weighing the mass of the filled container using the electronic scale (OHAUJ Company model AP11OS, resolution 0.1 mg). The VSM device provides the magnetization values in units of the electromagnetic mass unit (e.m.u.).

Samples were placed in the centre of the space between the sensing coils. The diameter of each coil is 12 cm and the distance between the coils is 3 cm. VSM is calibrated against high purity nickel sphere before sample measurements.

Figure 4.9. VSM equipment located at TÜBİTAK UME

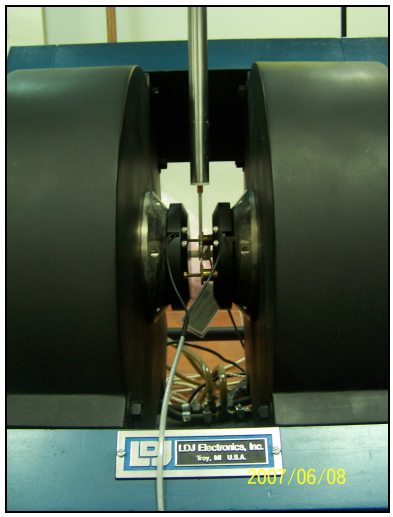

Figure 4.10. Vertical rod holding the sample between coils

4.1.5. Scanning Electron Microscopy (SEM)

Electrons are strongly scattered within the specimen, or even absorbed rather than transmitted. This is the limitation of TEM as the specimen must be used as ultra thin. Bulk, that is relatively thick, specimen can be used in SEM applications. The electron source used in the SEM can be a tungsten filament. Since the maximum accelerating voltage (typically 30 kV) is lower than that of a TEM, the electron gun is smaller, requiring less insulation. Axially-symmetric magnetic lenses are used but they are also smaller than those employed in the TEM. SEM produces an electronic map of the specimen which is displayed on a cathode ray tube (CRT). The signal produced by the secondary electrons is detected and sent to a CRT image. A SEM image contains information about the surface topography of the sample [94].

In order to characterize the silica in this study, Carl Zeiss EVO 40 model SEM instrument was used. The corresponding schematic diagramme of SEM is given in Figure 4.11.

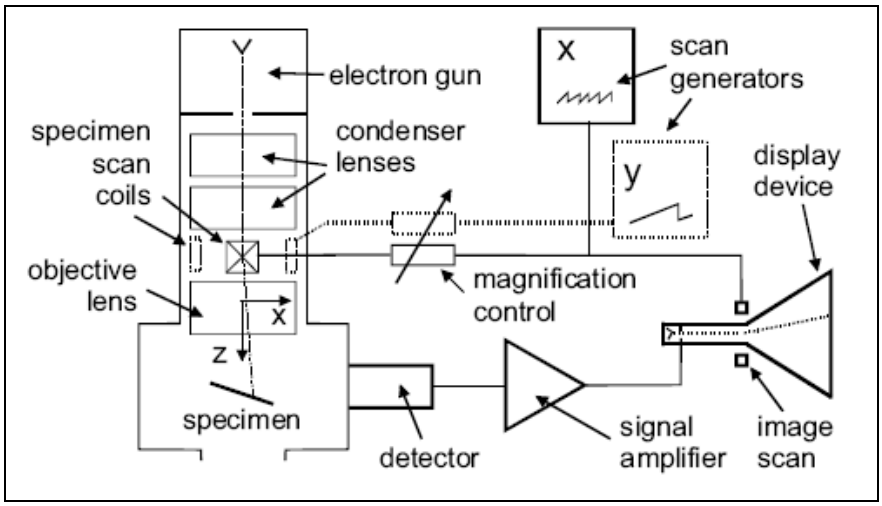

Figure 4.11. Schematic diagramme of a SEM [94]

4.2. THERMOPHYSICAL MEASUREMENT TECHNIQUES

4.2.1. Density

In this study thermophysical properties such as density, viscosity and thermal conductivity were analyzed using synthesized magnetite dispersed in water, hexane and heptane. In this study, a digital density meter Anton Paar DMA 4100 employing the oscillating U-tube principle was used. Below, the technical data are provided in the Table 4.3.

Table 4.3. Technical data for Anton Paar DMA 4100 [104]

Measuring Range	0 – 3 g/cm^3
Measuring Temperature	0 – 90 ^{o}C
Density Accuracy	0.0001 g/cm^3
Temperature Accuracy	0.05 ^{o}C
Density Repeatability	0.00005 g/cm^3
Temperature Repeatability	0.02 ^{o}C
Min. amount of sample	App. 1 mL
Measuring Time	30 Sec.

Figure 4.12. Density meter Anton Paar DMA 4100

The fluid sample to be measured was filled into an oscillating U-shaped glass tube vibrating at a certain frequency. The measurement of the density was based on the measurement of the vibration frequency which is related with the mass of the material to be measured. The greater the mass of the sample, the higher the vibration frequency is. The measuring principle is mainly based on the mass-spring model and the relationship between the oscillation frequency (*f*, in Hertz) and the sample density can be seen by following Equation (4.4)

$$f = \frac{1}{2}\pi\left[\frac{c}{(\rho V + m)}\right]^2 \tag{4.4}$$

where, ρ is the density of liquid in kg/m^3, V is the volume of the liquid in m^3, m is the cell mass in kg and c is the spring constant in kg.m^{2}s^{-2} . Since volume is highly temperature dependent, the density of a typical substance is also temperature dependent. A thermostat is connected with the density meter to control the temperature [105].

4.2.2. Viscosity

The Brookfield DV-III Ultra Programmable Rheometer measures fluid parameters of Shear Stress and Viscosity at given Shear Rates. Viscosity is a measure of a fluid's

resistance to flow. The principle of operation of the DV-III Ultra is to drive a spindle (which is immersed in the test fluid) through a calibrated spring. The viscous drag of the fluid against the spindle is measured by the spring deflection. Spring deflection is measured with a rotary transducer. The viscosity measurement range of the DV-III Ultra (in centipoise or cP) is determined by the rotational speed of the spindle, the size and shape of the spindle, the container the spindle is rotating in, and the full scale torque of the calibrated spring. The DV-III Ultra can also measure yield stress (in Pascals or Pa) [106].

The equivalent units of measurement in the SI system are calculated using the following conversions:

Table 4.4. Viscosity units of measurement [106]

Unit	**SI**	**CGS**
Viscosity	1 mPa•s	1 cP
Shear Stress	1 Newton/m^2	10 dyne/cm^2
Torque	1 N•m	107 dyne•cm

In order to see the volume concentration effect on the viscosity of a fluid viscosity, analyses of synthesized magnetite dispersed in water and heptane were performed using a Brookfield DV-III Ultra Programmable.

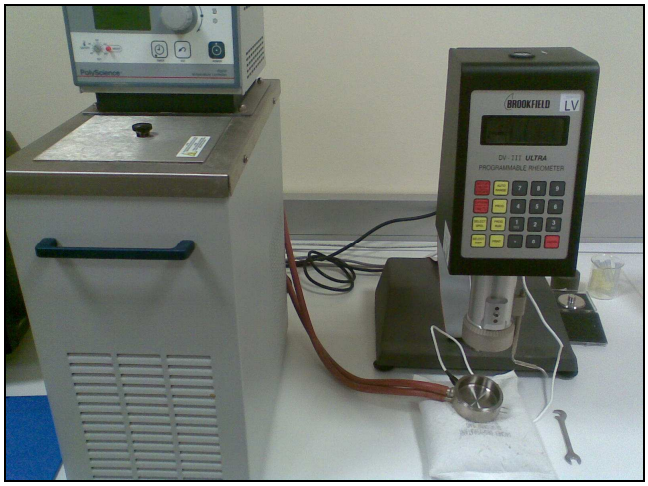

Figure 4.13. Brookfield DV-III Ultra Programmable Rheometer

Table 4.5. Rheometer specifications [106]

Specifications	
Speed Ranges for viscosity tests	0.01 RPM-250 RPM (0.01 increments from 0.01 to 0.99 RPM and 0.1 increments from 1.0 to 250 RPM)
Viscosity Accuracy	± 1.0% of F.S. range for a specific spindle running at a specific speed
Temperature sensing accuracies and range	±1.0 ^{o}C from -100 ^{o}C to 150^{o}C; ±2.0 ^{o}C from +150^{o}C to 300^{o}C
Torque Accuracy	±1.0% of full scale range
Torque Repeatability	±0.2%

The “gap” between the cone and the plate must be verified and adjusted before measurements are made. Besides, rheometer must be autozeroed before taking the measurements. This is done by moving the plate (built into the sample cup) up towards the cone until the pin in the centre of the cone touches the surface of the plate and then by separating (lowering) the plate by 0.0005 inch (0.013mm). This procedure was done due to the regulation given in the manual on page 85. The standard spindle supplied with the DV-III Ultra is designed to be used with a specific sample chamber that is 600 ml fluid for the viscosity measurements. Selecting the speed velocity determines the torque range for the measurements. An appropriate speed selection will result in measurements made between 10 and 100 on the instrument percent torque scale [106].

4.2.3. Thermal Conductivity

An instrument specifically designed by Flucon GmBH Lambda with PSL Systemtechnik LabTemp 30190 was used to measure the thermal conductivity of nanofluids in this study.

The transient hot-wire method has been widely used for determining the thermal conductivity of fluids with a high degree of accuracy (Pittman 1968, Haarman 1969, Mani 1971, de Groot *et a1* 1974, Castro *et a1* 1976 and Nagasaka and Nagashima 1981) [107].

This method was first suggested by Stalhane and Pyk in 1931 to measure the absolute thermal conductivity of powders. Many researchers have modified the method to make it more accurate. There are several advantages for the TWH method. The most attractive advantage of this method for application to fluids is its capacity for experimentally eliminating the error due to natural convection. In addition, this method is very fast compared to other techniques [108].

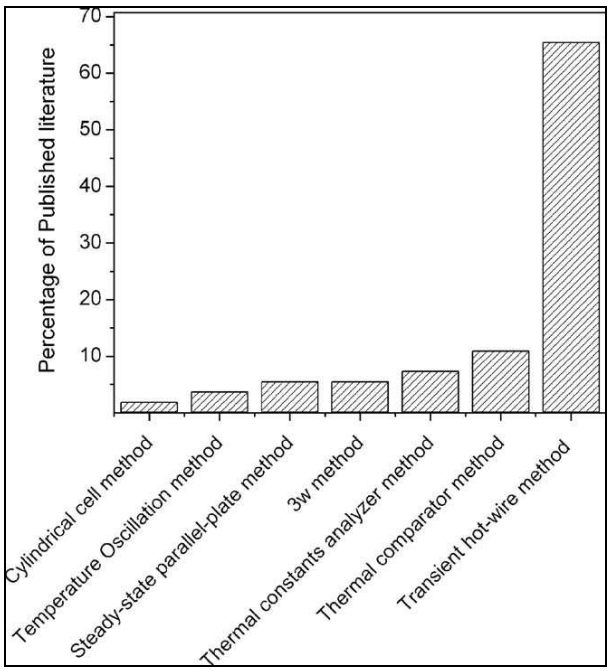

Figure 4.14 Comparison of the thermal conductivity measurement techniques for Nanofluids [108]

The thermal conductivity of a substance is a measure of the ability of that substance to transfer energy as heat in the absence of mass transport phenomena. Two basic techniques are commonly used for measuring thermal conductivities of liquids, the transient hot-wire method and the steady-state method. Most thermal property measurements of nanofluids have been done using transient method of measurement.

The hot wire method is a standard transient dynamic technique based on the measurement of the temperature rise in a defined distance from a linear heat source (hot wire) embedded in the test material. If the heat source is assumed to have a constant and uniform output along the length of test sample, the thermal conductivity can be derived directly from the resulting change in the temperature over a known time interval [109]. The heating wire as well as the temperature sensor (thermocouple) is encapsulated in a probe that electrically insulates the hot wire and the temperature sensor from the test material. A hot-wire system involves a wire suspended symmetrically in a liquid in a vertical cylindrical container. The wire serves both as heating element and as thermometer. Platinum is the general choice of the wire material [110].

If 'q' is the constant quantity of heat production per unit time and per unit length of the heating wire ($W.m^{-1}$), initiated at the time $t = 0$ (applied electric power), a radial heat flow around the wire occurs. The fundamental equation of the transit hot-wire technique method is based on the assumption that the hot wire is an ideal, infinite thin and long line heat source, which is in an infinite surrounding from homogeneous and isotropic material with constant initial temperature. The method is called transient because the power is applied abruptly and briefly. The working equation is based on a specific solution of Fourier's Law [110]:

$$\Delta T(r,t) = \frac{q}{4\pi k} \ln \frac{4at}{r^2 C} \tag{4.5}$$

where $\Delta T(r,t)$ is the temperature rise of the wire of radius "r" at time "t". Wheatstone bridge is used to measure the resistance difference that is related to the difference of the temperature rises. In addition, 'k' is the thermal conductivity ($W.m^{-1}.K^{-1}$), 'a' thermal diffusivity ($m^2.s^{-1}$) ($a=k/\rho c_p$) of the fluid, with 'ρ' is the density ($kg.m^{-3}$) and 'c_p' the heat capacity ($J.kg^{-1}.K^{-1}$) of the material and $C=exp(\gamma)$ where γ=0.5772 is the Euler's constant, r is the radius of the wire (m).

Thus the measurement of temperature rise as a function of time can be employed to determine the thermal conductivity 'k'. Calculating the slope of the linear portion of

temperature rise $\Delta T(r,t)$ versus natural logarithm of the time $ln(t)$ gives the thermal conductivity of the sample nanofluids [110].

$$k = \frac{q}{4\pi(T_2 - T_1)} \ln\left(\frac{t_2}{t_1}\right) \tag{4.6}$$

where $T_2 - T_1$ is the temperature rise of the wire between times t_1 and t_2.

Measurement in natural convection induced particle moving is not incorporated in the measurement. As particles move upon the application of a magnetic field, there may be an initial overestimation of the measured thermal conductivities.

Table 4.6. Thermal conductivity equipment specifications [111]

Specifications	
Measuring Media	Fluids, fluids with nanoparticles, gels, powders
Standard	Based on ASTM D 2717
Temperature range	Between -30 °C and +190 °C
Resolution/	0.1 °C
Accuracy	0.1 °C
Reproducability	1%
Cooling tap water temperature	Between +3 °C and +25 °C
Voltage Input	85 V-264 V~ (47 Hz -63 Hz)
Pressure range	Ambient or up to 35 bar (500 psi)

The system mainly enables to determine the thermal conductivity of fluids, powders, gels and fluids containing suspended nanoparticles. Only small amounts of sample (app. 50 ml) are sufficient to execute reliable measurements [111].

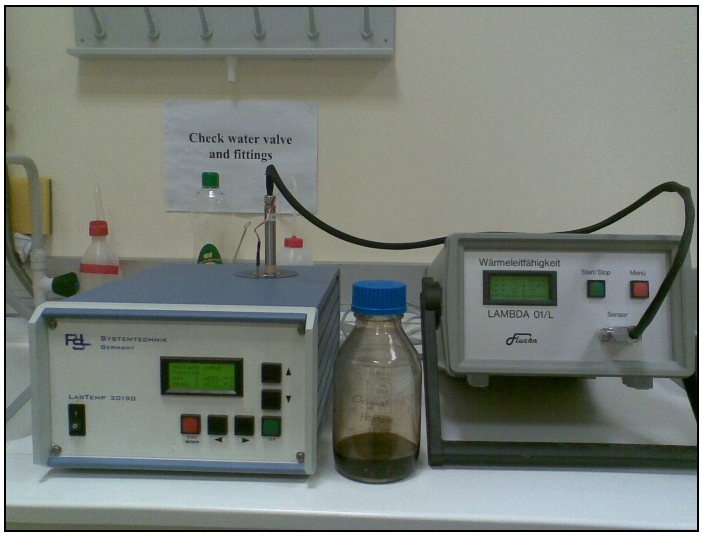

Figure 4.15. The thermal conductivity measuring device used in this study

5. RESULTS AND DISCUSSION

5.1. CHARACTERIZATION MEASUREMENTS OF THE SAMPLES

Nanoparticles synthesized by the above mentioned techniques were examined by Transmission Electron Microscopy (TEM), Dynamic Light Scattering (DLS), X-Ray diffraction (XRD) and Scanning Electron Microscopy (SEM) in order to obtain their structural information. In addition, VSM measurements have been performed to obtain magnetization behaviour of the magnetite samples.

5.1.1. Transmission Electron Microscopy (TEM) Analyses of Ferrofluids

The morphology and size of the synthesized particles were observed using transmission electron microscope. For imaging the magnetic nanoparticles, the Transmission Electron Microscope (TEM) Model FEI Company Tecnai™ G2 F30 Series operating at approximately 100 kV in UNAM, Bilkent, Türkiye was used. Magnetite nanoparticle samples for the analysis were prepared by placing a small amount of a very dilute dispersion of nanoparticles on amorphous carbon-coated copper grid and allowing the solvent to evaporate at room temperature.

Transmission electron microscopy (TEM) results revealed that the hydrophobic and hydrophilic magnetite particles synthesized are almost spherical although not very regular in shape with slight polydispersity in size with an average diameter of about 10 nm.

Hydrophobic nanoparticles have a core diameter of approximately 6 nm and a hydrodynamic diameter of 9.7 nm and the hydrophilic magnetite nanoparticles have a core diameter of 8 nm.

TEM images also indicate that both types of nanoparticles produced in this study have no noticeable agglomeration.

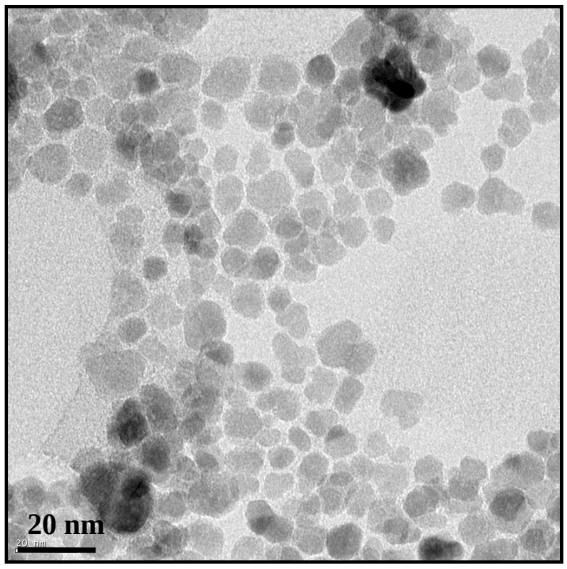

Figure 5.1. TEM image of magnetite nanoparticles (Fe_3O_4) prepared by water synthesis

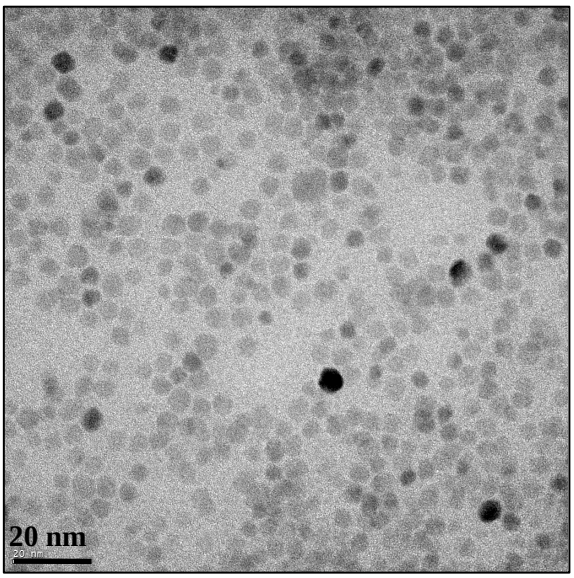

Figure 5.2. TEM image of magnetite nanoparticles (Fe_3O_4) prepared by oil synthesis

5.1.2. Dynamic Light Scattering (DLS) Analyses of Ferrofluids

The size distribution of these particles were obtained using dynamic light scattering (DLS, Malvern Zeta-Sizer Nano ZS) and the intensity averaged particle distribution was found to be between 5-20 nm with an average of approximately 10 nm, which is in perfect agreement with TEM results.

Small peak at large sizes disappears if distribution is based on the number average indicating that most particles are indeed isolated from each other. The size distribution of the synthesized particles is presented in Figure 5.3.

The analysis technique is mainly based on the principle of the particle diffusion speed due to Brownian motion. In a typical measurement, the intensity of the scattering light is measured where a very dilute amount of suspension is placed in a special cuvette and illuminated by laser light. Depending on the size of the particles, the intensities will vary and the particle size will be determined.

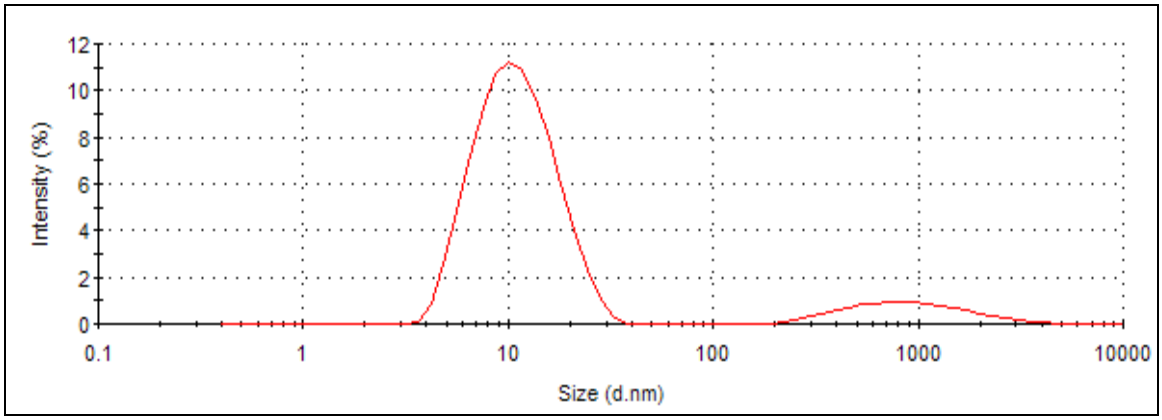

Figure 5.3. DLS Data for Fe_3O_4 particles

5.1.3. X-Ray Diffractometer (XRD) Analyses of Ferrofluid

Powder X-Ray Diffractometer (XRD) model Rigaku D/MAX-Ultima was used to obtain crystallographic information on the synthesized particles.

Powder X ray diffraction of particles confirmed that the particles were Fe_3O_4 (magnetite). The characteristic diffraction pattern of Fe_3O_4 obtained can be seen in Figure 5.4. The position and relative intensity of all diffraction peaks (*hkl* numbers are: 111, 220, 311, 400, 422, 511, 440, 620 and 533) were indexed as the corresponding standard magnetite powder diffraction data (reference code: JCPDS 01-088-0315) and according to the results it can be concluded that no characteristic peaks of impurities were observed.

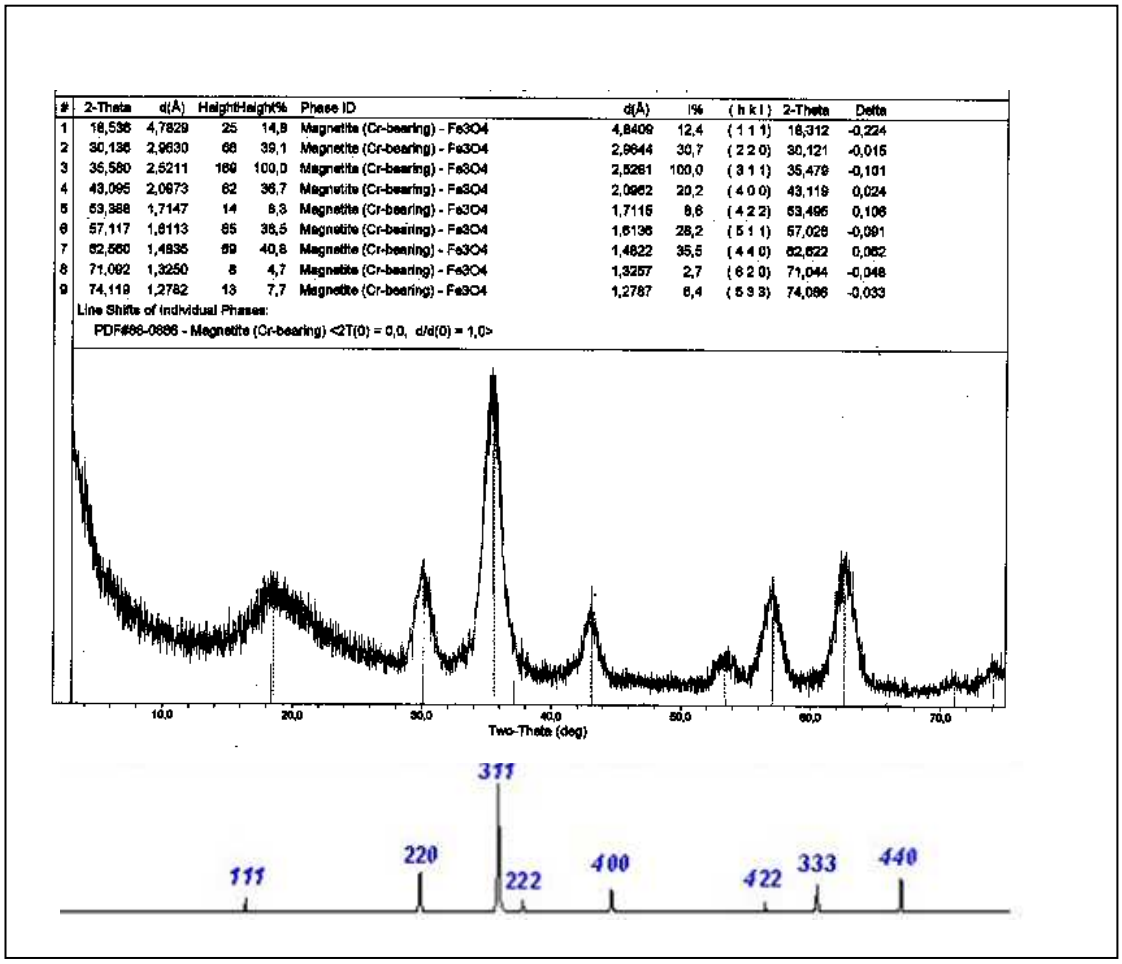

Figure 5.4. Magnetite – oil x-ray diffractogram

5.1.4. Vibrating Sample Magnetometer (VSM) Analyses of Ferrofluids

The magnetic properties of Fe3O4 samples suspended in heptane were analyzed by a Vibrating Sample Magnetometer (VSM) located at TÜBİTAK UME Magnetic Measurements Laboratory, Kocaeli, Türkiye. Figure 5.5 illustrates typical magnetization curves at different concentrations (1%, 3% and 5%).

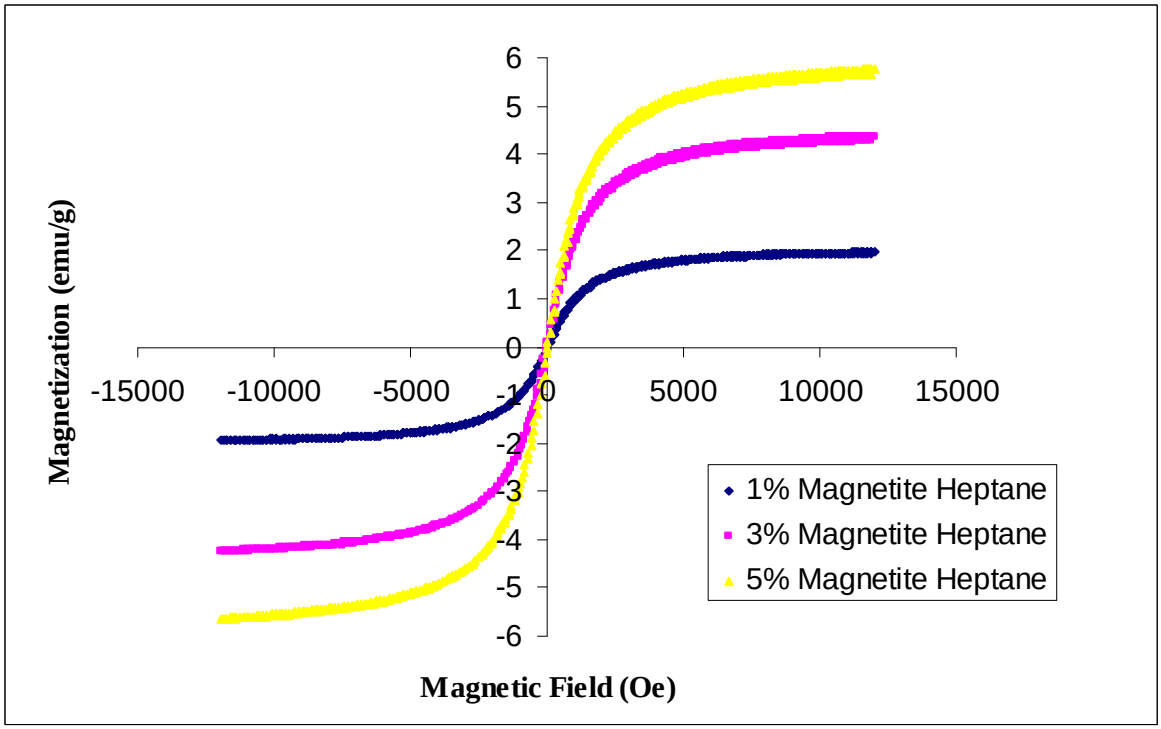

Figure 5.5. Magnetization curves at different concentrations of Fe_3O_4 particles suspended in heptane at 296 K

The saturation magnetization of synthesized magnetite nanoparticles were found to be equal to approximately 5.74 emu/g for 5 wt% of magnetite nanoparticles, 4.36 emu/g for 3 wt% of nanoparticles and 1.94 emu/g for 1 wt% of magnetite nanoparticles. In other words, from the magnetization curve, it can be concluded that the saturation magnetization (M_s) of the Fe_3O_4 nanoparticles increase from about 1.94 to 5.74 emu/g when the concentration of magnetite increases from 1 to 5 wt%, which can be attributed to the increase of weight and volume of magnetite nanoparticles [112].

We observed H (magnetic field)-dependence of the susceptibility of that material in this figure, which gives us characteristic sigmoidal shape of M-H curve. At the large values of H, magnetization approaches its saturation point. There is no hysteresis loop that means irreversibility in the magnetization process as expected. The result obtained in these measurements shows us superparamagnetism where the magnetic moment of the particle is free to react to thermal energy. Therefore, the curve here is anhysteretic. The magnetic fluids carrying superparamagnetism feature give no remanence and no coercivity field that

can be seen on the curves as expected [113]. It confirms that the magnetite nanoparticles are characteristic of superparamagnetic properties at room temperature leading to the net magnetization of fluid in the absence of an external field is zero. Superparamagnetic materials have no permanent magnetic moment and, hence, no hysteresis loops as a result.

At the lower field strength, a small change in the magnetic field causes a substantial change in the magnetization of the magnetic fluid as long as the magnetic field is below the saturation point. At the higher field strength, the magnetic moments of the particles align with the external field and reach its saturation value. This change in magnetization reduces significantly when the ferrofluid reaches saturation [114].

As seen in magnetization curves, initial magnetic susceptibility values increased with concentration. Increase in magnetic susceptibility with concentration was also observed by other researchers [115].

The slopes of the curves in Figure 5.6 can be used to determine the initial susceptibilities as $\chi_i = 0.01$, $\chi_i = 0.02$ and $\chi_i = 0.03$ for the 1%, 3% and 5% magnetite heptane, respectively.

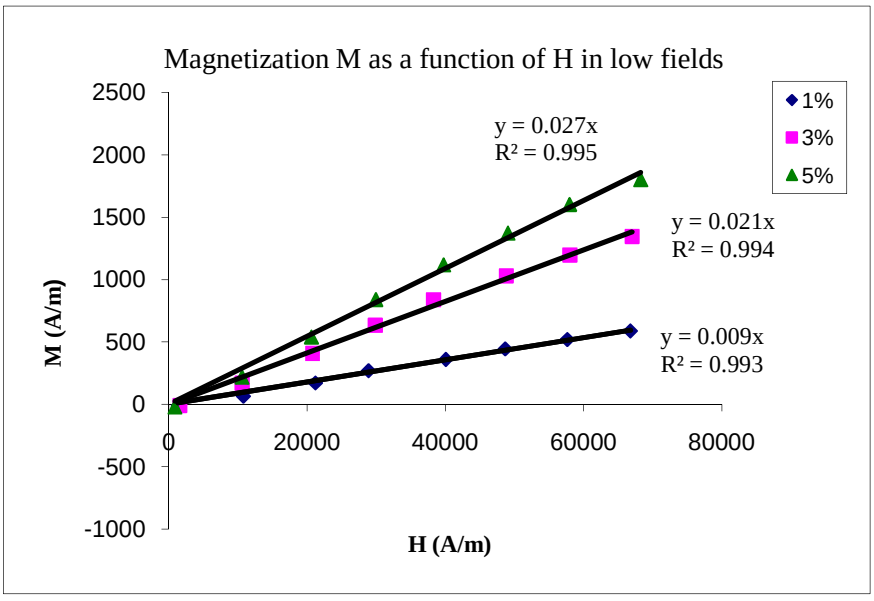

Figure 5.6. Magnetization as a function of H in low fields for magnetite heptane nanofluids

These curves state that the slope increase as weight percentage increases; thus, the magnetic susceptibility increases with weight percentage. This is an expected result since increased weight percentage causes the magnetization to increase.

5.1.5. Scanning Electron Microscopy (SEM) and DLS Analyses of Silica

The silica SEM images are presented in Figure 5.7 showing that nanoparticles are almost perfectly spherical shape with diameters near 100 nm.

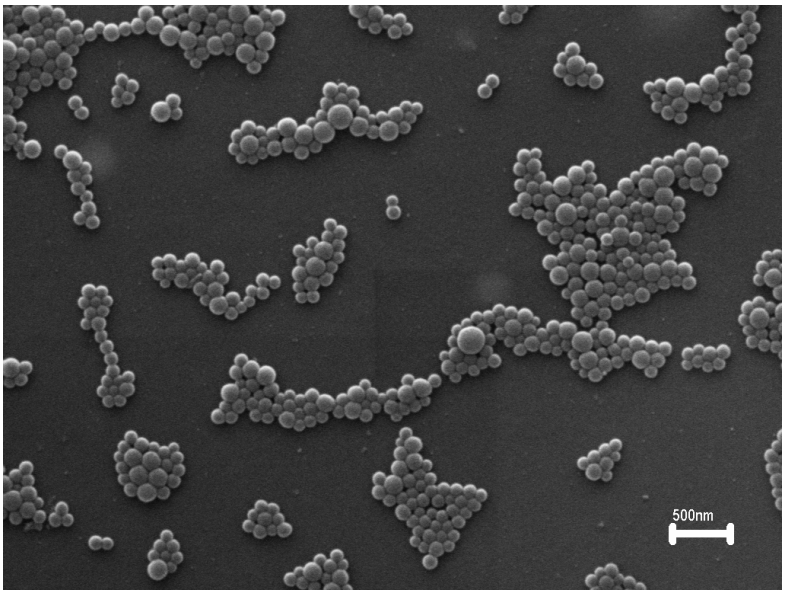

Figure 5.7. SEM image of Silica 2.86 N – 7T (SEM peak: 128.35 nm)

The size distribution of silica 2.86N-7T is shown in Figure 5.8. As seen, the curve maximizes at the size of 128 nm. This result is in perfect agreement with Figure 5.7.

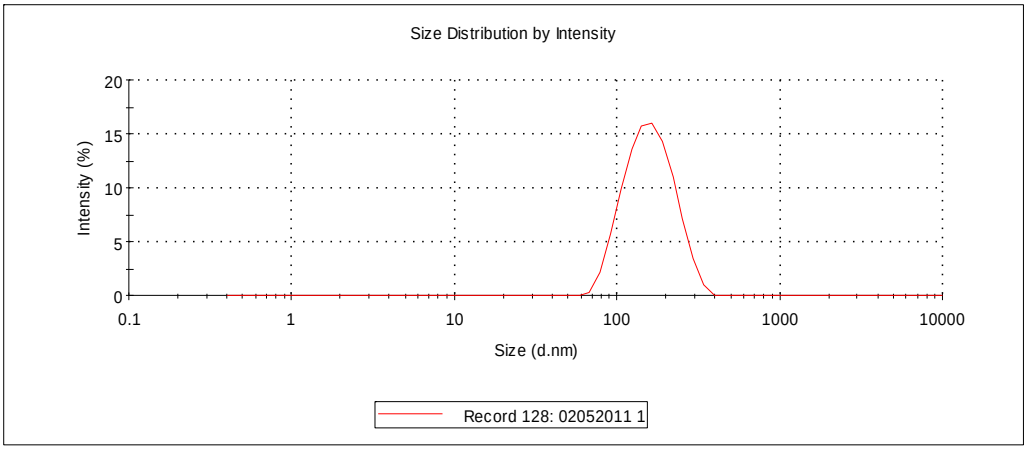

Figure 5.8. DLS results for 2.86 N – 7T Intensity: 165.7 - 160.2

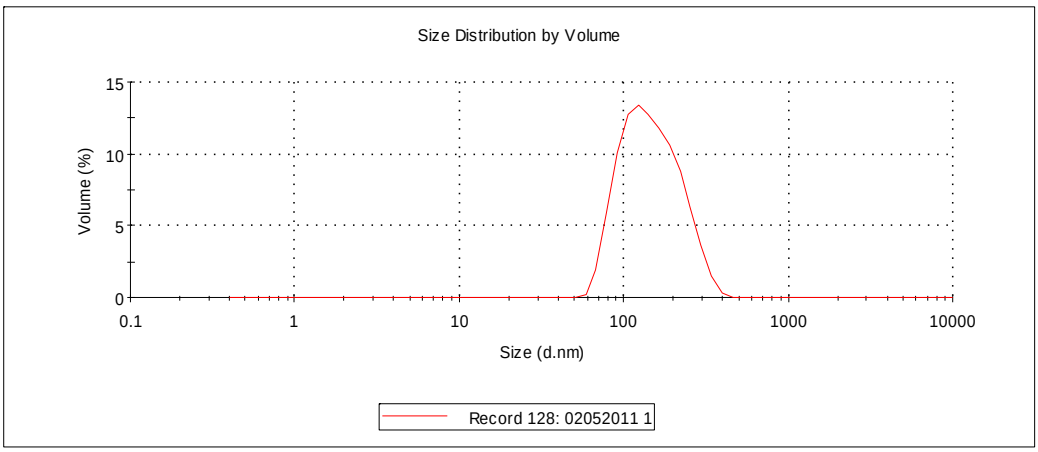

Figure 5.9. DLS results for 2.86 N – 7T Volume : 155.2 -149.6

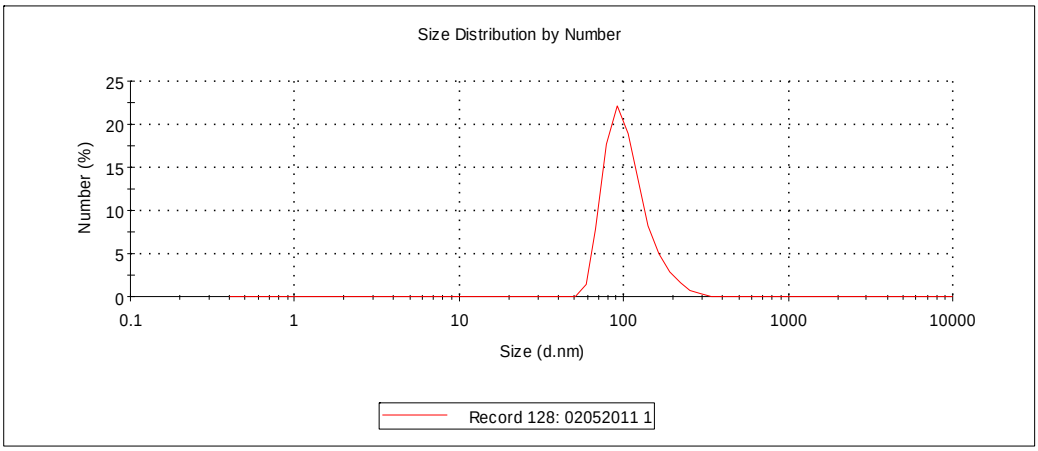

Figure 5.10. DLS results for 2.86 N – 7T Number : 108.4 -108.7

The DLS results for 2.86N-7T values 155.2-149.6 and 108.4-108.7 are presented in Figures 5.9 and 5.10. The peaks in these figures show that the sizes of cluster near 120 and 90 nm, respectively.

5.2. THERMOPHYSICAL MEASUREMENTS OF NANOFLUIDS

Some of these measurements were taken together with Ms student Miss. Merve Yüksel at Chemical Engineering Department of Yeditepe University.

5.2.1. Density Measurements of Ferrofluid

The densities of magnetite nanofluids containing various amounts of nanoparticles dispersed in heptane are measured over a temperature range from 25 ^{o}C to 60 ^{o}C given in Figure 5.11. The expected result is observed that the density increases with increasing nanoparticle concentration. The density enhancement of magnetite nanoparticles dispersed in heptane having a particle loading of 7 wt% is obtained as 7.78%, and the density enhancement of magnetite nanoparticles dispersed in heptane having a particle loading of 1 wt% is obtained as 0.90% both at 25 ^{o}C. The density enhancement of magnetite nanoparticles dispersed in heptane having a particle loading of 7 wt% is obtained as 7.86% calculated over average values.

Temperature effect on density can also be seen in measurements in the same Figure 5.11. Density values are decreased with increasing temperature as expected.

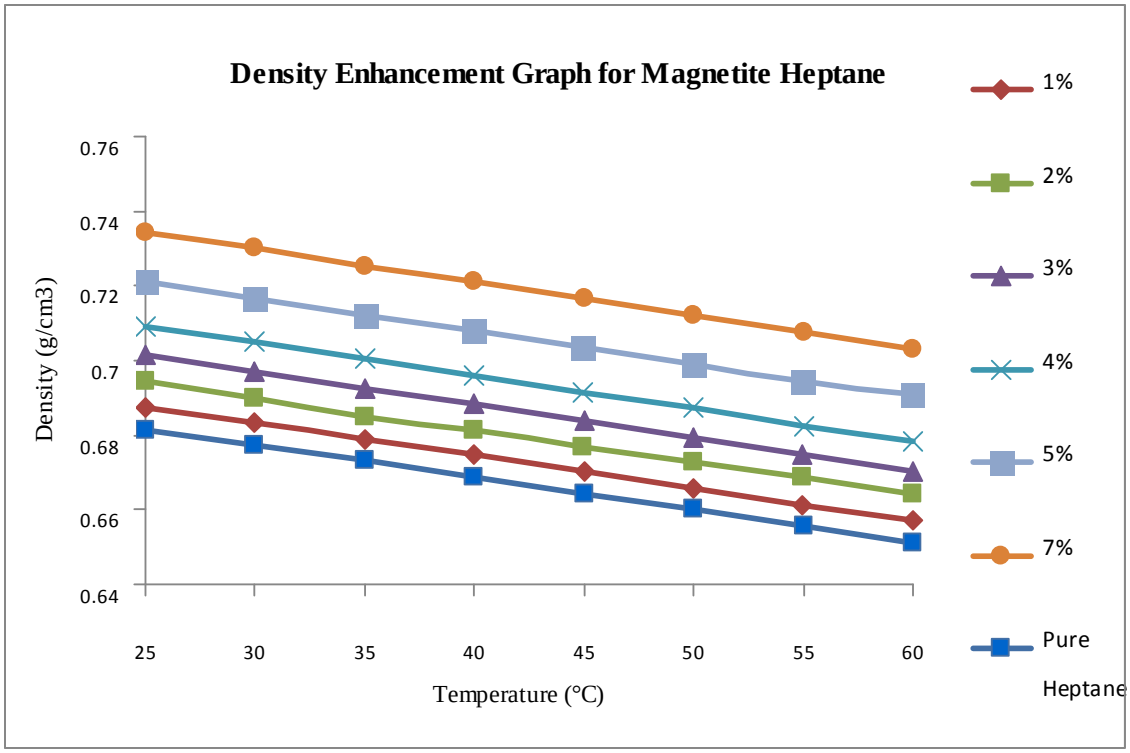

Figure 5.11. Density enhancement for magnetite nanoparticles dispersed in heptane

The theoretical model by Pak and Cho (1998) shows good agreement for magnetite nanofluids according to Figures 5.12 at all concentrations. For the magnetite heptane nanofluid at each volumetric concentration, the maximum deviation is 1.60% and the average is 0.67%. Furthermore, the percentage deviation increases with the increase in concentration.

In the investigation of the rheology of suspensions, the volume concentration, defined as the fraction of space of the total suspension occupied by the suspended material, is often used instead of mass concentration. The suspension rheology depends greatly on the hydrodynamic forces, which act on the surface of the particles or aggregates of particles. Hence, the volume concentration, not the mass concentration, is often used in defining concentration. However, it is much more difficult to make a dispersed liquid precisely at a desired volume concentration than at a desired mass concentration [114].

Therefore, in the present study, the volume concentration was determined from the mass concentration at the dispersed fluid by the following equation [114]:

$$\Phi_{\upsilon} = \frac{1}{\left(100/\Phi_m\right)\left(\rho_p/\rho_{bf}\right)+1} \times 100\mathbf{(\%)} \tag{5.1}$$

where ρ_p and ρ_{bf} are the densities of metallic oxide particles and base fluid, respectively, and Φ_{υ} and Φ_m are the volume and mass concentrations (%) of the dispersed fluid, respectively. Once the volume concentration is determined, the density of the dispersed liquid could be determined from the following equation [114]:

$$\rho = \left(1-\Phi_{\upsilon}\right)\rho_{bf} + \Phi_{\upsilon}\rho_p \tag{5.2}$$

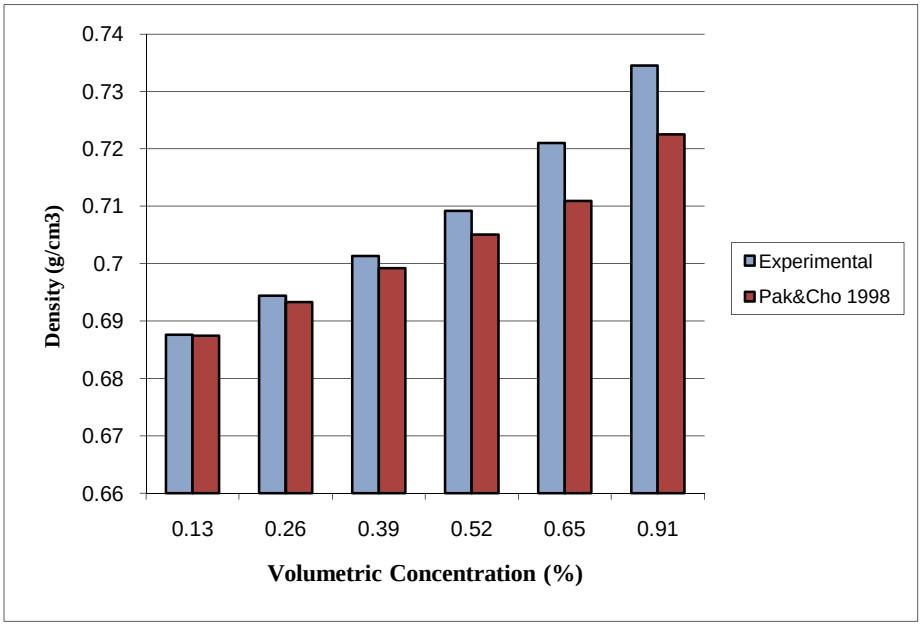

Figure 5.12. Comparison of density values for magnetite nanofluid at 25 °C

The theoretical density values were calculated from Eq.5.2 and the results were plotted along with experimental values. As a general trend, it is seen that experimental values are slightly higher than the theoretical density values. The type of the dispersed nanoparticles and the high particle weight fractions can be attributed to this discrepancy. Although the model represents good agreement with experimental data, Pak and Cho developed it for nanofluids with lower concentrations. This might be the reason why the deviations increase with the increase in the particle concentration.

5.2.2. Viscosity Measurements of Ferrofluid

The viscosity of nanofluids increases with increasing particle concentration and always becomes much higher than that of the base liquid. As a liquid behaviour, the viscosity of base fluids is decreased when the temperature is increased. At the same time, the Brownian motion of nanoparticles is increased as the temperature is increased, which affects the increased conductivity.

In this study, viscosities of magnetite nanoparticles dispersed in heptane were measured over the temperature range of 25 ^{o}C to 60 ^{o}C using a Brookfield viscometer and represented in the Figure 5.13. When the viscosities of the nanofluid are plotted against the temperature, an almost linear (R^2 ~ 0.99) relationship is found. Magnetite heptane nanofluid with varying particle loadings from 1% to 7%, viscosity enhancement is from 2.6% to 24.9%.

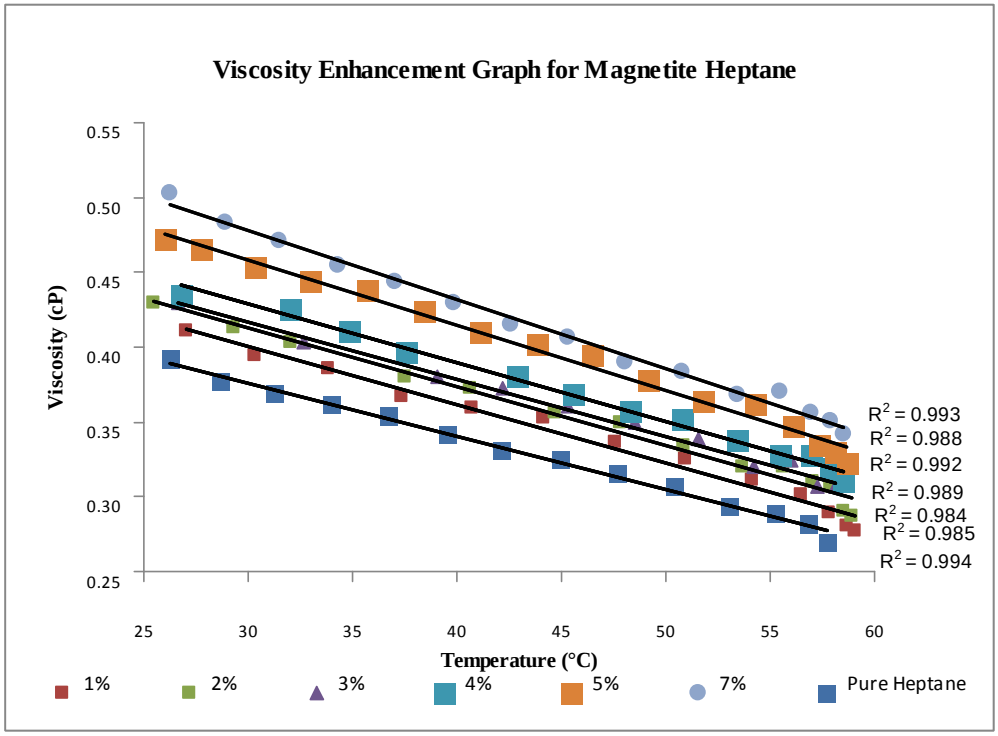

Figure 5.13. Viscosity enhancement for magnetite nanoparticles dispersed in heptane

On the other hand, the relative viscosity ($\mu_{nanofluid}/\mu_{basefluid}$) at 30 ^{o}C, for example, decreases from 1.28 to 1.05 for the particle concentrations between 7% and 1%. Relative viscosities at different temperature values given above are plotted against the particle weight fraction as percentage. Relative viscosity increased by increasing the weight fraction shown in Figure 5.14 although the slopes remained almost the same.

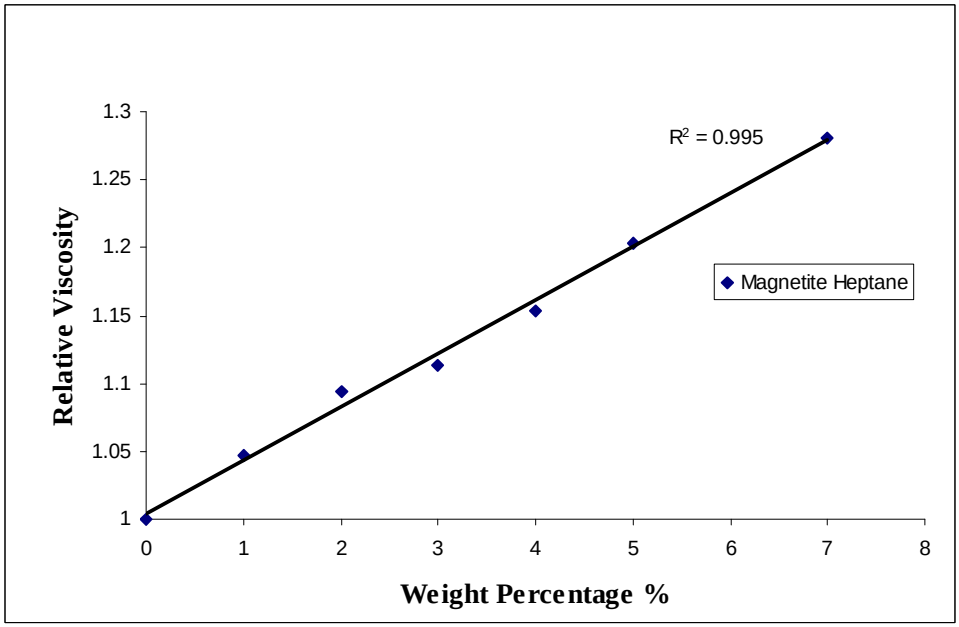

Figure 5.14. Relative viscosities of magnetite nanofluids at 30 ^{o}C

In summary, the viscosity of nanofluid increases considerably with increasing particle concentration. The reason of this effect is that particle concentration affects directly the fluid shear stress. On the other hand, the nanofluid viscosity decreases with increasing temperature since temperature affects the forces among nanoparticles.

There have been several models estimating the viscosities of nanofluids. Einstein's equation (1906) is the first derivation obtained. The viscosity values of nanofluids (μ_{nf}) for magnetite heptane nanofluids at a particular temperature (25^{o}C) and at different particle weight fractions between 1% and 7% are selected in order to compare to those of related theories given in Table 5.1. In this study, two estimations were used for the calculation of volumetric concentrations. One of them was given in Equation 5.1 and the second below [114, 115].

$$\Phi_{\upsilon} = \frac{\rho_{ff} - \rho_{hep}}{\rho_{Fe_3O_4} - \rho_{hep}} \times 100(\%) \tag{5.3}$$

where ρ_{ff} is the density of ferrofluid, ρ_{hep} is the density of heptane, $\rho_{Fe_3O_4}$ is the density of Fe_3O_4. The results are shown in Figure 5.15 and Figure 5.16.

Table 5.1. Viscosity theories and their formulae used in this study [18]

Model	Viscosity Formulae
Einstein (1906)	$\mu_{nf} = (1 + 2.5\phi)\mu_w$
Brinkman (1952)	$\mu_{nf} = \frac{1}{(1-\phi)^{2.5}}\mu_w$
Batchelor (1977)	$\mu_{nf} = (1 + 2.5\phi + 6.25\phi^2)\mu_w$
Ward	$\mu_{nf} = (1 + 2.5\phi + 6.25\phi^2 + 15.6\phi^3)\mu_w$
Wang (1999)	$\mu_{nf} = (1 + 7.3\phi + 123\phi^2)\mu_w$

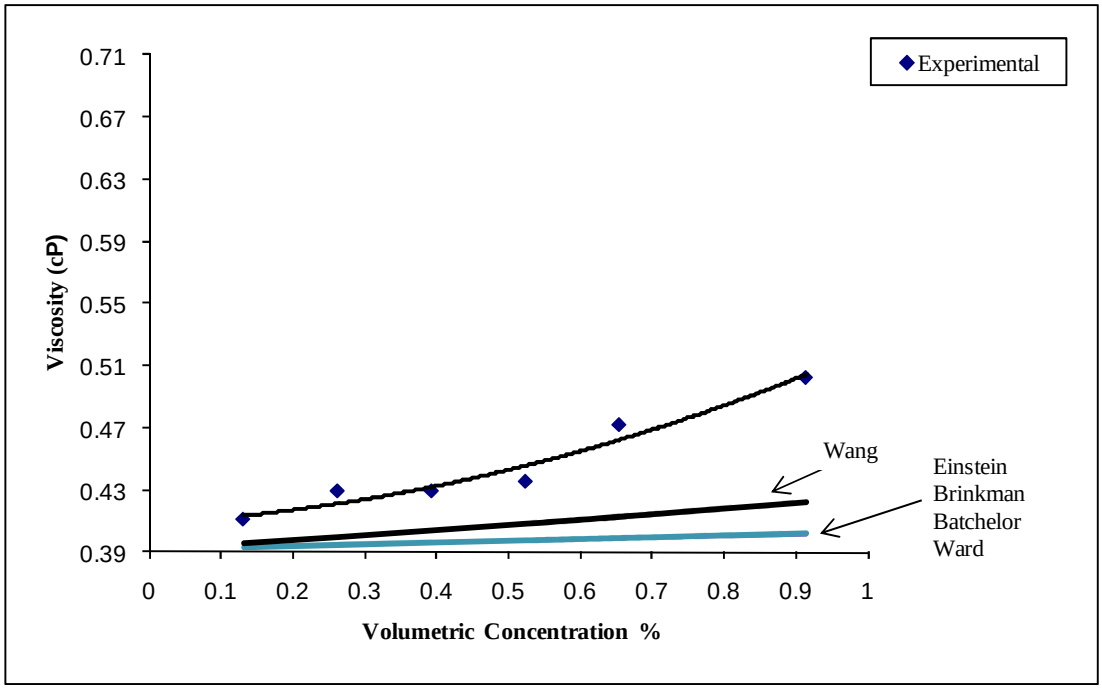

Figure 5.15 Comparison of the viscosity data with theories for magnetite heptanes nanofluid (volumetric concentration was calculated according to [114])

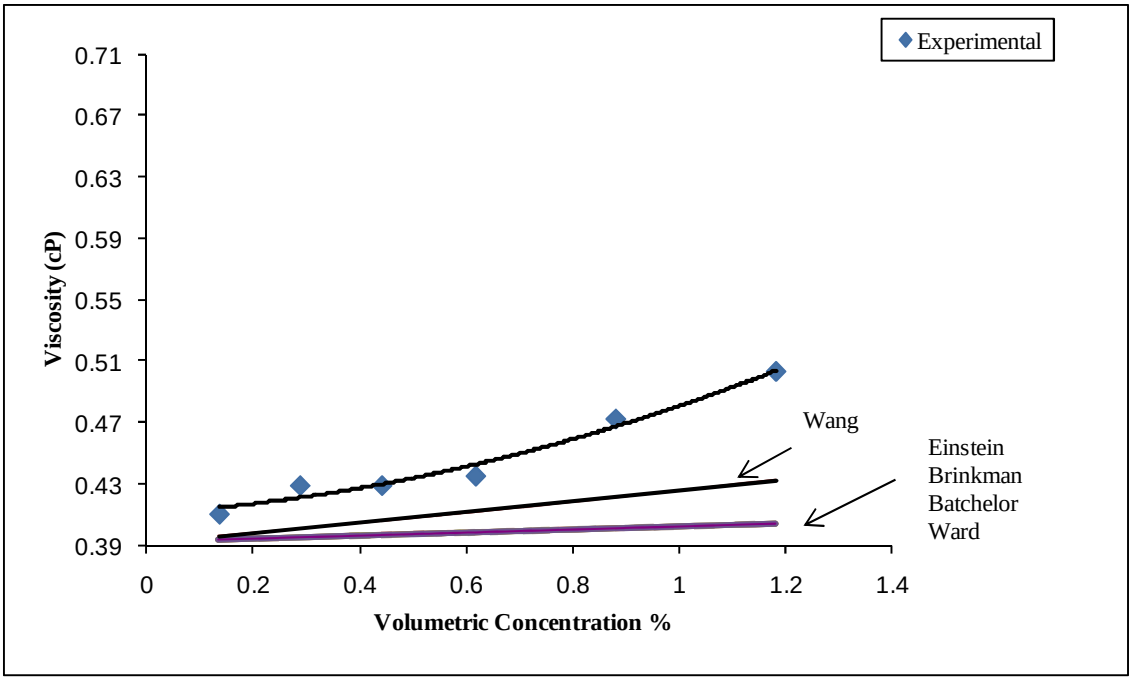

Figure 5.16 Comparison of the viscosity data with theories for magnetite heptane nanofluid (volumetric concentration was calculated according to [115])

The theoretical models used to estimate particle suspension viscosities are generally based on the assumption of a linearly viscous fluid containing dilute, suspended, spherical particles. Einstein's formula is valid for relatively low relative particle volume fractions (ϕ<0.02). For the values higher than this value, it underestimates the effective viscosity of the resulting fluid. In addition, the temperature values vary between 25 °C and 27 °C for each viscosity value, which may cause the fluctuation of the data. Therefore, there are discrepancies between the experimental and theoretical viscosity data as seen in Fig.5.15. But, the second approach is better than before since theoretical result and experimental result are relatively close to each other. Similar discrepancy was obtained by other researchers for SiC-deionized water nanofluids for Brinkman and Batchelor viscosity models [116].

5.2.3. Thermal Conductivity of Ferrofluids

Several measurements were performed over a temperature range covering 25 ^{o}C to 60 ^{o}C. For magnetite nanoparticles dispersed in heptane, 4.80, 3.58 and 0.86 % the

thermal conductivity improvements are measured at the particle fractions of 7, 5 and 1 wt% respectively. The results are presented in Figure 5.17. One can infer from those results that the thermal conductivity increases with weight percentage. This linear increase is best presented in Figure 5.18.

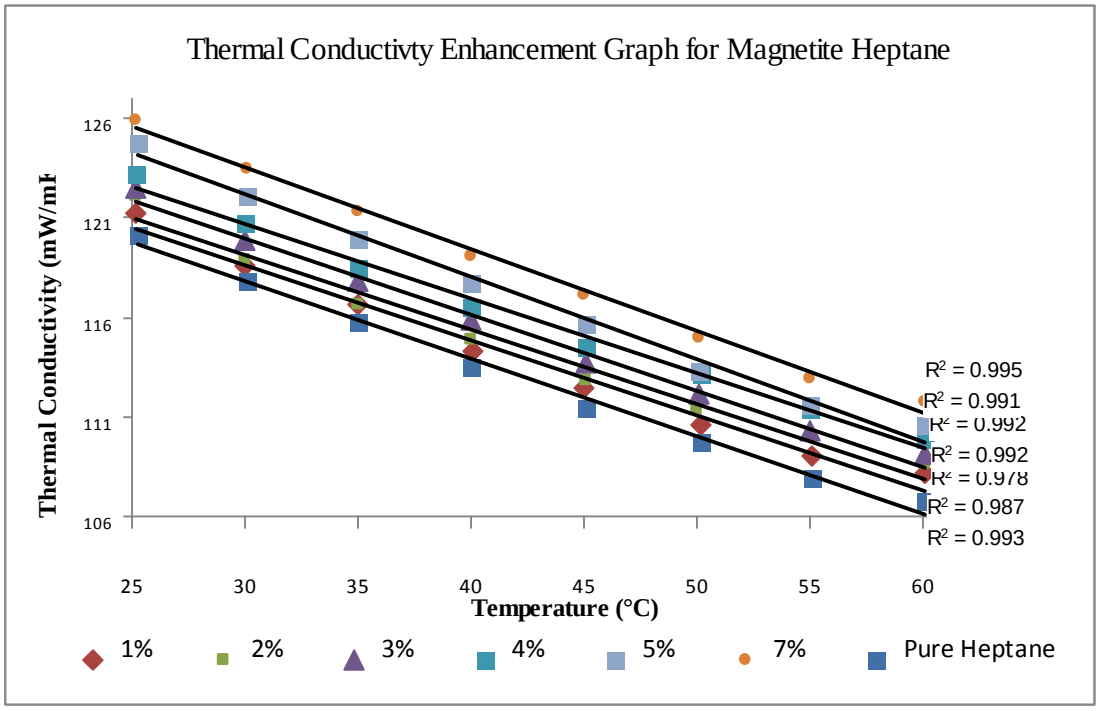

Figure 5.17. Thermal conductivity enhancement of magnetite nanoparticles dispersed in heptane

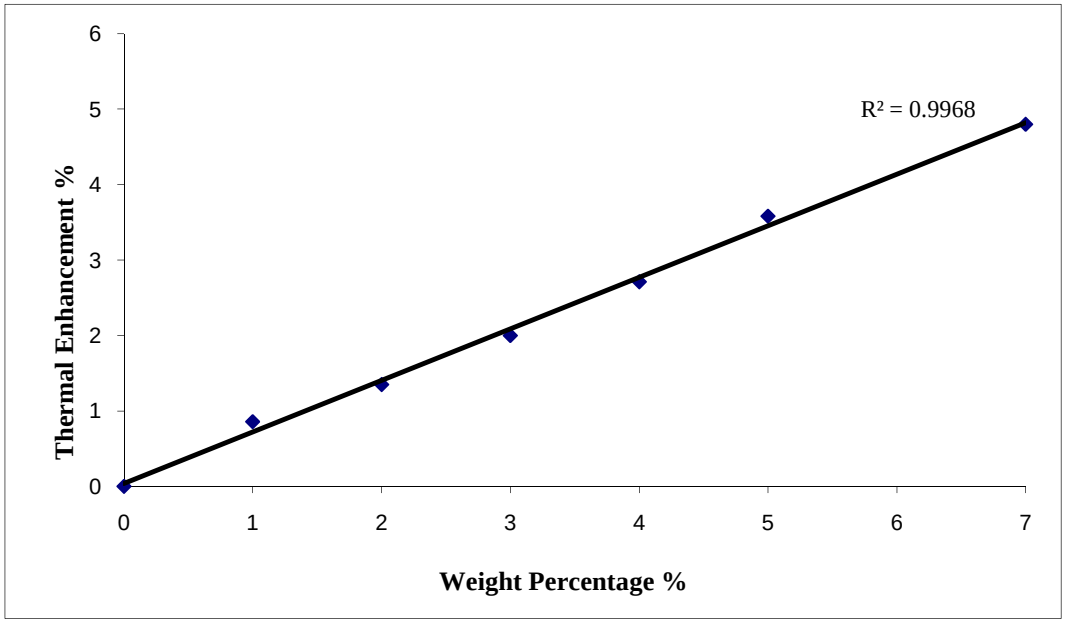

Figure 5.18. Thermal conductivity enhancement of magnetic heptane at each weight concentration

The experimental thermal conductivity results are evaluated in terms of relative thermal conductivities in order to investigate the effect of base fluid in the Figure 5.19 for magnetite heptane. Relative thermal conductivity is defined to be the ratio of the measured thermal conductivity of the nanofluid to the base fluid. The enhancement of thermal conductivity in heptane was found to be directly proportional to the particle concentration.

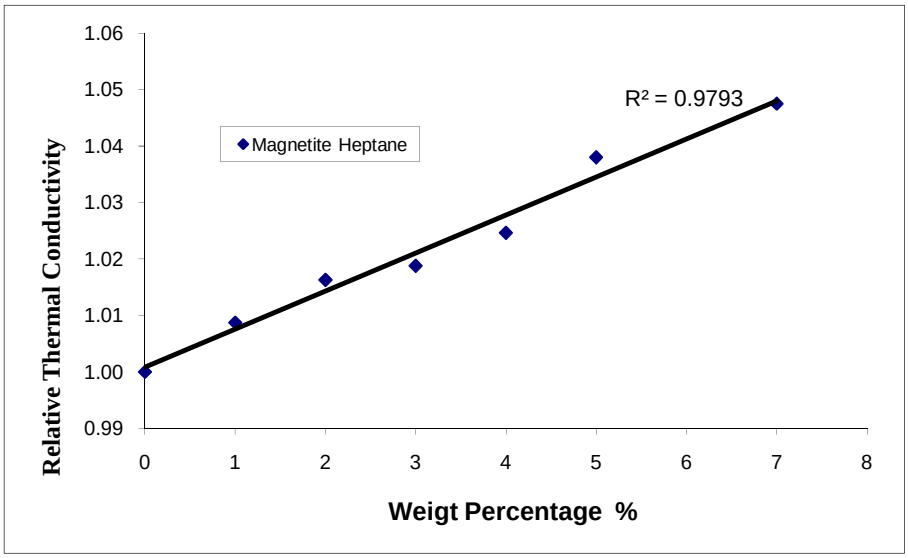

Figure 5.19. Relative enhancement of thermal conductivity upon addition of Fe_3O_4 in heptane as a function of concentration at 25^{o}C

The classical theory of thermal conductivity of fluids with suspended solid particles was developed by Maxwell assuming the nanoparticles to be spherical. However, the model is applicable for relatively large particles. A modified correlation is developed by Wasp (the model function is given in Ref.[21]) indicating that the effective thermal conductivity (k_{eff}) of nanofluids relies on the thermal conductivity of the spherical particle (k_p), base fluid (k_{bf}) and the volume fraction (ϕ) as given in Equation 5.4.

$$\frac{k_{eff}}{k_{bf}} = \frac{k_p + 2k_{bf} - 2\phi(k_{bf} - k_p)}{k_p + 2k_{bf} + \phi(k_{bf} - k_p)} \tag{5.4}$$

According to Figure 5.20, the results from Wasp model underestimate the thermal conductivity for the magnetite heptane nanofluid, although both models and experimental values show an almost linear increase of *k* by weight percentage.

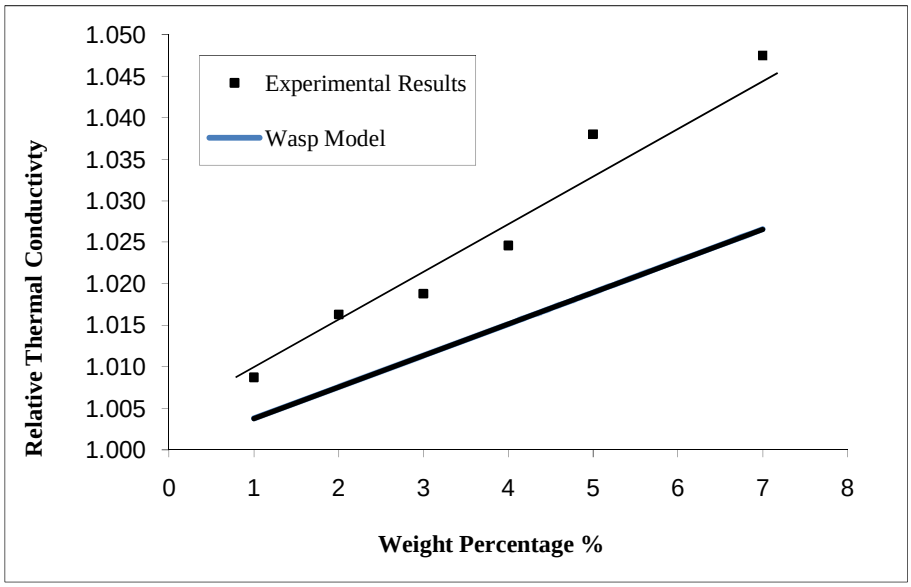

Figure 5.20. Comparison of Wasp model and experimental data obtained from this study for the thermal conductivity of Fe_3O_4 nanoparticles in heptane at 25 °C

5.2.4. Viscosity Measurements of Silica

Some experimental investigations into the viscosity of silicon dioxide (SiO_2) nanoparticles were conducted by several researchers suspended in different solutions such as ethylene glycol and water [57, 62]. On the other hand, the silica was chosen since silicon dioxide nanoparticles are the least expensive nanoparticles making it an ideal test subject. *Namburu et al* have conducted experiments using silicon dioxide nanoparticles with average diameters of 100, 50 and 20 nm in various volume percentages to explore the thermophysical properties of these nanofluids.

The viscosity values of the silicon dioxide particles (Code:2.86 N – 7T) dispersed in ethanol forming nanofluid with varying particle weight concentrations (1, 2, 5, and 10%) between temperatures of 25°C and °35 C are given Figure 5.21.

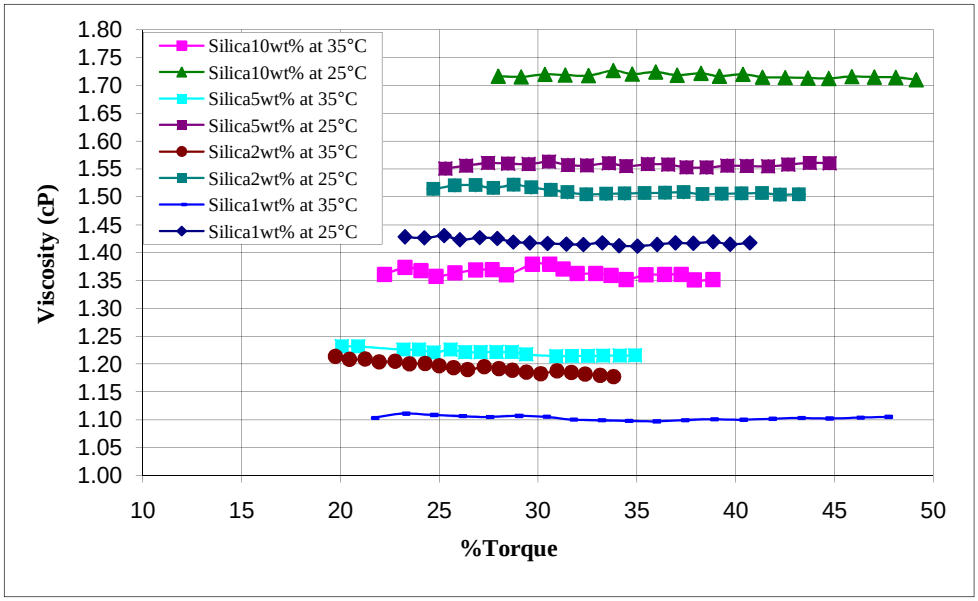

Figure 5.21. Experimental values of viscosity for varying weight concentrations of silicon dioxide nanofluids (128.35 nm) with respect to temperature

These results show that the viscosity (cPoise) is independent with the % torque of the measuring device but it is strongly dependent on the weight increase.

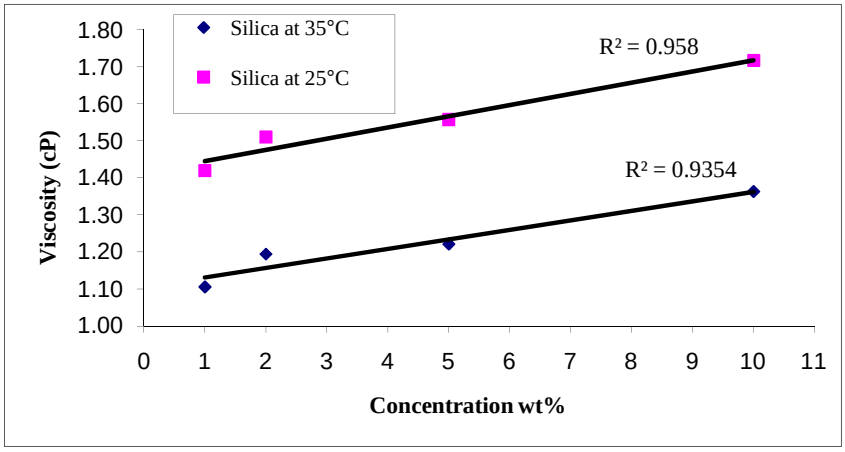

Figure 5.22. Experimental values of viscosity for varying weight concentrations of silicon dioxide nanofluids (128.35 nm) with respect to temperature

Figure 5.22 illustrates the plot of viscosity against weight concentration with increasing temperature. Data indicates that viscosity decreases as the sample fluid temperature increases. Furthermore, it shows that with higher nanoparticle concentrations, nanofluids possess higher viscosity. These behaviours are the same as the magnetite heptane's result given in Figure 5.13 and Figure 5.14. Similar behaviour of silica was obtained by *Namburu et al* [117]. They indicated that with higher nanoparticle concentrations, nanofluids possess higher viscosity. In contrary, viscosity diminishes exponentially as the sample fluid temperature increases.

In summary, the viscosity of nanofluid increases considerably with increasing particle concentration. The reason of this effect is that particle concentration affects directly the fluid shear stress.

5.3. MAGNETIC EFFECT MEASUREMENTS ON FERROFLUIDS

5.3.1. Magnetic Field Sources

Thermal conductivity measurements for magnetic heptane, water and magnetite hexane have been performed using two different magnetic sources. First two measurement have been done by using a simple magnetic coil and the last one by using a homemade U-core electromagnet with the relatively high magnetic field reaching up to 1.7 Tesla. The electromagnet was designed and constructed to get more homogeneous magnetic field. Some articles have been followed to succeed this goal [118, 119, 120, 121].

5.3.1.1. Magnetic Coil

Magnetic field was created by keeping a DC magnet (max. 0.2 Tesla) at a fixed distance from the container including nanofluid. Applied magnetic field was perpendicular to the hot wire equipment utilized in measuring the thermal conductivity (at ambient conditions). The magnet which provides external magnetic field is essentially composed of a cylindrical iron core of length 300 mm and diameter of 40 mm which includes 1500 turns of copper wires of 1.5 mm diameter. The magnet was connected to a DC power supply in order to achieve a steady current within the windings thus producing a steady magnetic

field. It is noted that this magnet was located on the right side of the tube carrying nanofluid, as shown in Figure 5.23.

For reducing the current within the system and suppress the unwanted temperature increase a ballast resistance was also used. The glass test tube which contains the magnetic fluid is located at a distance of 100 mm from the front face of cylindrical magnet and the thermal conductivity sensor which is immersed into the magnetic fluid was connected to the data acquisition system in order to monitor the changes of thermal conductivity. In the experiments, the magnetic fluid was placed in a cylindrical glass tube and exposed to the external magnetic field as shown in Figure 5.23. All measurements were done at ambient conditions and the time interval of measurements was selected to be nearly 35 sec.

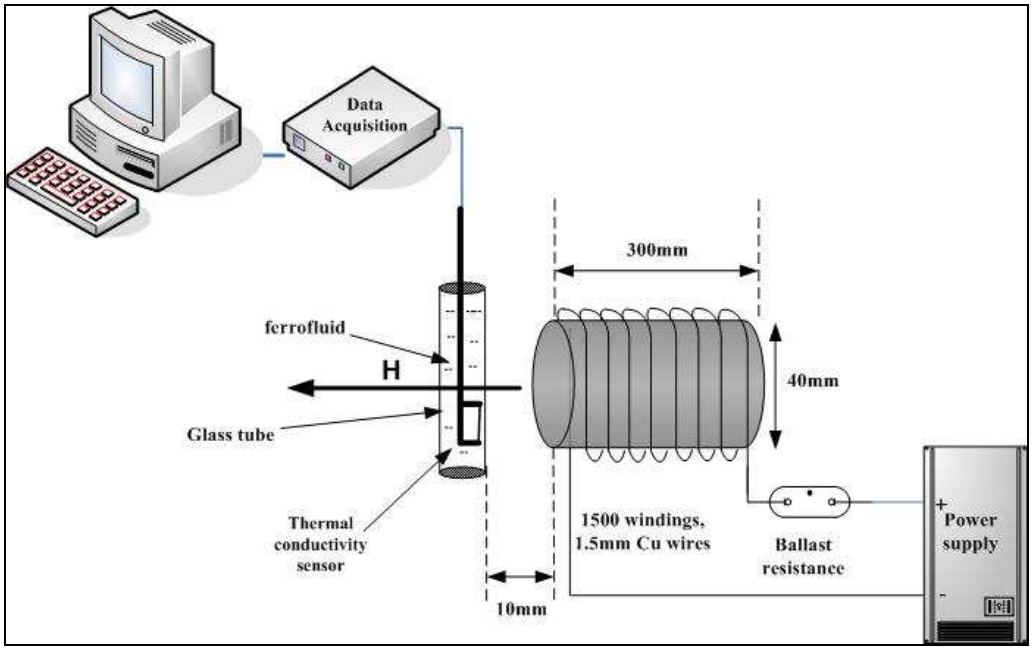

Figure 5.23. Experimental setup for the thermal conductivity measurements at the external magnetic field

5.3.1.2. Homemade U- core DC Electromagnet

The sketch of homemade electromagnet which produces a DC magnetic field through an iron yoke is shown in Figure 5.24.

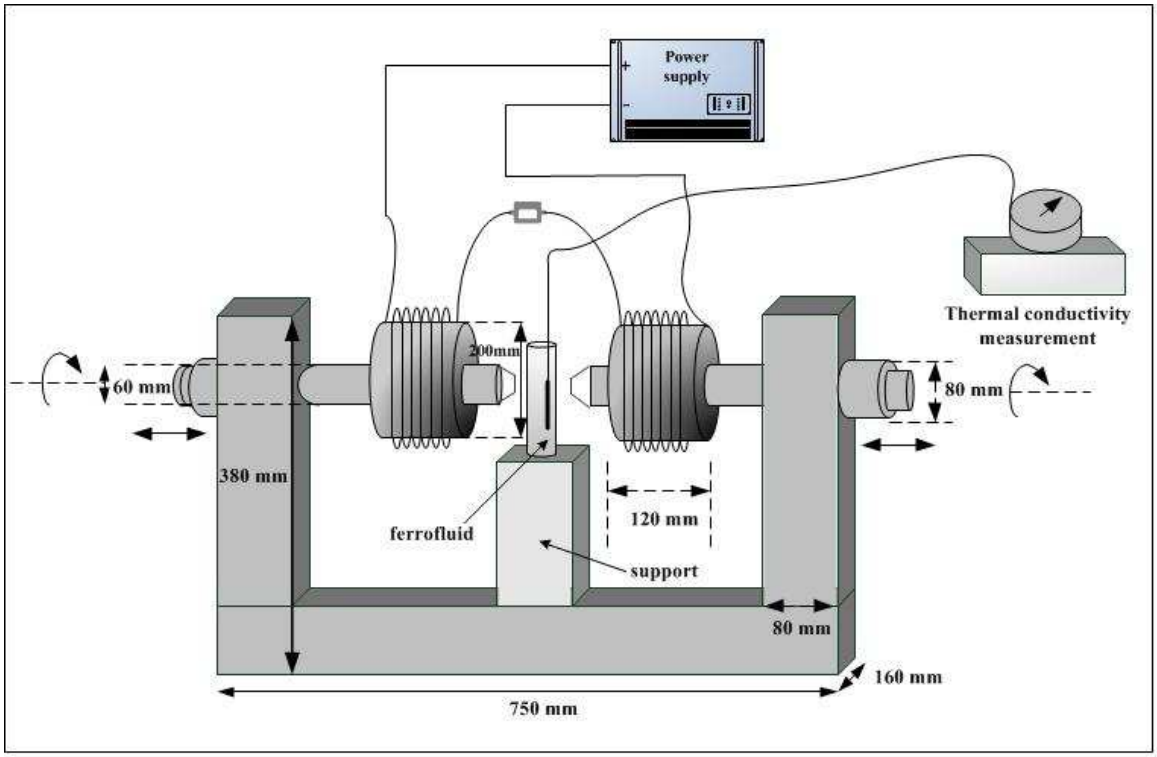

Figure 5.24. The U-core electromagnet and experimental setup for following experiments

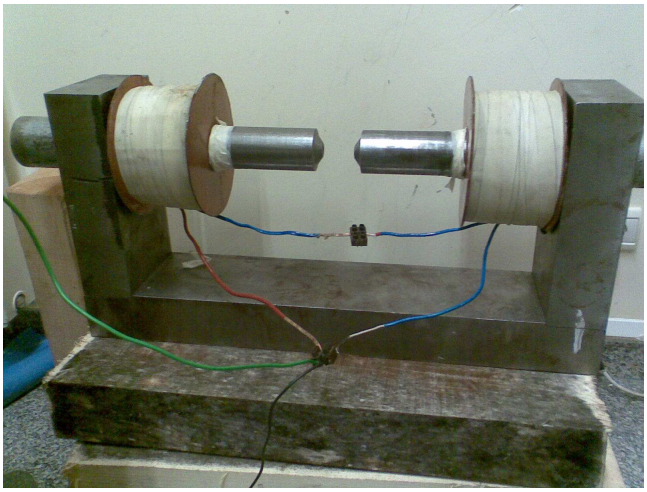

Figure 5.25. The picture of the U-core electromagnet used in this study

As illustrated in Figure 5.25, the poles can be adjusted by moving them back and forward as demand. In addition, the position of coils can also be changed in order to vary magnetic field strength created in the gap between poles. This allows a careful adjustment of the magnetic field by changing the positions of both the poles and coils. A DC power

supply is the main source of the magnetic field strength. According to the characteristic measurements of the magnet, the magnetic field increases linearly with increasing the current and decreases exponentially with increasing gap distance. The external circuit providing a full wave rectified DC voltage with capacitors used for electromagnet is schematically shown in Figure 5.26.

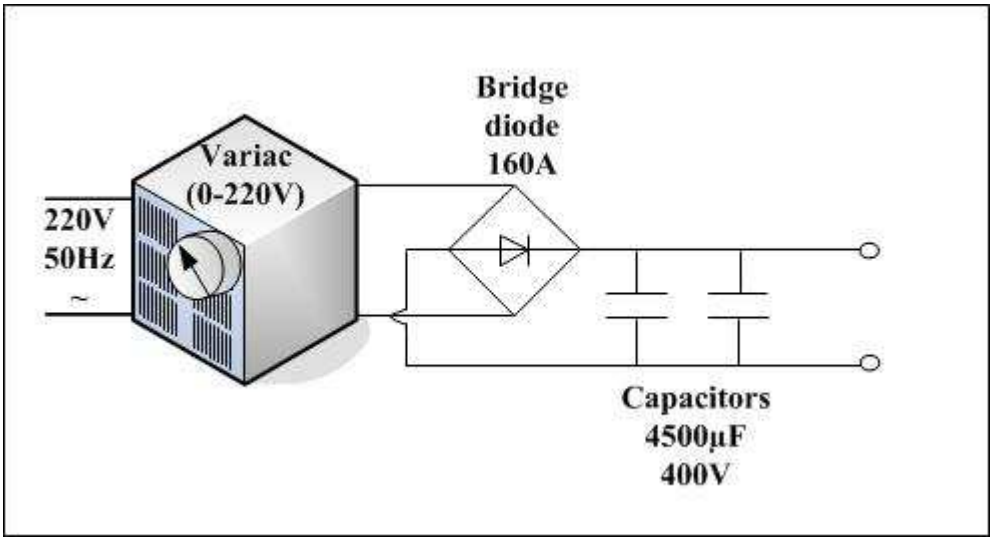

Figure 5.26. The full wave rectified DC circuit used for electromagnet

5.3.2. Thermal Conductivity of Magnetite Heptane and Water under magnetic effect

5.3.2.1. Using a Magnetic Coil

Thermal conductivities of magnetic particles dispersed in water and heptane were measured in the presence of a magnetic field. A magnetic field was created by keeping coils at fixed distances from the container with nanofluid. Applied magnetic field was perpendicular to the hot wire measuring thermal conductivity.

There are a few articles indicating the magnetic effect on thermal conductivity of magnetic nanofluids as mentioned earlier [28, 29, 30, 31, 32]. In one of these articles, Li *et al*. presented no change in the thermal conductivity of magnetic fluid under the magnetic field perpendicular to the temperature gradient. As applied magnetic field was kept parallel to the temperature gradient, they observed an increment in the thermal conductivity of the sample. They concluded that the orientation effect of the magnetic field can be explained

by the formation structure-chain-like aggregation in the sample. In our experiments, we observed a thermal conductivity change when the applied magnetic field was perpendicular to the hot wire measuring thermal conductivity.

Low magnetic fields were applied to samples (0.05 Tesla- 0.2 Tesla) to ensure that the particles are only gently moved in the fluid. Despite these low magnetic fields, it was observed that exposure to magnetic field over a period of time (few minutes) accumulates the particles on the walls of the container which results in the lack of particles (lowering of the concentration) from where thermal conductivity measurements are taken. Therefore, experiments were only carried out for short periods of time to minimize concentration gradient effects (less than 10 minutes).

For either base fluid, a sudden increase in thermal conductivity was observed for magnetic nanofluids upon application the external magnetic field. For a particle loading of 1.63 wt % in water, enhancement of thermal conductivity of 1.93 % and 5.5 % were obtained by applying external magnetic field with strengths of 0.05 Tesla and 0.1 Tesla respectively. On the other hand, for magnetic nanoparticles dispersed in heptane, 0.6 % and 2.7 % enhancement in thermal conductivity was achieved for 1.27 wt. % nanoparticle concentration by the application of 0.1 Tesla and 0.2 Tesla external magnetic fields, respectively.

It can also be seen that the thermal conductivity values become constant with some fluctuations after a period of time showing that the enhancements in thermal conductivity on application of external magnetic field increases the thermal conductivity up to a certain value for a distinct magnetic field strength and concentration.

Upon removal of magnetic field, the thermal conductivity values were observed to settle back to initial values. Enhancement of thermal conductivity on application of magnetic field for water and heptane are presented in Figure 5.27 and Figure 5.28, respectively. These results indicate that the thermal conductivity increases almost linearly by increasing applied magnetic field, as derived by Equation 3.68 in Chapter 3.4. This is presented by the plot given in Figure 5.29 which shows an almost linear increase of thermal conductivity by external magnetic field strength.

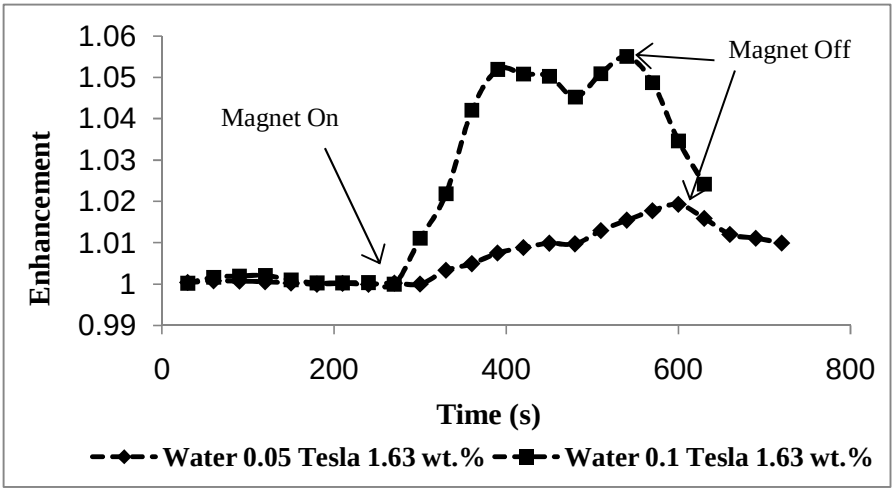

Figure 5.27. Relative enhancement of thermal conductivity in water-based magnetic fluid upon application of an external field

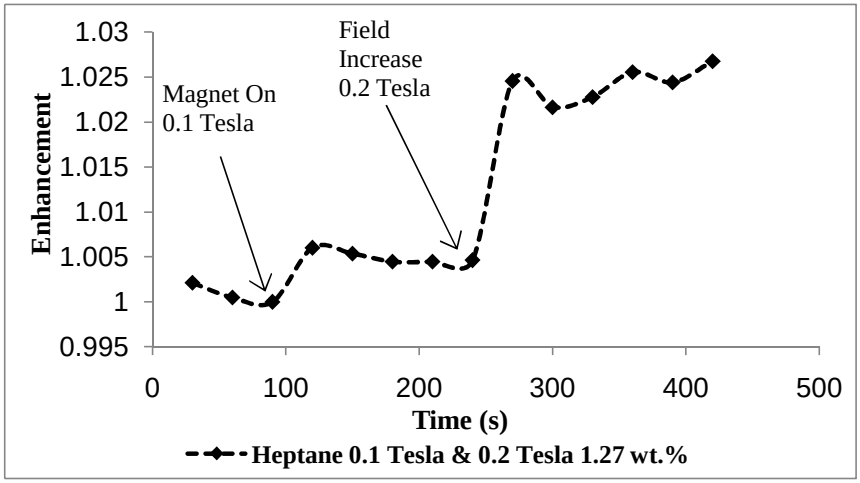

Figure 5.28. Relative enhancement of thermal conductivity in heptane-based magnetic fluid upon application of an external field

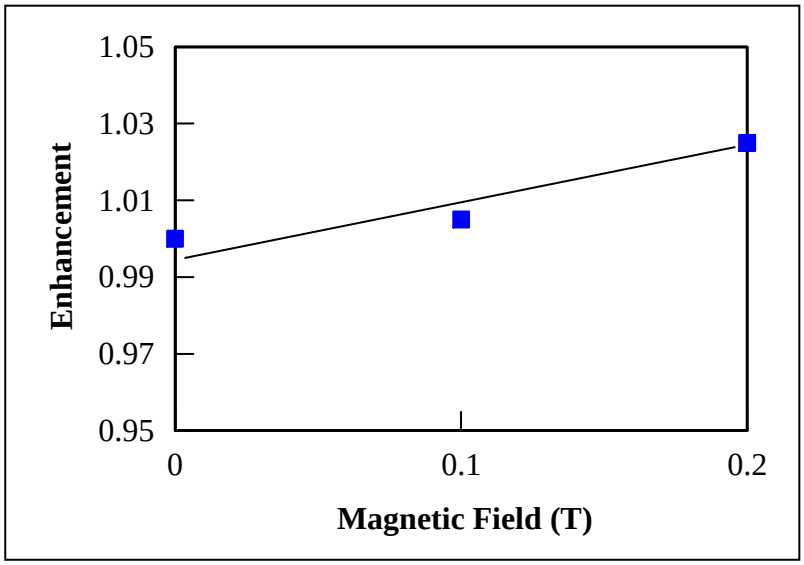

Figure 5.29. The thermal conductivity enhancement of heptane-based magnetic fluid which changes almost linearly by an external field

Due to the paramagnetic nature of particles, when an external magnetic field is applied, the magnetic moments of individual particles cause the particles move in the direction of the field resulting in the depletion of nanoparticles from the walls of the container facing magnet. Simultaneously, due to the heat produced by magnet, one expects that an uncontrolled temperature gradient is also being created parallel to the magnetic field.

The experimental data for both water and heptane clearly show an almost linear increase with increasing magnetic field intensity. This is in excellent agreement with Equation 3.68 derived in Chapter 3.4. This equation also shows a linear dependence of thermal conductivity on magnetic field intensity.

Although the general trend of enhancement upon application of an external field is similar, in comparison, water based fluids show a higher response to magnetic field than heptane based ones. Magnetic cores are identical in both heptane and water suspended particles so this difference cannot be attributed to any size change. Alternatively, the common belief is that the thermal conductivity enhancement is higher if the thermal conductivity of the base fluid is lower than that of particle [122], does not apply here. On the contrary, water has a much higher thermal conductivity than that of heptane as the base

fluids. At this point, although we do not have an explanation to this behaviour, we find it appropriate to present these results as important findings.

Very unusual enhancements of thermal conductivity due to alignment of particles in the magnetic field which results in effective heat transport through chainlike aggregates of nanoparticles were obtained [30]. In our case, both the magnetic fields applied and the concentration of particles were too small to induce these chainlike aggregates therefore the mechanism of thermal conductivity enhancement cannot be due to heat transport through chain formation.

It should be noted that although the particles indeed move when the magnetic field is applied, the measurement intervals are taken at a time scale that is far larger than the time scale of the motion induced by the magnetic field that the measured thermal conductivity is certainly not due to the translational motion of the particles in response to the field. As mentioned above, the particles do indeed move immediately towards the walls of the container, therefore if anything, depleting the medium of nanoparticles should give rise to a lowering of the measured thermal conductivity. But, as seen in both cases where heptane and water are used as solvents, thermal conductivity remains high as long as the magnetic field is on and drops down upon removal of the field.

Considering the low concentration of particles, coupled with low magnetic fields, the observed increase in thermal conductivity can only be attributed to induced motion of the particles which do not result in the formation of chains as described in the literature but rather an increase in the number of contacts between the particles, increasing the thermal transport, causing an enhancement in thermal conductivity.

5.3.2.2. Using U-core Electromagnet

The thermal conductivities of magnetic particles dispersed in heptane were measured in the presence of a magnetic field using U-core electromagnet at this time. Magnetic field was created by changing the supply current. The sample tube was located between the poles of electromagnet. The DC circuit given in Figure 5.26 was used without capacitors here; therefore, the applied voltage is bridged DC in this experiment. Applied

magnetic field was perpendicular to the hot wire measuring thermal conductivity shown in Figure 5.30 and Figure 5.31.

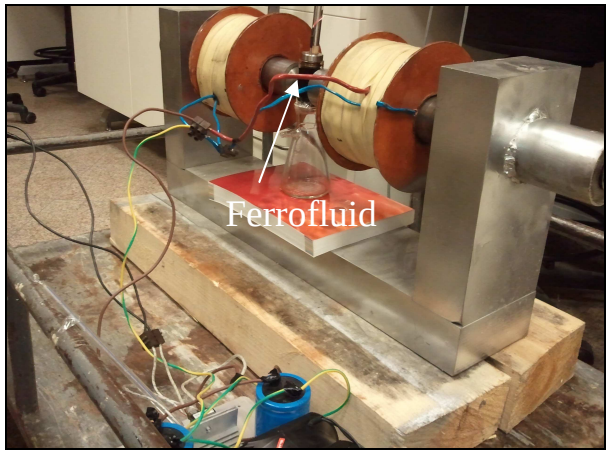

Figure 5.30. A picture of the thermal conductivity measurement with the effect of external magnetic field

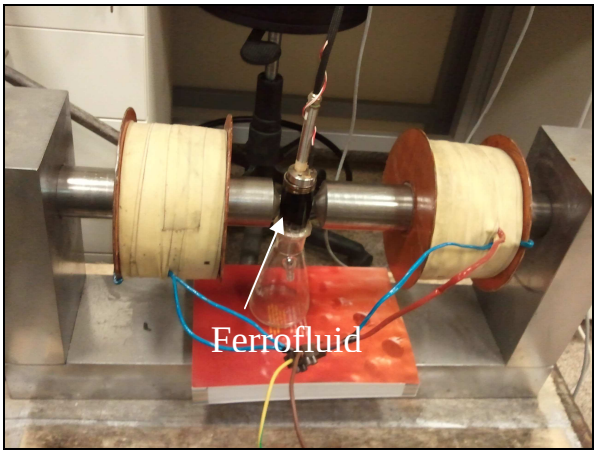

Figure 5.31. The ferrofluid located in the gap between magnetic poles

For magnetic nanoparticles dispersed in heptane, average 5.2 % enhancement in thermal conductivity was achieved for 1.27 wt. % of nanoparticle concentration by the application of 0.2 Tesla external magnetic field, which is higher than that of the obtained with the magnetic coil (Figure 5.32). The thermal conductivity values settle back to the almost initial values when the magnetic field is turned off. This behaviour was observed by several turning the magnet on and off for nearly 2200 seconds.

Although the data at t=1200s show strange behaviour (probably due to wrong measurement by device) all cases show similar sudden increase and decrease upon turning the magnet on and off. These results show that the ferrofluid does not have a memory effect and does not store the magnetic field applied externally. Figure 5.32 shows the relative enhancement of thermal conductivity in heptane-based magnetic fluid upon application of an external field.

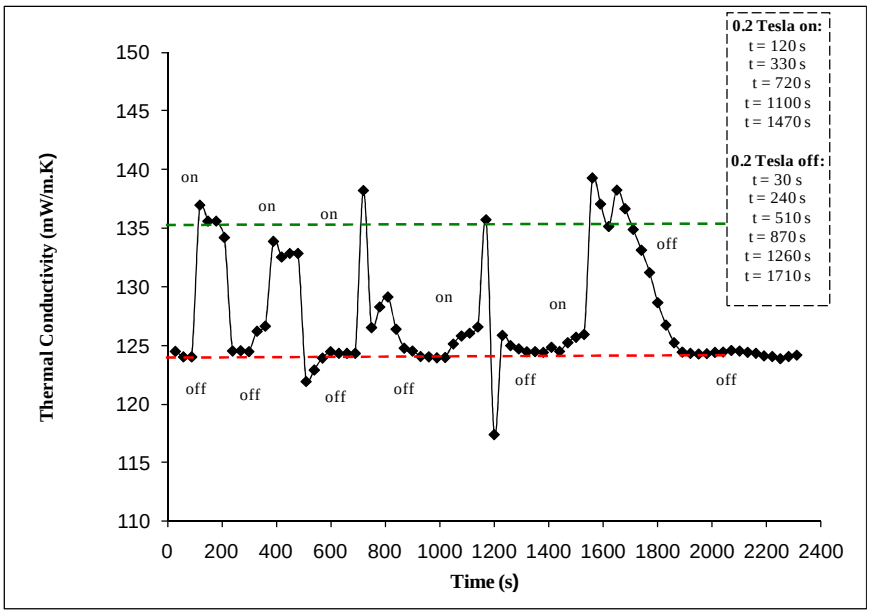

Figure 5.32. Relative enhancement of thermal conductivity in heptane-based magnetic fluid upon application of an external field

5.3.3. Thermal Conductivity of Magnetite Hexane under Magnetic Effect

Thermal conductivities of magnetic particles dispersed in hexane were measured in the presence of a magnetic field. Magnetic field was created by keeping an electromagnet at a fixed distance from the container with nanofluid in Figure 5.31. In this experiment, two capacitors of 4500 μF, 400 V were connected in parallel to rectify the power supply shown in Figure 5.26. In this case, a pure DC source was obtained. Applied magnetic field was perpendicular to the hot wire measuring thermal conductivity, as before.

Opposing previous findings, a sudden reduction in thermal conductivity was observed for magnetic nanofluids upon application of a small external magnetic field. For a

particle loading of 1.07 wt % in hexane, reduction of thermal conductivity of 1.13 %, 2.73 % and 2.76 % were obtained by applying external magnetic field with strengths of 0.1 Tesla, 0.18 Tesla and 0.3 Tesla respectively. This behaviour may be due to the chemical properties of the base fluid.

Hexane is not a suitable solvent for these experiments due to its low boiling point (69 ^{o}C). Heptane and water have similar boiling points, 97 ^{o}C and 100 ^{o}C respectively which allow experiments to be carried out at ambient temperatures without having to completely seal the system. Figure 5.33 shows the relative reduction of thermal conductivity in hexane-based magnetic fluid upon application of an rectified DC external field. These results show that either heptane or water should be used if thermal conductivity enhancement is desired upon magnetic field application.

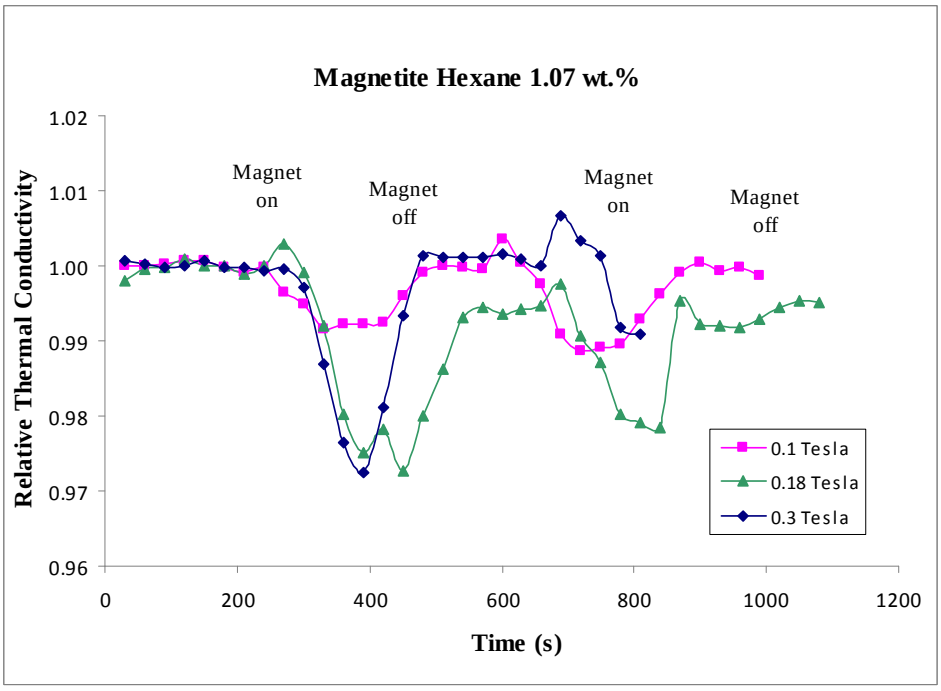

Figure 5.33. Relative reduction of thermal conductivity in hexane-based magnetic fluid upon application of an rectified DC external field

A reduction on thermal conductivity under the effect of magnetic field was also observed by several researchers [123, 124]. Djurek *et al.* measured thermal conductivities of ferrofluids (γ-Fe_2O_3 of 8–15 nm in water and in n-decane and $CoFe_2O_4$ dispersed in

water) at 25 °C in a magnetic field generated by an external coil receiving current from DC power supply and they observed a decrease on thermal conductivity with increasing the field strength up to 2–3 × 10^{-2} T, which was followed by field independence in higher fields. Magnetic field effects of thermal conductivities of four ferrofluid samples (Sample 1: $CoFe_2O_4$ dispersed in water (≈150 g/L), sample 2: γ-Fe_2O_3 dispersed in water (≈120 g/ L) with specific magnetization 55 emu/g; sample 3: γ-Fe_2O_3 dispersed in n-decane (≈300 g/ L), sample 4: γ-Fe_2O_3 dispersed in water (≈65 g/ L)) indicate a decrease with increasing the external field for low fields, and a rather constant value for higher fields. According to their results, the strongest relative decrease of thermal conductivity with the magnetic field was observed in $CoFe_2O_4$ nanoparticles (sample 1) dispersed in water [123].

According to Djurek *et al.*, the relative thermal conductivities reduces to about 0.96, 0.7 and 0.64 for about 0,01 Tesla, 0,018 Tesla and 0,03 Tesla for sample 3, respectively, and to about 0.93, 0.91 and 0.85 for about 0,01 Tesla, 0,018 Tesla and 0,03 Tesla for sample 2, respectively [123].

When a magnetic field is applied, the correlated motion in particle gas reduces the mass transport, or simply, the superparamagnetic state reduces the entropy when the magnetic field is exerted to it. An interesting result is the decrease of thermal conductivity with increasing mass of nanoparticles, which is hard to explain by the existing models and theories [123].

The other example is from the study of Shima *et al.* (2009) who investigated the magnetic field effect on magnetic nanofluid. To apply a uniform magnetic field to the fluid, the entire sample cell is kept inside a solenoid, where the field is varied by changing the current. They observed decreased k/k_f value from about 4 to about 1.7 by using magnetic field parallel to the temperature gradient in magnetic field range (82–283 G). Further, an increase in magnetic field leads to a stabilization of k/k_f at a marginal value of 1.41 [124].

As the external magnetic field is slowly increased from zero to a large value, bulk field responsive fluids such as magnetorheological fluids undergo several structural transitions from a gas of Brownian colloids to randomly distributed chains of colloids

aligned in the field direction. This aggregation into chains is known as head-to-tail aggregation. As the field is further increased, the chains of colloids begin to aggregate laterally in order to form clusters of zipped chains, which are known as zippering [125].

According to Shima *et al.*, the observed decrease in thermal conductivity above 82 G could be due either due to “zippering” of chains mentioned above. Mapping of the magnetic field within the probe area shows fairly uniform field and hence the possibility of induced body forces can be ruled out. However, the linear and thick aggregates with high aspect ratio due to zippering can collapse to the bottom of the cell and hence cannot be seen by the hotwire [124].

6. CONCLUSION AND FUTURE WORK

Nanoparticles forming the nanofluids were examined by Transmission Electron Microscopy (TEM), Dynamic Light Scattering (DLS), X-Ray diffraction (XRD) and Scanning Electron Microscopy (SEM) in order to obtain their size, shape and structural information. In addition, VSM measurements have been conducted to obtain the magnetization behaviour of the magnetite nanofluids by obtaining their M-H curves.

Transmission electron microscopy (TEM) results revealed that the hydrophobic and hydrophilic magnetite particles synthesized are almost spherical although not very regular in shape with slight polydispersity in size with an average diameter of about 10 nm. TEM images also indicate that both types of nanoparticles do not have any noticeable agglomeration.

The intensity averaged particle distribution obtained by DLS was found to be between 5-20 nm with an average of approximately 10 nm, which is in perfect agreement with TEM results for the size distribution measurements. According to the XRD results, it can be concluded that no characteristic peaks of impurities were observed for Fe_3O_4 nanoparticles.

VSM measurements taken for magnetic nanofluids showed that there is no hysteresis loop indicating the superparamagnetis. Therefore, the curves here are anhysteretic, but sinusoidal. The magnetic fluids carrying superparamagnetism feature gave no remanence and no the coercivity field as superparamagnetism behaviour , as expected. At the lower field strength, a small change in the magnetic field caused a substantial change in the magnetization of the magnetic fluid as long as the magnetic field is below the saturation point. At the higher field strength, the magnetic moments of the particles aligned with the external field and reached its saturation value. The curves obtained by experimentally state that the slopes increased as weight percentage increased meaning that the magnetic susceptibility increased with weight percentage. This is an expected result since increased weight percentage causes the magnetization increase.

The SEM image of silica (2.86N-7T) showed that nanoparticles are almost perfectly spherical shape with diameters near 100 nm. The size distribution of silica 2.86N-7T by DLS maximize at the size of 128 nm. This result is in perfect agreement with The SEM result. The DLS results for the same sample values 155.2-149.6 and 108.4-108.7 are found. The sizes of the cluster are near 120 and 90 nm, respectively.

Thermophyical measurements including density, viscosity and thermal conductivity were obtained without the effect of external magnetic field for nanofluids.

The densities of magnetite nanofluids containing various amounts of nanoparticles dispersed in heptane are measured over a temperature range from 25 ^{o}C and 60 ^{o}C. The density increased with increasing nanoparticle concentration as expected. The density enhancement of magnetite nanoparticles dispersed in heptane having a particle loading of 7 wt% is obtained as 7.78%, and the density enhancement of magnetite nanoparticles dispersed in heptane having a particle loading of 1 wt% is obtained as 0.90% both at 25 ^{o}C. The density enhancement of magnetite nanoparticles dispersed in heptane having a particle loading of 7 wt% is obtained as 7.86% calculated over average values. Density values are decreased with increasing temperature as expected. Experimental values were compared with the theoretical model (Pak and Cho) and the theoretical model showed good agreement for magnetite nanofluids at all concentrations. Experimental density values are higher than the theoretical density values. Although the model represents good agreement with experimental data, Pak and Cho developed it for nanofluids with lower concentrations. That’s why, the deviations increase with the increase in the particle concentration.

In this study, viscosities of magnetite nanoparticles dispersed in heptane were measured over the temperature range of 25 ^{o}C to 60 ^{o}C. Magnetite heptane nanofluid with varying particle loadings from 1% to 7%, viscosity enhancement is from 2.6% to 24.9%. The viscosities of nanofluids increased considerably with increasing particle concentration and decreased linearly with decreasing temperature. The viscosity values for magnetite heptane nanofluids at 25^{o}C and at different particle weight concentrations between 1% and 7% were selected in order to compare to those of related theories. Volumetric concentrations calculated by two different methods. There are discrepancies between the

experimental and theoretical viscosity data, but similar discrepancy was obtained by other researchers. The second approach used for calculating the volumetric concentrations was better than that of first method since theoretical result and experimental result relatively close to each other. Therefore, there are discrepancies between the experimental and theoretical viscosity data since the theoretical models used to estimate particle suspension viscosities are generally based on the assumption of a linearly viscous fluid containing dilute, suspended, spherical particles. In addition, the temperature values vary between 25 °C and 27 °C for each viscosity values, which may cause the fluctuation of the data. Similar discrepancy was obtained by other researchers.

Thermal conductivity measurements for magnetite nanoparticles dispersed in heptane were performed over a temperature range covering 25 ^{o}C to 60 ^{o}C. 4.80, 3.58 and 0.86 % thermal conductivity improvements were measured at the particle fractions of 7, 5 and 1 wt% respectively. One can infer from those results that the thermal conductivity increases with weight percentage. This is in excellent agreement with the theoretical derivations of thermal conductivity as a function of external field and weight percentage (see Equation 3.68 derived in Chapter 3.4). Wasp model was used to compare the experimental results. The thermal conductivity results from Wasp model underestimate for the magnetite heptane nanofluid, although both model and experimental values showed an almost linear increase of thermal conductivity by weight percentage.

The viscosity values of the silicon dioxide particles dispersed in ethanol forming nanofluid with varying particle weight concentrations (1, 2, 5, and 10%) between temperatures of 25°C and °35 C were measured. The results showed that the viscosity is independent with the % torque of the measuring device but it is strongly dependent on the weight increase. Data indicated that viscosity decreased as the sample fluid temperature increased. Data showed also that with higher nanoparticle concentrations, nanofluids possess higher viscosity.

Thermal conductivity measurements for magnetic heptane and water were taken using the magnetic coils reaching up to maximum 0.2 Tesla. A sudden increase in thermal conductivity was observed for magnetic nanofluids when an external magnetic field was applied to the sample. For a particle loading of 1.63 wt % in water, enhancement of

thermal conductivity of 1.93 % and 5.5 % were obtained by applying external magnetic field with strengths of only 0.05 Tesla and 0.1 Tesla respectively. On the other hand, for magnetic nanoparticles dispersed in heptane, 0.6 % and 2.7 % enhancement in thermal conductivity was achieved for 1.27 wt. % nanoparticle concentration by the application of 0.1 Tesla and 0.2 Tesla external magnetic fields, respectively. Thermal conductivity values become constant with some fluctuations after a period of time. Upon removal of magnetic field, the thermal conductivity values were observed to settle back to initial values. The experimental data for both water and heptane clearly show an almost linear increase with increasing magnetic field intensity. This is also in excellent agreement with Equation 3.68 derived in Chapter 3.4. This equation also shows a linear dependence of thermal conductivity on magnetic field intensity.

On the other hand, the thermal conductivities of magnetic particles dispersed in heptane were measured in the presence of the DC (full wave bridged by a bridge diode of 160 A) external magnetic field using homemade electromagnet as an alternative. For magnetic nanoparticles dispersed in heptane, average 5.2 % enhancement in thermal conductivity is achieved for 1.27 wt. % nanoparticle concentration by the application of 0.2 Tesla external magnetic field, which is higher than that of the obtained with the magnetic coil. The thermal conductivity values come back to the almost initial values when the magnetic field is turned off. These results showed that the ferrofluid does not have a memory effect and does not store the magnetic field applied externally.

As a last step, the thermal conductivities for magnetite hexane were measured using the homemade electromagnet by applying a DC (rectified by two capacitors of 4500 μF in parallel and bridge diodes of 160A) external magnetic field. Applied magnetic field was perpendicular to the hot wire measuring thermal conductivity. Opposing previous findings, a sudden decrease in thermal conductivity was observed for magnetic nanofluids upon the application of a small external magnetic field. For a particle loading of 1.07 wt % in hexane, decrease of thermal conductivity of 1.13 %, 2.73 % and 2.76 % were obtained by applying external magnetic field with strengths of 0.1 Tesla, 0.18 Tesla and 0.3 Tesla respectively.

As a conclusion, the theoretical derivation and experimental results for thermal conductivity for magnetite heptane and water matched well. The magnetic effects on thermal conductivity for magnetite heptane for DC (fully rectified) magnetic field can be investigated to understand the nature of the effect well. New set of experiments can be performed in the future for different types of ferrofluids at different concentrations by changing the magnetic field in a wide range.

APPENDIX A: UNCERTAINTY ESTIMATION AND ERROR ANALYSES OF THERMOPHYSICAL MEASUREMENTS

As a model function, Fourier's law of heat conduction is chosen for the uncertainty analyses thermal conductivity measurements. In the simplest arrangement, one needs to establish a steady one dimensional heat flow by the application of a known heat flux. Then by measuring the temperatures at two known locations along the direction of heat transmission one can estimate the thermal conductivity as follows:

$$k = \frac{q/A}{\Delta T/L} \tag{A.1}$$

where q is the magnitude of heat transmission through nanofluid and ΔT is the temperature difference across length L and cross-sectional area A. The uncertainty of thermal conductivity measurements was determined from the following equation according to GUM, ISO 1995 Guide to the Expression of Uncertainty in Measurement and EA-4/02-1999 Expression of the Uncertainty of Measurement in Calibration by taking $q=q_e-q_i$. Here $q_e=VI$ where V is the voltage and I is the current applied to the hotwire. By considering the uncertainties of these two quantities are about 0.5%, the uncertainty for the q_e is 0.7%.

$$u_k = \left[\left(\frac{\partial q_e}{q_e} \right)^2 + \left(\frac{\partial q_i}{q_i} \right)^2 + \left(\frac{\partial L}{L} \right)^2 + \left(\frac{\partial A}{A} \right)^2 + \left(\frac{\partial (\Delta T)}{\Delta T} \right)^2 \right] \tag{A.2}$$

Incidental heat transfer q_i is obtained from the calibration plot of q_i versus temperature difference (T_1-T_2) at the different times t_1 and t_2. The uncertainty in measurements of temperature is 0.1°C between the whole temperature ranges according to the device manual. At the mean temperature of 45 °C within the range of experiments, the uncertainty resulting from temperature is 0.2%. The uncertainty in length measurement can be taken as 0.5% for standard dimensional gage. On the other hand, the area is proportional to the square of the L, therefore the uncertainty in the area measurement is 1%. The

uncertainty in ΔT measurement results from T_1 and T_2. As a result, all components are given as follow:

$$u_k = \left[\left(\frac{\partial V}{V}\right)^2 + \left(\frac{\partial I}{I}\right)^2 + \left(\frac{\partial T_1}{T_1}\right)^2 + \left(\frac{\partial T_2}{T_2}\right)^2 + \left(\frac{\partial L}{L}\right)^2 + \left(2\frac{\partial L}{L}\right)^2 + \left(\frac{\partial T_1}{T_1}\right)^2 + \left(\frac{\partial T_2}{T_2}\right)^2 \right] \quad \text{(A.3)}$$

Finally, the standard uncertainty in measurement of thermal conductivity is calculated as 2.7%.

Table A.1. Comparison of experimental measurements of density of pure n-heptane with the literature values as a function of temperature at atmosferic pressure [126]

Temperature (K)	**Density (g/cm^3)**		**Relative Error (%)**
	Literature	**Experimental**	
298.15	0.6795	0.6815	0.3
303.15	0.6755	0.6773	0.3
313.15	0.6675	0.6687	0.2
323.15	0.6591	0.6600	0.1

Table A.2. Comparison of experimental measurements of viscosity of pure n-heptane with the literature values as a function of temperature at atmosferic pressure [126]

Temperature (K)	**Viscosity (mPa.s)**		**Relative Error (%)**
	Literature	**Experimental *(Best Fit)***	
298.15	0.3912	0.3934	0.6
303.15	0.3707	0.3759	1.4
313.15	0.3352	0.3409	1.7
323.15	0.3041	0.3059	0.6

APPENDIX B: UNITS FOR MAGNETIC PROPERTIES

Table B.1. Units for magnetic properties [127]

Physical quantity	**Symbol**	**Gaussian & cgs emu[a]**	**Conversion factor, C[b]**	**SI & rationalized mks[c]**
Magnetic flux density, magnetic induction	*B*	Gauss (G)[d]	10^{-4}	Tesla (T), Wb/m^2
Magnetic potential difference, magnetomotive force	*U, F*	gilbert(Gb)	$10/4\pi$	ampere (A)
Magnetic field strength, magnetizing force	*H*	oersted (Oe), [e] Gb/cm	$10^3/4\pi$	A/m[f]
(Volume) magnetization[g]	*M*	emu/cm^{3h}	10^3	A/m
(Volume) magnetization	$4\pi M$	G	$10^3/4\pi$	A/m
Magnetic polarization, intensity of magnetization	*J, I*	emu/cm^3	$4\pi \times 10^{-4}$	T, Wb/m^{2i}
(Mass) magnetization	*σ, M*	emu/g	1 $4\pi \times 10^{-7}$	$A \cdot m^2/kg$ $Wb \cdot m/kg$
Magnetic moment	*m*	emu,erg/G	10^{-3}	$A \cdot m^2$, joule per tesla (J/T)
Magnetic dipole moment	*j*	emu,erg/G	$4\pi \times 10^{-18}$	$Wb \cdot m^i$

Table B.1. Units for magnetic properties [127] (*continue*)

Physical quantity	**Symbol**	**Gaussian & cgs emu[a]**	**Conversion factor, C[b]**	**SI & rationalized mks[c]**
(Volume) susceptibility	χ, κ	dimensionless, emu/cm^3	$4\pi\ (4\pi)^2 \times 10^{-7}$	Dimensionless henry per meter (H/m), Wb/(A · m)
(Mass) susceptibility	χ_ρ, κ_ρ	cm^3/g, emu/g	$4\pi \times 10^{-3}$ $(4\pi)^2 \times 10^{-10}$	m^3/kg $H \cdot m^2/kg$
(Molar) susceptibility	χ_{mol}, κ_{mol}	cm^3/mol, emu/mol	$4\pi \times 10^{-6}$ $(4\pi)^2 \times 10^{-13}$	m^3/mol $H \cdot m^2/mol$
Permeability	μ	dimensionless	$4\pi \times 10^{-7}$	H/m, Wb/(A · m)
Relative Permeability[j]	μ_r	not defined	-	Dimensionless
(Volume) energy density, energy product[k]	W	erg/cm^3	10^{-1}	J/m^3
Demagnetization factor	D, N	dimensionless	$1/4\pi$	Dimensionless
Magnetic flux	Φ	maxwell (Mx), $G \cdot cm^2$	10^{-8}	Weber (Wb), Volt · second (V· s)

[a]Gaussian units and cgs emu are the same for magnetic properties. The defining relation is $B = H + 4\pi M$.

[b]Multiply a number of C to convert it to SI (e.g. $1G \times 10^{-4} T/G = 10^{-4} T$).

[c]SI (*Syst`eme International d'Unit´es*) has been adopted by the National Bureau of Standards. Where two conversion factors are given, the upper one is recognized under, or consistent with, SI and is based on the definition $B = \mu_0 H + J$, where the symbol I is often used in place of J .

[d]1 gauss = 10^5 gamma (γ).

[e]Both oersted and gauss are expressed as $cm^{-1/2} \cdot g^{-1/2} \cdot s^{-1}$ in terms of base units.

[f] A/m was often expressed as 'ampere-turn per meter' when used for magnetic field strength.

[g]Magnetic moment per unit volume.

[h]The designation 'emu' is not a unit.

[i]Recognized under SI, even though based on the definition $B = \mu_0 H + J$. See footnote *c*.

[j]$\mu_r = \mu/\mu_0 = 1 + \chi$, all in SI. Relative permeability μ_r is equal to Gaussian μ

[k]$B \cdot H$ and $\mu_0 M \cdot H$ have SI units J/m^3; $M \cdot H$ and $B \cdot H/4\pi$ have Gaussian units erg/cm^3.

REFERENCES

1. Wooding, A., Kilner, M., Lambrick, D.B., *Studies of the double surfactant layer stabilization of water-based magnetic fluids*, J. Colloid Interface Sci., Vol. 144, pp. 236-242, 1991.

2. Feynman, R., *There's plenty of room at the bottom*, Engineering & Science 23, pp. 22-36, 1960.

3. *International Competitive Strategies: Nanotechnology and Turkey*, TÜSİAD Competitive Strategies Series-11, No:TÜSİAD-T/2008-11/474, November 2008.

4. Eastman, J.A., Phillpot, S.R., Choi, S.U.S., Keblinski, P., *Thermal Transport In Nanofluids*, Annu. Rev. Mater. Res., Vol. 34, pp. 219–46, 2004.

5. Maxwell, J.C., *A Treatise on Electricity and Magnetism*, 2nd Ed., Vol. 1, Clarendon Pres, Oxford, pp. 435, 1881.

6. Ahuja, A.S., *Augmentation of heat transport in laminar flow of polystyrene suspensions. I. Experiments and results*, Journal of Applied Physics, Vol. 46, No. 8, pp. 3408-3416, 1975.

7. Ahuja, A.S., *Augmentation of heat transport in laminar flow of polystyrene suspensions. II. Analysis of the data*, Journal of Applied Physics, Vol. 46, No. 8, pp. 3417-3425, 1975.

8. Choi, S.U.S. and Eastman, J.A., *Enhancing thermal conductivity of fluids with nanoparticles*, ASME International mechanical engineering congress & exposition, November 12-17, 1995.

9. Das, S. K., Choi, S.U.S., Patel, H.E., *Heat Transfer in Nanofluids—A Review*, Heat Transfer Engineering, Vol. 27, No. 10, pp. 3–19, 2006.

10. Xuan, Y., Li, Q., *Heat transfer enhancement of nanofluids*, International Journal of Heat and Fluid Flow, Vol. 21, pp. 58-64, 2000.

11. Masuda, H., Ebata, A., Teramea, K., Hishinuma, N., *Alteration of thermal conductivity and viscosity of liquid by dispersing ultra-fine particles*, Netsu Bussei (Japan), Vol. 4, pp. 227-233, 1993.

12. Choi, S.U.S., Eastman, J.A., *Enhancing Thermal Conductivity of Fluids with Nanoparticles*, ASME International Mechanical Engineering Congress & Exposition, pp. 12-17, November 1995.

13. Li, Y., Zhou, J., Tung, S., Schnedier, E., Xi, A., *A review on development of nanofluid preparation and characterization*, Powder Technology, Vol. 196, pp. 89-101, 2009.

14. Murshed, S.M.S., Leong, K.C., Yang, C., *Thermophysical and electrokinetic properties of nanofluids – A critical review*, Applied Thermal Engineering, Vol. 28, pp. 2109–2125, 2008.

15. Eastman, J.A., Phillpot, S.R., Choi, S.U.S., Keblinski, P., *Thermal Transport in Nanofluids1*, Annu. Rev. Mater. Res., Vol. 34, pp. 219–46, 2004.

16. Singh, A.K., *Thermal Conductivity of Nanofluids*, Defence Science Journal, Vol. 58, No. 5, pp. 600-607, September 2008.

17. Yu , Wenhua, France, David M., Routbort, Jules L., Choi, Stephen U.S., *Review and Comparison of Nanofluid Thermal Conductivity and Heat Transfer Enhancements*, Heat Transfer Engineering, Vol. 29, No. 5, pp. 432–460, 2008.

18. Wang, Xiang-Qi, Mujumdar, Arun S., *A review on nanofluids – part I: theoretical and numerical investigations*, Brazilian Journal of Chemical Engineering, Vol. 25, No. 4, pp. 613-630, October-December, 2008.

19. Wen, Dongsheng, Lin, Guiping, Vafaei, Saeid, Zhang, Kai, *Review of nanofluids for heat transfer applications*, Particuology, Vol. 7, pp. 141–150, 2009.

20. Das, Sarit Kumar, Choi, Stephen U.S., Patel, Hrishikesh E., *Heat Transfer in Nanofluids— A Review*, Heat Transfer Engineering, Vol. 27, No. 10, pp. 3–19, 2006.

21. Wang, Xiang-Qi, Mujumdar, Arun S., *Heat transfer characteristics of nanofluids: a review*, International Journal of Thermal Sciences, Vol. 46, pp. 1–19, 2007.

22. Manna, Indranil, *Synthesis, Characterization and Application of Nanofluid—An Overview*, Journal of the Indian Institute of Science, Vol. 89, No.1, January–March 2009.

23. Shinkai, Masashige, *Review : Functional Magnetic Particles for Medical Application*, Journal of Bioscience and Bioengineering, Vol. 94, No. 6, pp. 606-613, 2002.

24. Wang, Xiang-Qi, Mujumdar, Arun S., *A review on nanofluids – part II : experiments and applications*, Brazilian Journal of Chemical Engineering, Vol. 25, No. 4, pp. 631 - 648, October - December, 2008.

25. Özerinç, S., Kakaç, S., Yazıcıoğlu, A.G., *Enhanced thermal conductivity of nanofluids: a state-of-the-art review*, Microfluid Nanofluid., DOI 10.1007/s10404-009-0524-4, Vol. 8, No. 2, pp. 145-170, 2010.

26. Li, Yanjiao, Zhou, Jing'en, Tung, Simon, Schneider, Eric, Xi, Shengqi, *Review : A review on development of nanofluid preparation and characterization*, Powder Technology, Vol. 196, pp. 89–101, 2009.

27. Wong, Kaufui V., De Leon, Omar, *Review Article : Applications of Nanofluids: Current and Future*, Hindawi Publishing Corporation, Advances in Mechanical Engineering, Vol. 2010, Article ID 519659, pp. 11, 2010.

28. Li, Q., Xuan, Y, Wang, J., *Experimental investigations on transport properties of magnetic fluids*, Experimental Thermal and Fluid Science, Vol. 30, pp. 109–116, 2005.

29. Li, Q., Xuan, Y., *Experimental investigation on heat transfer characteristics of magnetic fluid flow around a fine wire under the influence of an external magnetic field*, Experimental Thermal and Fluid Science, Vol. 33, pp. 591–596, 2009.

30. Philip, J., Shima, P.D., Raj, B., *Enhancement of thermal conductivity in magnetite based nanofluid due to chainlike structures*, Appl. Phys. Letters 91, 203108-1-3, 2007.

31. Shima, P.D., Philip, John, Raj, Baldev, *Magnetically controllable nanofluid with tunable thermal conductivity and viscosity*, Applied Physics Letters, Vol. 95, 133112, 2009.

32. Lajvardi, M., Rad, J.M., Hadi, I., Gavili, A., Isfahani, T.D., Zabihi, F., Sabbaghzadeh, J., *Experimental investigation for enhanced ferrofluid heat transfer under magnetic field effect*, Journal of Magnetism and Magnetic Materials, Vol. 322, pp. 3508–3513, 2010.

33. Xie, H., Fujii, M., Zhang, X., *Effect of interfacial nanolayer on the effective thermal conductivity of nanoparticle-fluid mixture*, Int. J. Heat Mass Transfer, Vol. 48, pp. 2926-2932, 2005.

34. Lee, S., Choi, S.U.S., Li, S., Eastman, J.A., *Measuring thermal conductivity of fluids containing oxide nanoparticles*, J. Heat Transfer, Vol. 121, pp. 280-289, 1999.

35. Liu, M.-S., Lin, M.C.-C., Huang, I.-T., Wang, C.-C., *Enhancement of thermal conductivity with carbon nanotube for nanofluids*, Int. Commun. Heat Mass Transfer, Vol. 32, pp. 1202-1210, 2005.

36. Murshed, S.M.S., Leong, K.C., Yang, C., *Enhanced thermal conductivity of TiO_2-water based nanofluids*, Int. J. Thermal Sci., Vol. 44, pp. 367-373, 2005.

37. Hwang, Y.J., Ahn, Y.C., Shin, H.S., Lee, C.G., Kim, G.T., Park, H.S., Lee, J.K., *Investigation on characteristics of thermal conductivity enhancement of nanofluids*, Current Appl. Phys., Vol. 6, pp. 1068-1071, 2005.

38. Xuan, Y., Li, Q., *Heat transfer enhancement of nanofluids*, Int. J. Heat Fluid Flow, Vol. 21, pp. 58-64, 2000.

39. Masuda, H., Ebata, A., Teramea, K., Hishinuma, N., *Alteration of thermal conductivity and viscosity of liquid by dispersing ultra-fine particles*, Netsu Bussei (Japan), Vol. 4, pp. 227-233, 1993.

40. Patel, H. E., Das, S. K., Sundararagan, T., Nair, A. S., Geoge, B., Pradeep, T., *Thermal conductivities of naked and monolayer protected metal nanoparticle based nanofuids: Mani-festation of anomalous enhancement and chemical effects*, Appl. Phys. Lett., Vol. 83, pp. 2931-2933, 2003.

41. Eastman, J.A., Choi, U.S., Li, S., Thompson, L.J., Lee, S., *Enhanced thermal conductivity through the development of nanofluids*, Materials Research Society Symposium – Proceedings, Vol. 457, pp. 3-11, 1997.

42. Hong, T.K., Yang, H.S., Choi, C.J., *Study of the enhanced thermal conductivity of Fe nanofluids*, J. Appl. Phys., Vol. 97, pp. 1-4, 2005.

43. Xie, H., Wang, J., Xi, T., Liu, Y., *Thermal conductivity of suspensions containing nanosized SiC particles*, Int. J. Thermophysics, Vol. 23, pp. 571-580, 2002.

44. Choi, S.U.-S., Zhang, Z.G., Yu, W., Lockwood, F.E., Grulke, E.A., *Anomalous thermal conductivity enhancement in nanotube suspensions*, Appl. Phys. Letters, Vol. 79, pp. 2252-2254, 2001.

45. Buongiorno, J., *et al.*, *A benchmark study on the thermal conductivity of nanofluids*, J.of Applied Physics 106 094312, 2009, J. of magnetism and magnetic materials, Vol. 322, pp. 3895-3901, 2010.

46. Abareshi, M., Goharshadi, E., Zebarjad, S.M., Fadafan, H.K., Youssefi, A., *Fabrication, characterization and measurement of thermal conductivity of Fe_3O_4 nanofluids*, J.of Magnetism and Magnetism Material, Vol. 322, pp. 3895-3901, 2010.

47. Garg, J., *et al., Enhanced Thermal Conductivity and Viscosity of copper nanoparticles in ethylene glycol nanofluid*, Journal of Applied Physics, Vol. 103, 0744301-1-0744301-6, 2008.

48. Phuoc, Tran X. and Massoudi, M., *Experimental observations of the effects of shear rates and particle concentration on the viscosity of Fe_2O_3-deionized water nanofluids*, Int. Journal of Thermal Sciences, Vol. 48, pp. 1294-1301, 2009.

49. Duangthongsuk, W., *et al., Measurement of temperature-dependent thermal conductivity and viscosity of TiO_2-water nanofluids*, Experimental Thermal and Fluid Science, Vol. 33, pp. 706-714, 2009.

50. Chandrasekar, M., et al., *Experimental investigations and theoretical determination of thermal conductivity and viscosity of Al_2O_3/water nanofluid*, Experimental and Fluid Science, Vol. 34, pp. 210-216, 2010.

51. Chen, H., *et al., Rheological behaviour of ethylene glycol based titania nanofluids*, Chemical Physics Letters, Vol. 444, pp. 333-337, 2007.

52. Hojjat, M., *et al., Rheological characteristics of non-Newtonian nanofluids: Experimental investigation*, Int. Commun.*Heat and Mass Transfer*, Article in press, 2011.

53. Tamjid, E., and Guenther, B.H., *Rheology and colloidal structure of silver nanoparticles dispersed in diethylene glycol*, Powder Technology, Vol. 197, pp. 49-53, 2010.

54. Tseng, W.J., and Lin, K., *Rheology and colloidal structure of aqueous TiO_2 nanoparticle suspensions*, Material Science and Engineering, A355, pp. 186-192, 2003.

55. Turgut, A., et al., *Thermal conductivity and viscosity measurements of water-based TiO_2 nanofluids*, Int.J.Thermopphys, Vol. 30, pp. 1213-1226, 2009.

56. Kwak, K., Kim, C., *Viscosity and thermal conductivity of copper oxide nanofluid dispersed in ethylene glycol*, Korea-Australia Rheology Journal, Vol. 17, No. 2, pp. 35-40, 2005.

57. Namburu, P.K., *et al.*, *Experimental Investigation of viscosity and specific heat of silicon dioxide nanofluids*, Micro &Nano Letters, Vol. 2, No. 3, pp. 67-71, 2007.

58. Nguyen, C.T., *et al.*, *Temperature and particle-size dependent viscosity data for water-based nanofluids-Hysteresis phenomenon*, Int.J.Heat and Fluid Flow, Vol. 28, pp. 1492-1506, 2007.

59. Masoumi, N., *et al.*, *A new model for calculating the effective viscosity of nanofluids*, J.of Physics D:Applied Physics, Vol. 42, 055501, pp. 6, 2009.

60. Yu, W., *et al.*, *Investigation of thermal conductivity and viscosity of ethylene glycol bsed ZnO nanofluid*, Thermpchimica Acta, Vol. 491, pp. 92-96, 2009.

61. Murshed, S.M.S., *et al.*, *Investigations of thermal conductivity and Viscosity of nanofluids*, Int.Journal of Thermal Sci., Vol. 47, pp. 560-568, 2008.

62. Kang H.U., *et al.*, *Estimation of thermal conductivity of nanofluid using experimental effective particle volume*, Experimental Heat Transfer, Vol. 19, No. 3, pp. 181-191, 2006.

63. Masuda, *et al., Alteration of thermal conductivity and viscosity of liquid by dispersing ultra-fine particles (dispersion of Al_2O_3, SiO_2 and TiO_2 ultra-fine particles)*, Netsu Bussei (Japan), Vol. 4, pp. 227-233, 1993.

64. Wang, X., *et al., Thermal conductivity of nanoparticle–fluid mixture*, Journal of Thermophysics and Heat Transfer, Vol. 13, pp. 474-480, 1999.

65. Pak, B.C., *et al., Hydrodynamic and heat transfer study of dispersed fluid with submicron metallic oxide particles*, Exp.Heat Transfer, Vol. 11, pp. 151-170, 1998.

66. Das, S.K., *et al., Temperature dependence of thermal conductivity enhancement for nanofluids*, ASME Transactions, Jour.of Heat Transfer, Vol. 125, pp. 567-574, 2003.

67. Prasher, R., *et al., Measurement of nanofluids viscosity and its implications for thermal applications*, Appl. Phys. Lett., Vol. 89, 133108-1133108-3, 2006.

68. Timofeeva, E.V., *et al., Thermal conductivity and particle agglomeration in alumina nanofluids: experiment and theory*, Phys. Review E, Vol. 76, 061203, 2007.

69. He, Y., *et al., Heat transfer and flow behaviour of aqueous suspensions of TiO_2 nanofluids flowing upward through a vertical pipe*, Int.J.of Heat and Mass Transfer, Vol. 50, pp. 2272-2281, 2007.

70. Lee, J.H., *et al., Effective viscosities and thermal conductivities of aqueous nanofluids containing low volume consentrations of Al_2O_3 nanoparticles*, Int.J.of Heat and Mass Transfer, Vol. 51, pp. 2651-2656, 2008.

71. Xinfang, L., *et al., Experimental investigation on viscosity of Cu-H_2O nanofluids*, J.Wuhan Unv.Technol.Mater. Sci.Ed., 24, 48-52, 2009.

72. Rosenzweig , R.E., *Ferrohydrodynamics*, Cambiridge Press, Cambridge, 1985.

73. Odenbach, S., (Editor), *Ferrofluids: Magnetically controllable fluids and their applications,* Springer, Berlin, 2002.

74. Leslie-Pelecky, D.L., Rieke, R. D., *Magnetic Properties of Nanostructured Materials, Chem. Mater.*, Vol. 8, pp. 1770-1783, 1996.

75. Neuringer, J. and Rosensweig, R.E., *Ferrohydrodynamics*, The Physics of Fluids, Vol. 7, No. 12, pp. 1927-1937, 1964.

76. Scherer, C. and Figueiredo Neto, A.M., *Ferrofluis: Preparation and Applications*, Brazialian Journal of Ferrofluids, Vol. 35, No. 3A, September 2005.

77. Odenbach, S., (Editor), *Ferrofluids: Magnetically controllable fluids and theirapplications,* Springer, Berlin, 2002.

78. Rohsenow , Warren M., Choi , Harry Y. , *Heat, Mass and Momentum Transfer*, Prentice-Hall Inc.,New Jersey, 1961.

79. Welty, James R., Wicks, Charles E., Wilson, Robert E., *Fundementals of Momentum, Heat and Mass Transfer*, Third Edition, John Wiley&Sons, USA, 1984.

80. Keblinski, P., Phillpot, S.R., Choi, S.U.S., Eastman, J.A., *Mechanisms of heat flow in suspensions of nano-sized particles (nanofluids),* Int. J. Heat Mass Trans., Vol. 45, pp. 855–63, 2002.

81. Eastman, J.A., Phillpot, S.R., Choi, S.U.S., Keblinski, P., *Thermal Transport in Nanofluids1*, Annu. Rev. Mater. Res., Vol. 34, pp. 219–46, 2004.

82. Wang, X., Xu, X. and Choi, S. U. S., *Thermal Conductivity of Nanoparticle-Fluid Mixture,* Journal of Thermophysics and Heat Transfer, Vol. 13, No. 4, pp. 474–480, 1999.

83. Xuan, Y., and Li, Q., *Heat Transfer Enhancement of Nanofluids*, International Journal of Heat and Fluid Flow, Vol. 21, pp. 58–64, 2000.

84. Chon, C. H., Kihm, K. D., *Thermal conductivity enhancement of nanofluids by Brownian motion*, Journal of Heat Transfer, Vol. 127, pp. 810, 2005.

85. Long, Gary J. and Grandjean, Fernande, *Supermagnets, Hard Magnetic Materials*, Kluwer Academic Publishers, pp. 32-37, 1990.

86. McCaig, Malcolm, Clegg, Alan G., *Permanent Magnets in Theroy and Pratice*, Second Edition, , Pentech Press London, pp. 11-24, 1977.

87. Pankhurst, Q.A, Connolly, J., Jones, S. K. and Dobson, J., *Applications of magnetic nanoparticles in biomedicine*, J. Phys. D: Appl. Phys., Vol. 36, R167–R181, 2003.

88. Li, Y., Zhou, J., Tung, S., Schnedier, E., Xi, A., *A review on development of nanofluid preparation and characterization*, Powder Technology, Vol. 196, pp. 89-101, 2009.

89. V.E. Buravtsova, E.A. Gan'shina, V.S. Gushchin, S.I. Kasatkin, A.M. Murav'ev, N.V. Plotnikova, F.A. Pudonin, Magnetic and magnetooptical properties of multilayer ferromagnet-semiconductor nanostructures, Phys. the Solid State, Vol. 46, pp. 891-901, 2004.

90. Love, L. J. *et al*, *Ferrofluid Field Induced Flow for Microfluidic Applications*, ASME Transactions on Mechatronics, Vol. 10, No. 1, 2005.

91. R.Bayron Birth, Transport Phenomena, John Wiley and Son's Inc., 2007.

92. Leach, Richard K., *Fundemental Principles of Engineering Nanometrolgy*, Elsvier Inc. USA, pp. 201-202, 2010.

93. http://cimewww.epfl.ch/people/cayron/Fichiers/thesebook-chap3.pdf

94. Egerton, Ray F., *Physical Principles of Electron Microscopy, An Introduction to TEM, SEM, and AEM*, Springer, p. 84, 1st ed. 2005, Corr. 2nd printing 2008. XII.

95. FEI Company Tools for NanoTech, *Tecnai GF30 The benchmark for high performancenanoanalysis*,http://www.nano.org.tr/files/tem/2007_07_TecnaiF2_30_ds.pdf, 2007.

96. Sartor, M., *Dynamic Light Scattering*, University of California San Diego (UCSD), http://physics.ucsd.edu/neurophysics/courses/physics_173_273/dynamic_light_scattering_03.pdf, 2006.

97. Malvern, *Dynamic Lights Scattering (DLS)*, Zetasizer Nano Series, Mano 317 User Manual, Issue 5, 2009.

98. Scintag Inc., *Basics of X-ray Diffraction*, Chapter 7, http://epswww.unm.edu/xrd/xrdbasics.pdf, 1999.

99. Waseda, Yoshio, Matsubara, Eiichiro, Shinoda, Kozo, *X-Ray Diffraction Crystallography: Introduction, Examples and Solved Problems*, Springer, 2011.

100. Cullity, B.D, *Natural Sciences; Physics; Physical nature of matter*, Publisher: Addison-Wesley Publishing Company, Inc.1956.

101. Fiorillo, Fausto, *Measurement and Caharacterization of Magnetic Materials*, Elsevier Inc. Academic pres, pp. 500-508, 2004.

102. Long, Gary J. and Grandjean, Fernande , *Supermagnets, Hard Magnetic Materials*, Kluwer Academic Publishers, pp. 398-399, 1990.

103. Bertotti, Giorgio, *Hysteresis in magnetization*, Academic press, pp. 9-10, 1998.

104. Anton Paar Unique Density and Concentration Meters, *DMA 4100 Product Specifications*,http://www.uniontek.com.cn/images/antonapaar/%D7%CA%C1%CF-DMA-4100.pdf.

105. Anton Paar, *Operation Manual for Anton Paar DMA 4100*, 2006.

106. *Brookfield DV-III Ultra Programmable Rheometer Operating Instruction Manual*, Brookfield Engineering Laboratories Inc., Manual No. M/98-211-B0104, http://www.viscometers.org/PDF/Manuals/laboratory/DV-III%20Ultra.pdf.

107. Nagasaka, Y. and Nagashima, A., *Absolute measurement of the thermal conductivity of electrical I y conducting liquids by the transient hot-wire method*, J. Phys. E: Sci. Instrum., Vol. 14, pp. 1435-1440, 1981.

108. Paul, G., Chopkar, M., Mana, I., Das, P.K., *Techniques for measuring the thermal conductivity of nanofluids: A review*, Renewable and Sustainable Energy Reviews, Vol. 14, pp. 1913–1924, 2010.

109. Xie, H., Fujii, M., Zhang, X., *Effect of interfacial nanolayer on the effective thermal conductivity of nanoparticle-fluid mixture*, Int. J. Heat Mass Transfer, Vol. 48, pp. 2926-2932, 2005.

110. Lee, S., Choi, S.U.-S., Li, S., Eastman, J.A., *Measuring thermal conductivity of fluids containing oxide nanoparticles*, J. Heat Transfer, Vol. 121, pp. 280-289, 1999.

111. PSL Systemtechnik, *Measuring of Thermal Conductivity with the Measuring System Lambda*, http://www.psl-systemtechnik.de/thermal_conductivity.html?&L=1.

112. Sun, J., Zhou, S., Hou, P., Yang, Y., Weng, J., Li, X. and Li, M., *Synthesis and characterization of biocompatible Fe_3O_4 nanoparticles*, Wiley InterScience, 2006.

113. Pankhurst, Q.A., Connolly, J., Jones, S.K. and Dobson, J., *Applications of magnetic nanoparticles in biomedicine*, J. Phys. D: Appl. Phys., Vol. 36, R167–R181, 2003.

114. Pak, B.C. and Cho, Y.I., *Hydrodynamic and Heat Transfer Study of Dispersed Fluids with Submicron Metallic Oxide Particles*, Experimental Heat Transfer, Vol. 11, pp. 151-170, 1998.

115. Huang, Wei, Wu, Jianmin, Guo, Wei, *Initial susceptibility and viscosity properties of low concentration e-Fe3 N based magnetic fluid*, Nanoscale Res Lett, 2:155–160, 2007.

116. S. W. Lee, S.D. Park, S. Kang, I. C. Bang, J. H. Kim, "*Investigation of viscosity and thermal conductivity of SiC nanofluids for heat transfer applications*", International Journal of Heat and Mass Transfer, Vol. 54, pp. 433–438, 2011.

117. Namburu, P.K., Kulkarni, D.P., Dandekar, A. and Das, D.K., *Experimental investigation of viscosity and specific heat of silicon dioxide nanofluids*, Micro & Nano Letters, Vol. 2, No. 3, pp. 67–71, 2007.

118. Bates, L.F., Lloyd-Evans, B.J., *A compact electromagnet for general purposes*, Proceedings of the Physical Society, Vol. 45, No. 3, pp. 425-433, 1933.

119. Hudson R.P., *A Simply-constructed Small Electromagnet of High Performance*, Journal of Scientific Instruments, Vol. 26, No. 12, pp. 401-404, 1949.

120. Snellman, Olle, Burge, E.J., *The Uppsala Electromagnet*, Journal of Scientific Instruments, Vol. 26, No. 10, pp. 331-335, 1949.

121. Sucksmith, W., Anderson, S.P., *A general purpose electromagnet*, Journal of Scientific Instruments, Vol. 33, No. 6, pp. 234-236, 1956.

122. Buongiorno J. *et al.*, *A benchmark study on the thermal conductivity of nanofluids*, Journal of Applied Physics, Vol. 106, 094312, 2009.

123. Djurek, I., Znidarsic, A., Kosak, A., and Djurek, D., *Thermal Conductivity Measurements of the $CoFe_2O_4$ and γ-Fe_2O_3 based Nanoparticle Ferrofluids*, Croatica Chemica ACTA, CCACAA, Vol. 80, No.3-4, pp. 529-532, 2007.

124. Shima, P. D., Philip, J., and Raj, B. *Magnetically controllable nanofluid with tunable thermal conductivity and viscosity*, Applıed Physics Letters, Vol. 95, 133112 , 2009.

125. Haghgooie, R. and Doyle P. S., *Transition from two-dimensional to three-dimensional behaviour in the self-assembly of magnetorheological fluids confined in thin slits*, Physical Review E **75**, 061406, 2007.

126. Assael, M. J. and Papadaki, M., *Measurements of the Viscosity of n-Heptane, n-Nonane, and n-Undecane at Pressures up to 70 MPa*, International Journal of Thermophysics, Vol. 12, No. 5, 1991.

127. Varadan, V., Chen, L.F., Xie, J., *Nanomedicine: Design and Applications of Magnetic Nanomaterials, Nanosensors and Nanosystems*, John Wiley & Sons, Ltd, 2008.